Chapter 2

Earthquake Ground Motion and Response Spectra

Bijan Mohraz, Ph.D., P.E.
Southern Methodist University, Dallas, Texas

Fahim Sadek, Ph.D.
Mechanical Engineering Department, Southern Methodist University, Dallas, Texas. On assignment at the National Institute of Standards and Technology, Gaithersburg, Maryland

Key words: Earthquake Engineering, Earthquake Ground Motion, Earthquake Energy, Ground Motion Characteristics, Peak Ground Motion, Power Spectral Density, Response Modification Factors, Response Spectrum, Seismic Maps, Strong Motion Duration.

Abstract: This chapter surveys the state-of-the-art work in strong motion seismology and ground motion characterization. Methods of ground motion recording and correction are first presented, followed by a discussion of ground motion characteristics including peak ground motion, duration of strong motion, and frequency content. Factors that influence earthquake ground motion such as source distance, site geology, earthquake magnitude, source characteristics, and directivity are examined. The chapter presents probabilistic methods for evaluating seismic risk at a site and development of seismic maps used in codes and provisions. Earthquake response spectra and factors that influence their characteristics such as soil condition, magnitude, distance, and source characteristics are also presented and discussed. Earthquake design spectra proposed by several investigators and those recommended by various codes and provisions through the years to compute seismic base shears are described. The latter part of the chapter discusses inelastic earthquake spectra and response modification factors used in seismic codes to reduce the elastic design forces and account for energy absorbing capacity of structures due to inelastic action. Earthquake energy content and energy spectra are also briefly introduced. Finally, the chapter presents a brief discussion of artificially generated ground motion.

2.1 INTRODUCTION

Ground vibrations during an earthquake can severely damage structures and equipment housed in them. The ground acceleration, velocity, and displacement (referred to as ground motion) when transmitted through a structure, are in most cases amplified. This amplified motion can produce forces and displacements, which may exceed those the structure can sustain. Many factors influence ground motion and its amplification; therefore, an understanding of how these factors influence the response of structures and equipment is essential for a safe and economical design.

Earthquake ground motion is usually measured by strong motion instruments, which record the acceleration of the ground. The recorded accelerograms, after they are corrected for instrument errors and baseline (see next section), are integrated to obtain the velocity and displacement time-histories. The maximum values of ground motion (peak ground acceleration, peak ground velocity, and peak ground displacement) are of particular interest in seismic analysis and design. These parameters, however, do not by themselves describe the intensity of shaking that structures or equipment experience. Other factors, such as earthquake magnitude, distance from the fault or epicenter, duration of strong shaking, soil condition of the site, and the frequency content of the motion also influence the response of a structure. Some of these effects such as the amplitude of the motion, frequency content, and local soil conditions are best represented through a response spectrum [2-1 to 2-4] which describes the maximum response of a damped single-degree-of-freedom (SDOF) oscillator with various frequencies or periods to ground motion. The response spectra from a number of records are often averaged and smoothed to obtain design spectra which specify the seismic design forces and displacements at a given frequency or period.

This chapter presents earthquake ground motion and response spectra, and the influence of earthquake parameters such as magnitude, duration of strong motion, soil condition, source distance, source characteristics, and directivity on ground motion and response spectra. The evaluation of seismic risk at a given site and development of seismic maps are also discussed. Earthquake design spectra proposed by several investigators and those recommended by various agencies and organizations are presented. The latter part of the chapter includes the inelastic earthquake spectra and response modification factors (*R*-factors) that several seismic codes and provisions recommend to account for the energy absorbing capacity of structures due to inelastic action. Earthquake energy content and energy spectra are also presented. Finally, the chapter presents a brief discussion of artificially generated ground motion.

2.2 RECORDED GROUND MOTION

Ground motion during an earthquake is measured by strong motion instruments, which record the acceleration of the ground. Three orthogonal components of ground acceleration, two in the horizontal direction and one in the vertical, are recorded by the instrument. The instruments may be located on free-field or mounted in structures. Typical strong motion accelerograms recorded on free-field and the ground floor of the Imperial County Services Building during the Imperial Valley earthquake of October 15, 1979 [2-5] are shown in Figure 2-1.

Analog accelerographs, which record ground accelerations on photographic paper or film, were used in the past. The records were then digitized manually, but later the process was automated. These instruments were triggered by the motion itself and some part of the initial motion was therefore lost, resulting in permanent displacements at the end of the record. Today, digital recording instruments

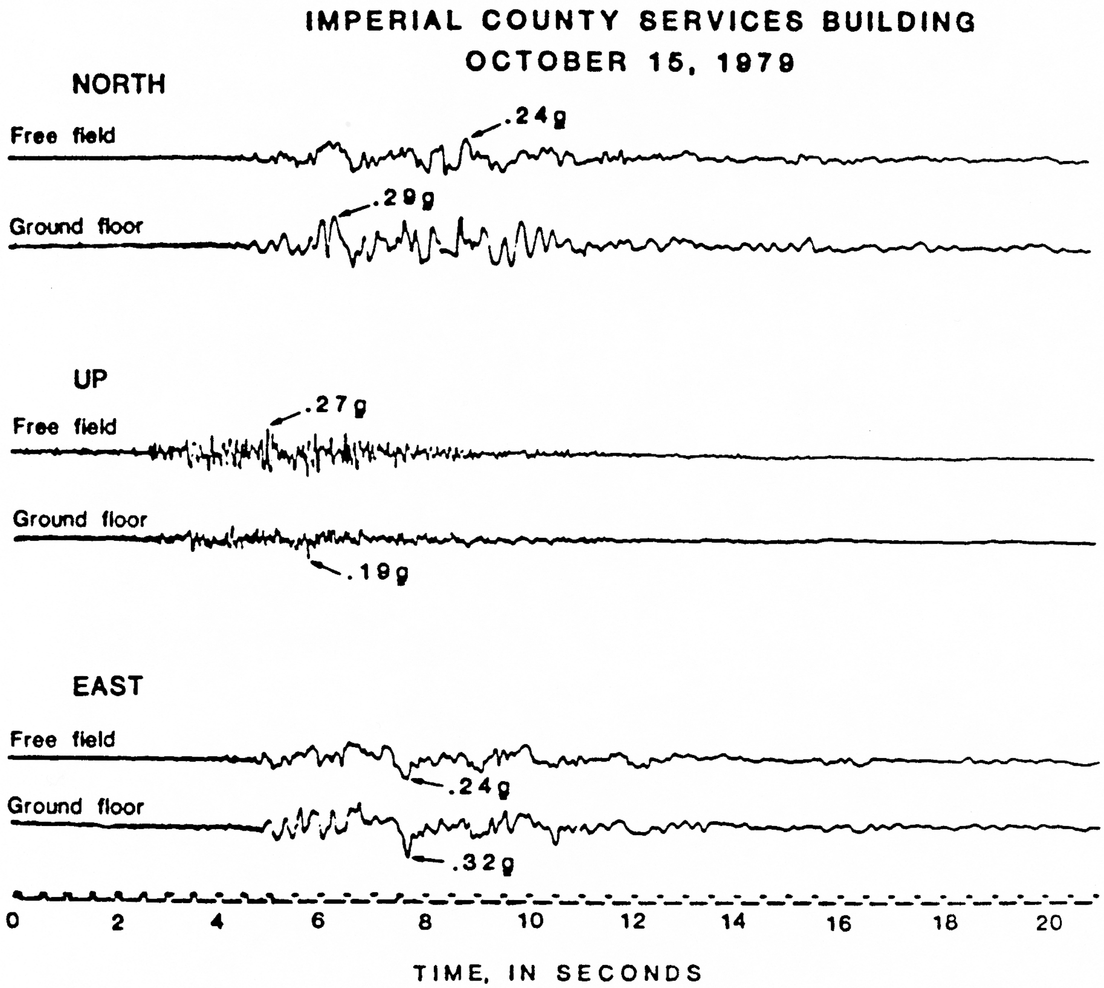

Figure 2-1. Strong motion accelerograms recorded on free field and ground floor of the Imperial County Service Building during the Imperial Valley earthquake of October 15, 1979. [After Rojahn and Mork (2-5).]

using force-balance accelero-meters are finding wider application because these instruments produce the transducer output in a digital form that can be automatically disseminated via dial up modems or Internet lines. In addition to having low noise and greater ease in data processing, digital instruments eliminate the delays in recording the motion and the loss of accuracy due to digitizing traces on paper or film. They also permit recovery of the initial portion of the signal.

Accelerations recorded on accelerographs are usually corrected to remove the errors associated with digitization (transverse play of the recording paper or film, warping of the paper, enlargement of the trace, etc.) and to establish the zero acceleration line before the velocity and displacement are computed. Small errors in establishing the zero acceleration baseline can result in appreciable errors in the computed velocity and displacement. To minimize the errors, a correction is applied by assuming linear zero acceleration and velocity baselines and then using a least square fit to determine the parameters of the lines. For a detailed description of the procedure used in digitizing and correcting accelerograms, one should refer to Trifunac [2-6], Hudson et al. [2-7], and Hudson [2-8]. Another procedure which assumes a second degree polynomial for the zero acceleration baseline has also been used in the past [2-9]. The Trifunac-Hudson procedure, however, is more automated and has been used extensively to correct accelerograms. The corrected accelerograms are then integrated to obtain the velocity and displacement time-histories.

For accelerograms obtained from digital recording instruments, the initial motion is preserved, thereby simplifying the task of determining the permanent displacement. Iwan et al. [2-10] proposed a method for processing digitally recorded data by computing the average ordinates of the acceleration and velocity over the final segment of the record and setting them equal to zero. A constant acceleration correction is applied to the strong shaking portion of the record which may be defined as the time segment between the first and last occurrence of accelerations of approximately 50 cm/sec^2. A different constant acceleration correction is applied to the remaining final segment.

In the United States, the digitization, correction, and processing of accelerograms have been carried out by the Earthquake Engineering Research Laboratory of the California Institute of Technology in the past and currently by the United States Geological Survey (USGS) and other organizations such as the California Strong Motion Instrumentation Program (CSMIP) of the California Division of Mines and Geology (CDMG). A typical corrected accelerogram and the integrated velocity and displacement for the S00E component of El Centro, the Imperial Valley earthquake of May 18, 1940 are shown in Figure 2-2.

2.3 CHARACTERISTICS OF EARTHQUAKE GROUND MOTION

The characteristics of ground motion that are important in earthquake engineering applications are:

1. Peak ground motion (peak ground acceleration, peak ground velocity, and peak ground displacement),
2. duration of strong motion, and
3. frequency content.

Each of these parameters influences the response of a structure. Peak ground motion primarily influences the vibration amplitudes. Duration of strong motion has a pronounced effect on the severity of shaking. A ground motion with a moderate peak acceleration and a long duration may cause more damage than a ground motion with a larger acceleration and a shorter duration. Frequency content strongly affects the response characteristics of a structure. In a structure, ground motion is amplified the most when the frequency content of the motion and the natural frequencies of the structure are close to each other. Each of these characteristics are briefly discussed below:

2.3.1 Peak ground motion

Table 2-1 gives the peak ground acceleration, velocity, displacement, earthquake magnitude, epicentral distance, and site description for typical records from a number of seismic events from the western United States. Some of these records are frequently used in earthquake engineering applications. Peak ground acceleration had been widely used to scale earthquake design spectra and acceleration time histories. Later studies recommended that in addition to peak ground acceleration, peak ground velocity and displacement should also be used for scaling purposes. Relationships between ground motion parameters are discussed in Section 2.6.

Table 2-1. Peak Ground Motion, Earthquake Magnitude, Epicentral Distance, and Site Description for Typical Recorded Accelerograms

Earthquake and location	Mag.	Epicentral distance (km)	Comp.	Peak Acc. (g)	Peak Vel. (in/sec)	Peak Disp. (in)	Site Description
Helena, 10/31/1935	6.0	6.3	S00W	0.146	2.89	0.56	Rock
Helena, Montana Carroll College			S90W	0.145	5.25	1.47	
			Vert	0.089	3.82	1.11	
Imperial Valley, 5/18/1940	6.9	11.5	S00E	0.348	13.17	4.28	Alluvium, several 1000 ft
El Centro site			S90W	0.214	14.54	7.79	
			Vert	0.210	4.27	2.19	
Western Washington, 4/13/1949	7.1	16.9	N04W	0.165	8.43	3.38	Deep cohesionless soil,
Olympia, Washington Highway Test			N86E	0.280	6.73	4.09	420 ft
Lab			Vert	0.092	2.77	1.59	
Northwest California, 10/7/1951	5.8	56.2	S44W	0.104	1.89	0.94	Deep cohesionless soil,
Ferndale City Hall			N46W	0.112	2.91	1.08	500 ft
			Vert	0.027	0.87	0.64	
Kern County, 7/21/1952	7.2	41.4	N21E	0.156	6.19	2.64	40 ft of alluvium over
Taft Lincoln School Tunnel			S69E	0.179	6.97	3.60	poorly cemented
			Vert	0.105	2.63	1.98	sandstone
Eureka, 12/21/1954	6.5	24.0	N11W	0.168	12.44	4.89	Deep cohesionless soil,
Eureka Federal Building			N79E	0.258	11.57	5.53	250 ft deep
			Vert	0.083	3.23	1.83	
Eurkea, 12/21/1954	6.5	40.0	N44W	0.159	14.04	5.58	Deep cohesionless soil,
Ferndale City Hall			N46E	0.201	10.25	3.79	500 ft deep
			Vert	0.043	2.99	1.54	
San Francisco, 3/22/1957	5.3	11.5	N10E	0.083	1.94	0.89	Rock
San Francisco Golden Gate Park			S80E	0.105	1.82	0.33	
			Vert	0.038	0.48	0.27	
Hollister, 4/8/1961	5.7	22.2	S01W	0.065	3.06	1.12	Unconsolidated alluvium
Hollister City Hall			N89W	0.179	6.75	1.51	over partly consolidated
			Vert	0.050	1.85	0.85	gravel
Parkfield, 6/27/1966	5.6	56.1	N05W	0.355	9.12	2.09	Alluvium
Cholame Shandon, California Array			N89E	0.434	10.02	2.80	
No. 5			Vert	0.119	2.87	1.35	
Borrego Mountain, 4/8/1968	6.4	67.3	S00W	0.355	9.12	2.09	Alluvium
El Centro site			S90W	0.434	10.02	2.80	
			Vert	0.119	2.87	1.35	
San Fernando, 2/9/1971	6.4	21.1	N00W	0.255	11.81	5.87	Alluvium
8244 Orion Blvd., 1st Floor			S90W	0.134	9.42	5.45	
			Vert	0.171	12.58	5.76	
San Fernando, 2/9/1971	6.4	29.5	N21E	0.315	6.76	1.66	Sandstone
Castaic Old Ridge Route			N69W	0.271	10.95	3.74	
			Vert	0.156	2.54	1.38	
San Fernando, 2/9/1971	6.4	7.2	S15W	1.170	44.58	14.83	Highly jointed diorite
Pacoima Dam			S74W	1.075	22.73	4.26	gneiss
			Vert	0.709	22.96	7.61	
San Fernando, 2/9/1971	6.4	32.5	S00W	0.180	8.08	2.87	Granitic
Griffith Park Observatory			S90W	0.171	5.73	2.15	
			Vert	0.123	2.92	1.33	
Loma Prieta, 10/17/1989	7.0	7.0	90	0.479	18.70	4.54	Landslide deposits
Corralitos, Eureka Canyon Road			360	0.630	21.73	3.76	
			Vert	0.439	7.33	3.06	
Loma Prieta, 10/17/1989	7.0	16.0	90	0.409	8.36	2.68	Limestone
Santa Cruz – UCSC/LICK Lab			360	0.452	8.36	2.60	
			Vert	0.331	4.71	2.65	
Loma Prieta, 10/17/1989	7.0	43.0	360	0.219	13.16	5.45	Bay sediments/alluvium
Sunnyvale – Colton Avenue			270	0.215	13.42	4.98	
			Vert	0.103	2.91	1.21	
Landers, 6/28/1992	7.3	1.8	350	0.800	12.91	28.32	Stiff alluvium overlying
SCE Lucerne Valley Station			260	0.730	58.84	107.21	hard granitic rock
			Vert	0.860	16.57	17.03	
Northridge, 1/17/1994	6.6	19.3	265	0.434	12.05	1.97	Highly jointed diorite
Pacoima Dam			175	0.415	17.59	1.83	gneiss
			Vert	0.184	6.33	1.03	
Northridge, 1/17/1994	6.6	22.5	90	0.883	16.44	5.64	Alluvium
Santa Monica – City Hall Ground			360	0.370	9.81	2.57	
			Vert	0.232	5.52	1.49	
Northridge, 1/17/1994	6.6	15.8	90	0.604	30.29	5.99	Alluvium
Sylmar – County Hospital Parking			360	0.843	50.74	12.81	
Lot			Vert	0.535	7.34	2.97	

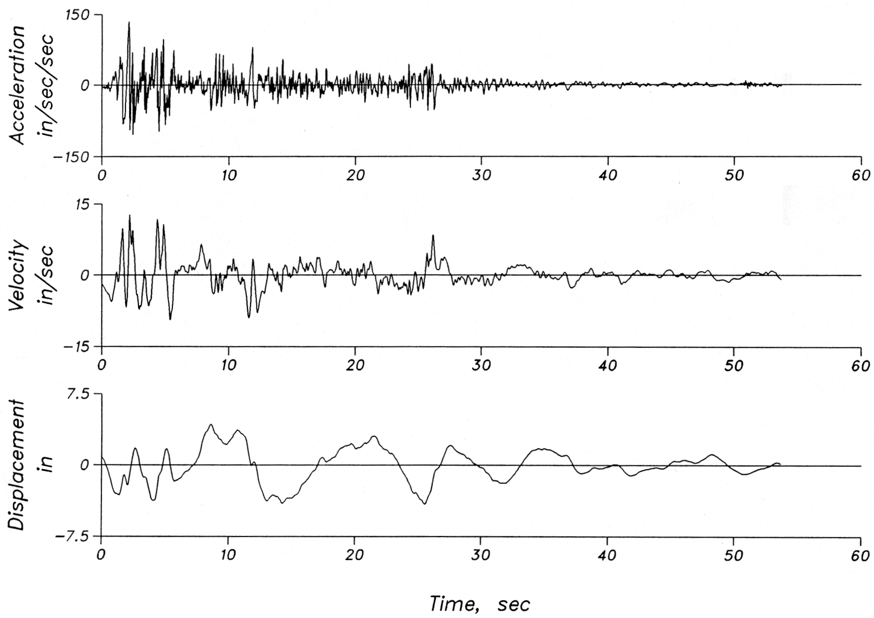

Figure 2-2. Corrected accelerogram and integrated velocity and displacement time-histories for the S00E component of El Centro, the Imperial Valley Earthquake of May 18, 1940.

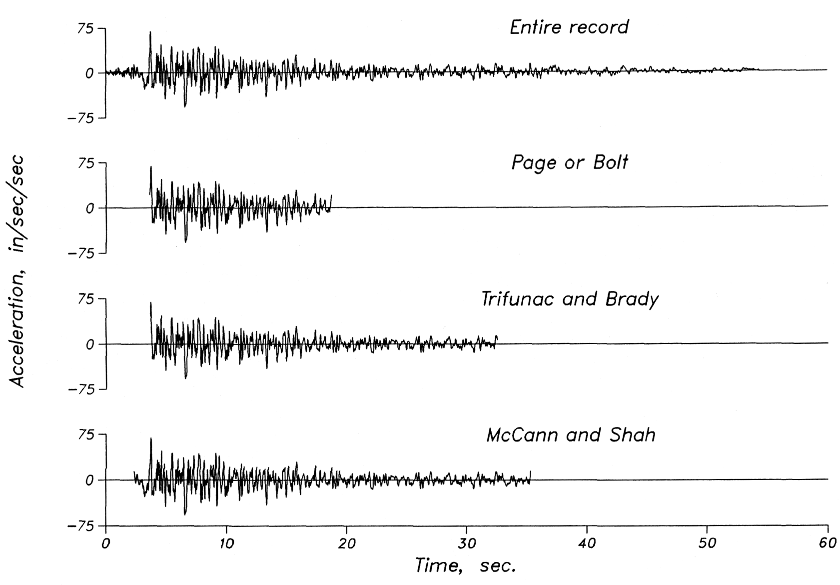

Figure 2-3. Comparison of strong motion duration for the S69E component of the Taft, California earthquake of July 21, 1982 using different procedures.

2.3.2 Duration of strong motion

Several investigators have proposed procedures for computing the strong motion duration of an accelerogram. Page et al. (2-11) and Bolt (2-12) proposed the "bracketed duration" which is the time interval between the first and the last acceleration peaks greater than a specified value (usually 0.05*g*). Trifunac and Brady (2-13)[1] defined the duration of the strong motion as the time interval in which a significant contribution to the integral of the square of acceleration ($\int a^2 dt$) referred to as the accelerogram intensity takes place. They selected the time interval between the 5% and the 95% contributions as the duration of strong motion. A third procedure suggested by McCann and Shah (2-15) is based on the average energy arrival rate. The duration is obtained by examining the cumulative root mean square acceleration (*rms*)[2] of the accelerogram. A search is performed on the rate of change of the cumulative *rms* to determine the two cut- off times. The final cut-off time T_2 is obtained when the rate of change of the cumulative *rms* acceleration becomes negative and remains so for the remainder of the record. The initial time T_1 is obtained in the same manner except that the search is performed starting from the "tail-end" of the record.

Figure 2-3 shows a comparison among the strong motion durations extracted from a typical record using different procedures. Table 2-2 gives the initial time T_1, the final Time T_2, the duration of strong motion ΔT, the *rms* acceleration, and the percent contribution to ($\int a^2 dt$) for several records. The comparisons show that these procedures result in different durations of strong motion. This is to be expected since the procedures are based on different criteria. It should be noted that since there is no standard definition of strong motion duration, the selection of a procedure for computing the duration for a certain study depends on the purpose of the intended application. For example, it seems reasonable to use McCann and Shah's definition, which is based on *rms* acceleration when studying the stationary characteristics of earthquake records and in computing power spectral density. On the other hand, the bracketed duration proposed by Page et al. (2-11) and Bolt (2-12) may be more appropriate for computing elastic and inelastic response and assessing damage to structures.

Based on the work of Trifunac and Brady (2-13), Trifunac and Westermo (2-16) developed a frequency dependent definition of duration where the duration is considered separately in several narrow frequency bands. They define the duration as the sum of time intervals during which the integral ($\int f^2(t)dt$) -- where $f(t)$ is the ground acceleration, velocity, or displacement -- has the steepest slope and gains a significant portion (90%) of its final value. This definition considers the duration being composed of several separate segments with locations specified by the slopes of the integral. The procedure is to band-pass filter the signal $f(t)$ using two Ormsby filters in different frequency bands with specified central frequencies. The duration for each frequency band is computed as the sum of several time intervals where the smoothed integration function ($\int f^2(t)dt$) has the steepest slope. The study by Trifunac and Westermo (2-16) indicated that the duration of strong motion increases with the period of motion.

2.3.3 Frequency content

The frequency content of ground motion can be examined by transforming the motion from a time domain to a frequency domain through a Fourier transform. The Fourier amplitude spectrum and power spectral density, which are based on this transformation, may be used to characterize the frequency content. They are briefly discussed below:

[1] An earlier study by Husid et al. (2-14) used a similar definition for the duration of strong motion.

[2] See Section 2.3.3 for definition of *rms*

Table 2-2. Comparison of Strong Motion Duration for Eight Earthquake Records

Record	Comp.	Method*	T_1 (sec)	T_2 (sec)	ΔT (sec)	RMS (cm/sec2)	$\int a^2 dt$
El Centro, 1940	S00E	A	0.00	53.74	53.74	46.01	100
		B	0.88	26.74	25.86	65.16	97
		C	1.68	26.10	24.42	64.75	90
		D	0.88	26.32	25.44	65.60	96
	S90W	A	0.00	53.46	53.46	38.85	100
		B	1.24	26.64	25.40	54.88	95
		C	1.66	26.20	24.54	54.39	90
		D	0.80	26.62	25.82	24.73	96
Taft, 1952	N21E	A	0.00	54.34	54.34	25.03	100
		B	3.44	22.94	19.50	38.50	85
		C	3.70	34.24	30.54	31.70	90
		D	2.14	36.46	34.32	30.85	96
	S69E	A	0.00	54.38	54.38	26.10	100
		B	3.60	18.72	15.12	44.61	82
		C	3.66	32.52	28.86	33.96	90
		D	2.34	35.30	32.96	32.71	95
El Centro, 1934	S00W	A	0.00	90.28	90.28	19.48	100
		B	1.92	14.78	12.86	46.89	83
		C	2.82	23.92	21.10	38.27	90
		D	1.92	23.88	21.96	38.38	94
	S90W	A	0.00	90.22	90.22	20.76	100
		B	1.98	20.10	18.12	44.58	93
		C	2.86	23.14	20.28	41.57	90
		D	1.62	20.10	18.48	44.26	93
Olympia, 1949	N04W	A	0.00	89.06	89.06	22.98	100
		B	0.74	22.30	22.30	44.25	93
		C	1.78	25.80	25.80	40.51	90
		D	0.08	22.94	22.94	43.73	93
	N86E	A	0.00	89.02	89.02	28.10	100
		B	1.00	21.04	21.04	56.00	94
		C	4.34	18.08	18.08	59.22	90
		d	0.28	21.52	21.52	55.48	94

* A: Entire Record
B: Page or Bolt (2-11 or 2-12)
C: Trifunac and Brady (2-13)
D: McCann and Shah (2-15)

Fourier amplitude spectrum. The finite Fourier transform $F(\omega)$ of an accelerogram $a(t)$ is obtained as

$$F(\omega) = \int_0^T a(t) e^{-i\omega t} dt \text{ , } i = \sqrt{-1} \qquad (2\text{-}1)$$

Where T is the duration of the accelerogram. The Fourier amplitude spectrum $FS(\omega)$ is defined as the square root of the sum of the squares of the real and imaginary parts of $F(\omega)$. Thus,

$$FS(\omega) = \sqrt{\left[\int_0^T a(t)\sin\omega t dt\right]^2 + \left[\int_0^T a(t)\cos\omega t dt\right]^2} \quad (2\text{-}2)$$

Since $a(t)$ has units of acceleration, $FS(\omega)$ has units of velocity. The Fourier amplitude spectrum is of interest to seismologists in characterizing ground motion. Figure 2-4 shows a typical Fourier amplitude spectrum for the S00E component of El Centro, the Imperial Valley earthquake of May 18, 1940. The figure indicates that most of the energy in the accelerogram is in the frequency range of 0.1 to 10 Hz, and that the largest amplitude is at a frequency of approximately 1.5 Hz.

It can be shown that subjecting an undamped single-degree-of-freedom (SDOF) system to a base acceleration $a(t)$, the velocity response of the system and the Fourier amplitude spectrum of the acceleration are closely related. The equation of motion of the system can be written as

$$\ddot{x} + \omega_n^2 x = -a(t) \quad (2\text{-}3)$$

In which x and $\ddot{x}$ are the relative displacement and acceleration, and ω_n is the natural frequency of the system. Using Duhamel's integral, the steady-state response can be obtained as

$$x(t) = \frac{1}{\omega_n}\int_0^t - a(\tau)\sin\omega_n(t-\tau)d\tau \quad (2\text{-}4)$$

The relative velocity $\dot{x}(t)$ follows directly from Equation 2-4 as

$$\dot{x}(t) = \int_0^t - a(\tau)\cos\omega_n(t-\tau)d\tau \quad (2\text{-}5)$$

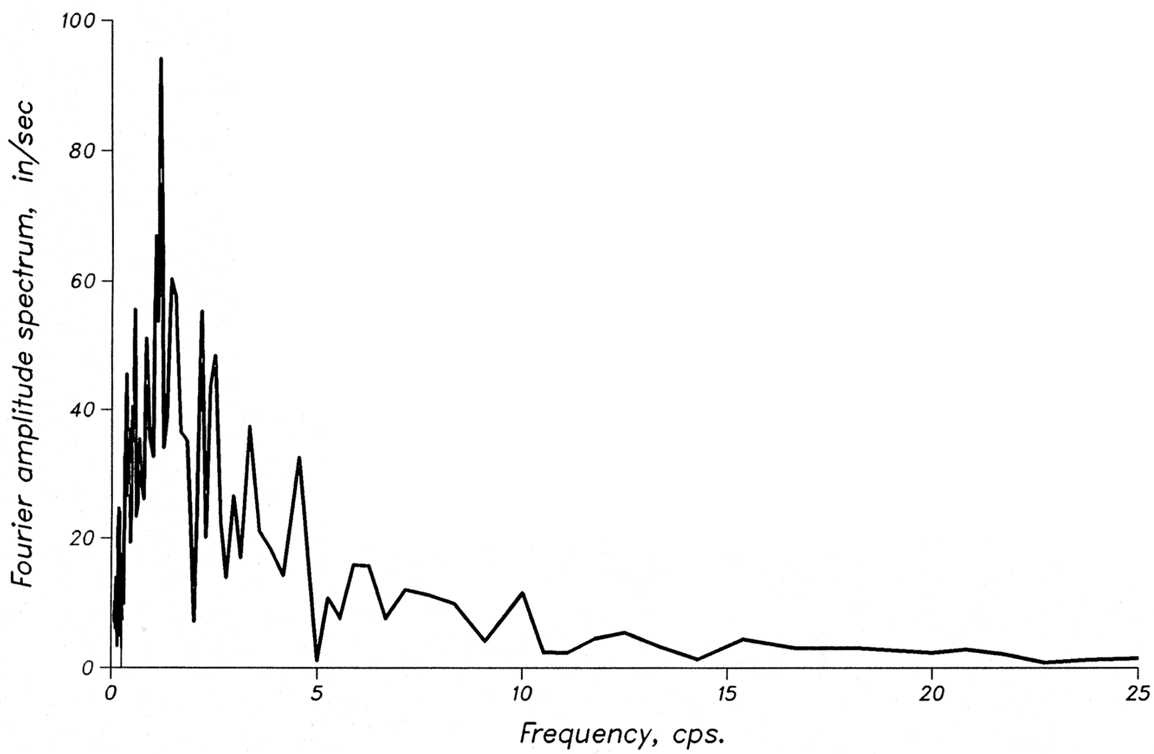

Figure 2-4. Fourier amplitude spectrum for the S00E component of El Centro, the Imperial Valley earthquake of May 18, 1940.

Equation 2-5 can be expanded as

$$\dot{x}(t) = -\left[\int_0^t a(\tau)\cos\omega_n \tau d\tau\right]\cos\omega_n t - \left[\int_0^t a(\tau)\sin\omega_n \tau d\tau\right]\sin\omega_n t \quad (2\text{-}6)$$

Denoting the maximum relative velocity (spectral velocity) of a system with frequency ω by *SV(ω)* and assuming that it occurs at time t_v, one can write

$$SV(\omega) = \sqrt{\left[\int_0^{t_v} a(\tau)\sin\omega\tau d\tau\right]^2 + \left[\int_0^{t_v} a(\tau)\cos\omega\tau d\tau\right]^2} \quad (2\text{-}7)$$

The pseudo-velocity *PSV(ω)* defined as the product of the natural frequency ω and the maximum relative displacement or the spectral displacement *SD(ω)* is close to the maximum relative velocity (see Section 2.7). If *SD(ω)* occurs at t_d then

$$PSV(\omega) = \omega SD(\omega) = \sqrt{\left[\int_0^{t_d} a(\tau)\sin\omega\tau d\tau\right]^2 + \left[\int_0^{t_d} a(\tau)\cos\omega\tau d\tau\right]^2} \quad (2\text{-}8)$$

Comparison of Equations 2-2 and 2-7 shows that for zero damping, the maximum relative velocity and the Fourier amplitude spectrum are equal when $t_v=T$. A similar comparison between Equations 2-2 and 2-8 reveals that the pseudo-velocity and the Fourier amplitude spectrum are equal if $t_d=T$. Figure 2-5 shows a comparison between *FS(ω)* and *SV(ω)* for zero damping for the S00E component of El Centro, the Imperial Valley earthquake of May 18, 1940. The figure indicates the close relationship between the two functions. It should be noted that, in general, the ordinates of the Fourier amplitude spectrum are less than those of the undamped pseudo-velocity spectrum.

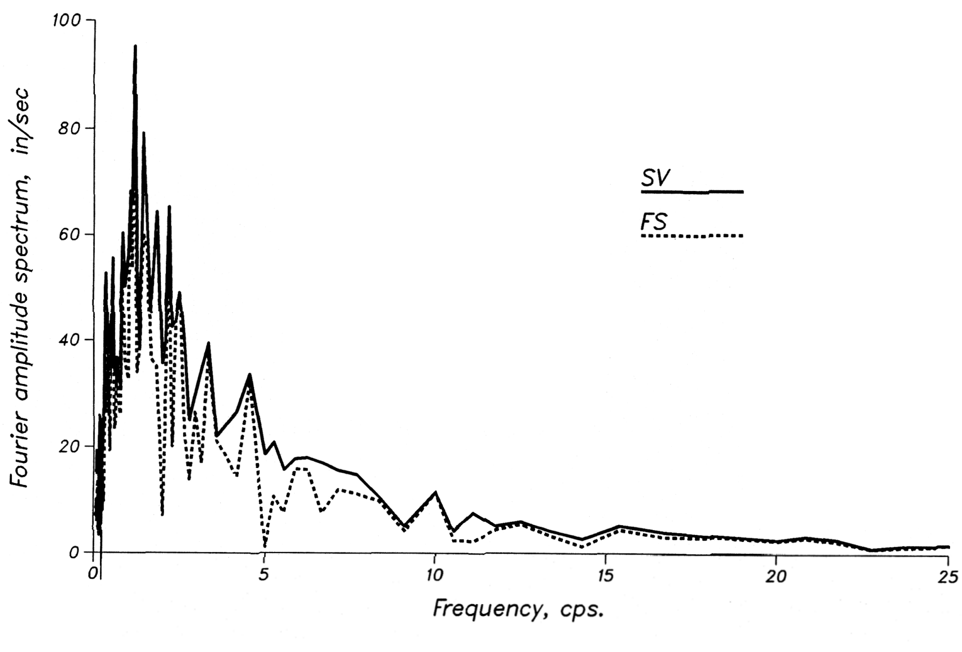

Figure 2-5. Comparison of Fourier amplitude spectrum and velocity spectrum for an undamped single-degree-of-freedom system for the S00E component of El Centro, the Imperial Valley earthquake of May 18, 1940.

Power spectral density. The inverse Fourier transform of $F(\omega)$ *is*

$$a(t) = \frac{1}{\pi}\int_0^{\omega_0} F(\omega)e^{i\omega t}\,d\omega \tag{2-9}$$

where ω_o is the maximum frequency detected in the data (referred to as Nyquist frequency). Equations 2-1 and 2-9 are called Fourier transform pairs. As mentioned previously, the intensity of an accelerogram is defined as

$$I = \int_0^T a^2(t)dt \tag{2-10}$$

Based on Parseval's theorem, the intensity I can also be expressed in the frequency domain as

$$I = \frac{1}{\pi}\int_0^{\omega_o} \left|F(\omega)\right|^2 d\omega \tag{2-11}$$

The intensity per unit of time or the temporal mean square acceleration ψ^2 can be obtained by dividing Equation 2-10 or 2-11 by the duration T. Therefore,

$$\psi^2 = \frac{1}{T}\int_0^T a^2(t)dt = \frac{1}{\pi T}\int_0^{\omega_0} \left|F(\omega)\right|^2 d\omega \tag{2-12}$$

The temporal power spectral density is defined as

$$G(\omega) = \frac{1}{\pi T}\left|F(\omega)\right|^2 \tag{2-13}$$

Combining Equations 2-12 and 2-13, the mean square acceleration can be obtained as

$$\psi^2 = \int_0^{\omega_0} G(\omega)d\omega \tag{2-14}$$

In practice, a representative power spectral density of ground motion is computed by averaging across the temporal power spectral densities of an ensemble of N accelerograms (see for example reference 2-17). Therefore,

$$G(\omega) = \frac{1}{N}\sum_{i=1}^{N} G_i(\omega) \tag{2-15}$$

where $G_i(\omega)$ is the power spectral density of the ith record. The power spectral density is frequently presented as the product of a normalized power spectral density $G^{<n>}(\omega)$ (area = 1.0) and a mean square acceleration as

$$G(\omega) = \psi^2 G^{<n>}(\omega) \tag{2-16}$$

Figure 2-6 shows a typical example of a normalized power spectral density computed for an ensemble of 161 accelerograms recorded on alluvium. Studies [2-17, 2-18] have shown that strong motion segment of accelerograms constitutes a locally stationary random process and that the power spectral density can be presented as a time-dependent function $G(t,\omega)$ in the form:

$$G(t,\omega) = \psi^2 S(t) G^{<n>}(\omega) \tag{2-17}$$

where $S(t)$ is a slowly varying time-scale factor which accounts for the local variation of the mean square acceleration with time.

Power spectral density is useful not only as a measure of the frequency content of ground motion but also in estimating its statistical properties. Among such properties are the *rms* acceleration ψ, the central frequency ω_c, and the shape factor δ defined as

$$\psi = \sqrt{\lambda_0} \tag{2-18}$$

$$\omega_c = \sqrt{\lambda_2 / \lambda_0} \tag{2-19}$$

$$\delta = \sqrt{1 - (\lambda_1^2 / \lambda_0 \lambda_2)} \tag{2-20}$$

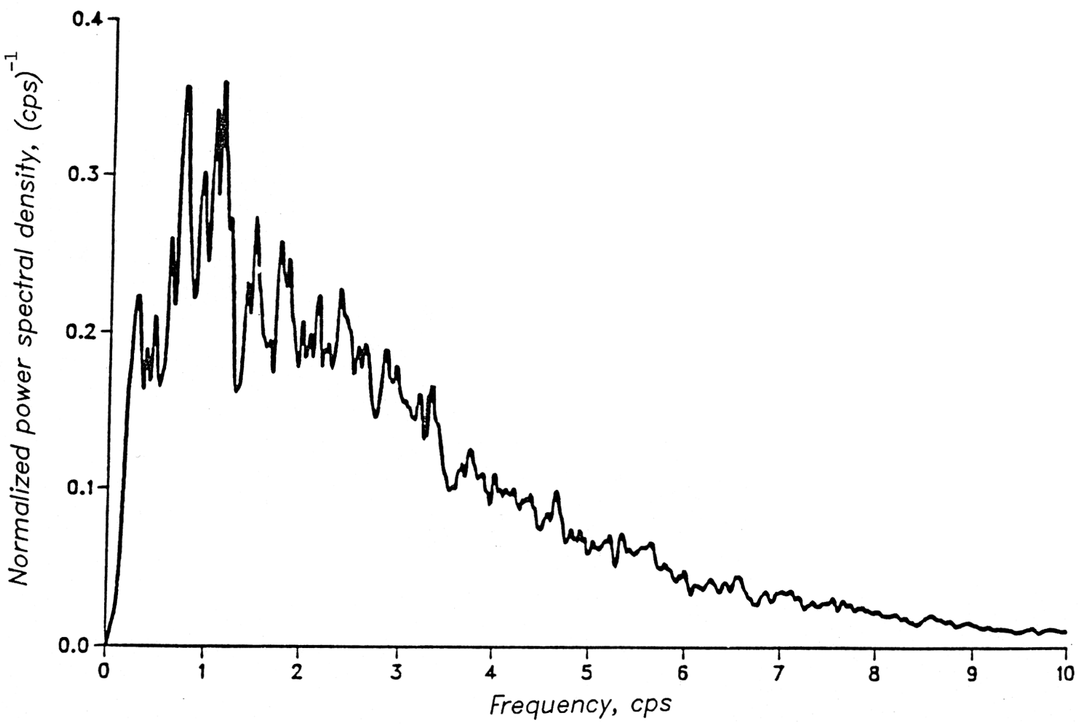

Figure 2-6. Normalized power spectral density of an ensemble of 161 horizontal components of accelerograms recorded on alluvium. [After Elghadamsi et al. (2-18).]

where λ_r is the r-th spectral moment defined as

$$\lambda_r = \int_0^{\omega_0} \omega^r G(\omega) d\omega \tag{2-21}$$

Smooth power spectral density of the ground acceleration has been commonly presented in the form proposed by Kanai [(2-19)] and Tajimi [(2-20)] as a filtered white noise ground excitation of spectral density G_0 in the form

$$G(\omega) = \frac{1 + 4\xi_g^2 (\omega / \omega_g)^2}{\left[1 - (\omega / \omega_g)^2\right]^2 + (2\xi_g \omega / \omega_g)^2} G_0 \tag{2-22}$$

The Kanai-Tajimi parameters ξ_g, ω_g, and G_0 represent ground damping, ground frequency, and ground shaking intensity. These parameters are computed by equating the *rms* acceleration, the central frequency, and the shape factor, Equations 2-18 to 2-20, of the smooth and the raw (unsmooth) power spectral densities [(2-18, 2-21)]. Table 2-3 gives the values of ξ_g, ω_g, and G_0 for the normalized power spectral densities on different soil conditions. Also shown are the central frequency ω_c and the shape factor δ. Using the Kanai-Tajimi parameters in Table 2-3, normalized power spectral densities for horizontal and vertical motion on various soil conditions were computed and are presented in Figures 2-7 and 2-8. The figures indicate that as the site becomes stiffer, the predominant frequency increases and the power spectral densities spread over a wider frequency range. This observation underscores the influence of site conditions on the frequency content of seismic excitations. The figures also show that the power spectral densities for horizontal motion have a sharper peak and span over a narrower frequency region than the corresponding ones for vertical motion.

Table 2-3. Central Frequency, Shape Factor, Ground Frequency, Ground Damping, and Ground Intensity for Different Soil Conditions. [After Elghadamsi et al. (2-18)]

Site Category	No. of Records	Central Frequency f_c (Hz)	Shape Factor δ	Ground Frequency f_g (Hz)	Ground Damping ξ_g	Ground Intensity G_0 (1/Hz)
Horizontal						
Alluvium	161	4.10	0.65	2.92	0.34	0.102
Alluvium on rock	60	4.58	0.59	3.64	0.30	0.078
Rock	26	5.41	0.59	4.30	0.34	0.070
Vertical						
Alluvium	78	6.27	0.63	4.17	0.46	0.080
Alluvium on rock	29	6.68	0.62	4.63	0.46	0.072
Rock	13	7.53	0.55	6.18	0.46	0.053

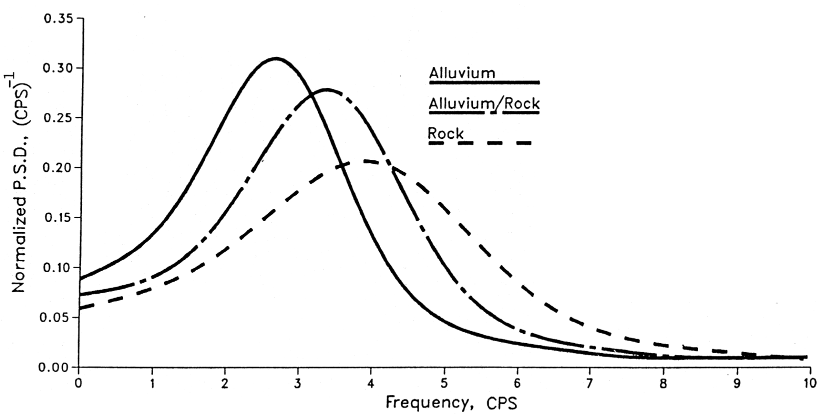

Figure 2-7. Normalized power spectral densities for horizontal motion. [After Elghadamsi et al. (2-18).]

Clough and Penzien (2-22) modified the Kanai-Tajimi power spectral density by introducing another filter to account for the numerical difficulties expected in the neighborhood of *ω=0*. The cause of these difficulties stems from dividing Equation 2-22 by ω^2 and ω^4, respectively, to obtain the power spectral density functions for ground velocity and displacement. The singularities close to *ω=0* can be removed by passing the process through another filter that attenuates the very low frequency components. The modified power spectral density takes the form

$$G(\omega)= \frac{1+4\xi_g^2(\omega/\omega_g)^2}{\left[1-(\omega/\omega_g)^2\right]^2+(2\xi_g\omega/\omega_g)^2}\times \frac{(\omega/\omega_1)^4}{\left[1-(\omega/\omega_1)^2\right]+4\xi_1^2(\omega/\omega_1)^2}(G_0) \qquad (2\text{-}23)$$

Where ω_1 and ξ_1 are the frequency and damping parameters of the filter.

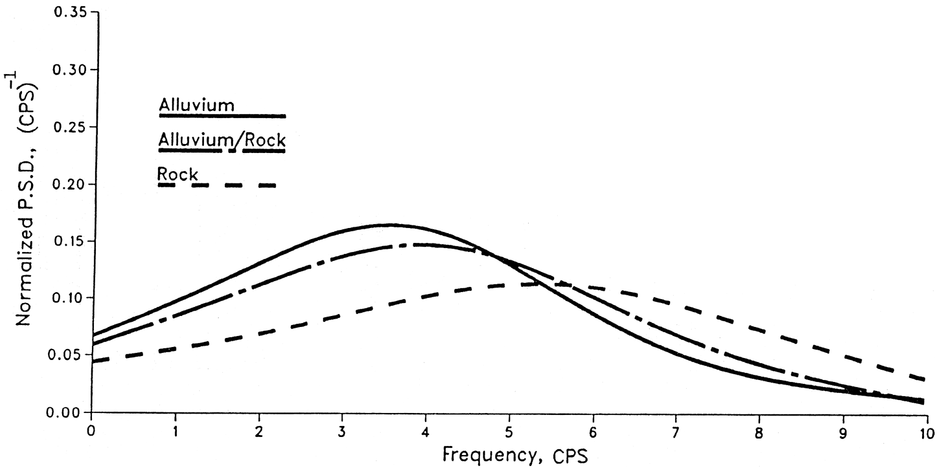

Figure 2-8. Normalized power spectral densities for vertical motion. [After Elghadamsi et al. (2-18).]

Lai [(2-21)] presented empirical relationships for estimating ground frequency ω_g and central frequency ω_c for a given epicentral distance R in kilometers or local magnitude M_L. These relationships are

$$\omega_g = 27 - 0.09R \quad 10 \leq R \leq 60 \qquad (2\text{-}24)$$

$$\omega_g = 65 - 7.5M_L \quad 5 \leq M_L \leq 7 \qquad (2\text{-}25)$$

$$\omega_g = 1.12\omega_c - 5.15 \qquad (2\text{-}26)$$

Using these relationships and the acceleration attenuation equations (see Section 2.4.1), Lai proposed a procedure for estimating a smooth power spectral density for a given strong motion duration and ground damping.

Once the power spectral density of ground motion at a site is established, random vibration methods may be used to formulate probabilistic procedures for computing the response of structures. In addition, the power spectral density of ground motion may be used for other applications such as generating artificial accelerograms as discussed in Section 2.12.

2.4 FACTORS INFLUENCING GROUND MOTION

Earthquake ground motion is influenced by a number of factors. The most important factors are: 1) earthquake magnitude, 2) distance from the source of energy release (epicentral distance or distance from the causative fault), 3) local soil conditions, 4) variation in geology and propagation velocity along the travel path, and 5) earthquake source conditions and mechanism (fault type, slip rate, stress conditions, stress drop, etc.). Past earthquake records have been used to study some of these influences. While the effect of some of these parameters such as local soil conditions and distance from the source of energy release are fairly well understood and documented, the influence of source mechanism is under investigation and the variation of geology along the travel path is complex and difficult to quantify. It should be noted that several of these influences are interrelated; consequently, it is difficult to discuss them individually without incorporating the others. Some of the influences are discussed below:

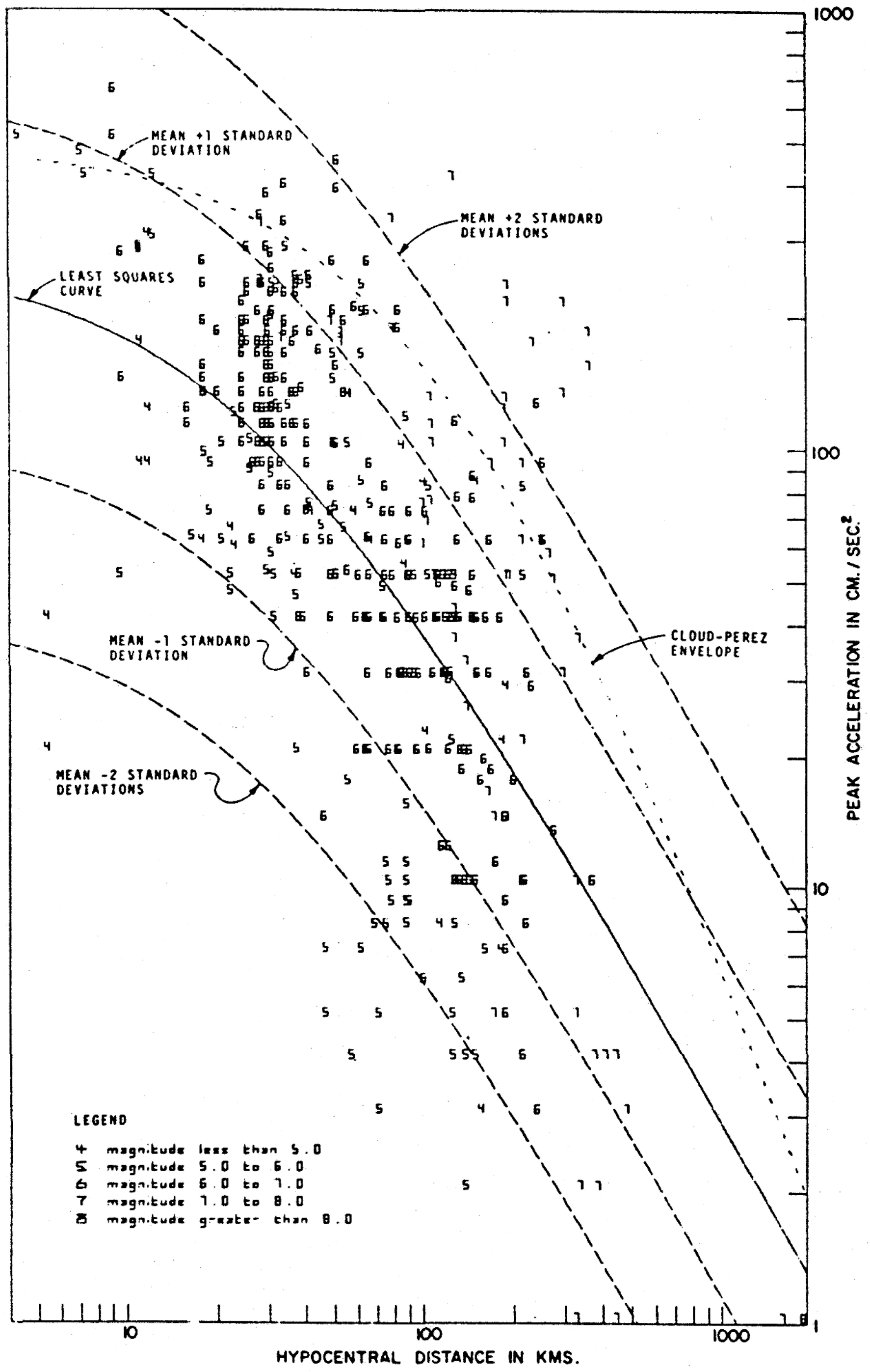

Figure 2-9. Peak ground acceleration plotted as a function of fault distance obtained from worldwide set of 515 strong motion records without normalization of magnitude. [After Donovan (2-23).]

2.4.1 Distance

The variation of ground motion with distance to the source of energy release has been studied by many investigators. In these studies, peak ground motion, usually peak ground acceleration, is plotted as a function of distance. Smooth curves based on a regression analysis are fitted to the data and the curve or its equation is used to predict the expected ground motion as a function of distance. These relationships, referred to as motion attenuation, are sometimes plotted independently of earthquake magnitude. This was the case in the earlier studies because of the lack of sufficient number of earthquake records. With the availability of a large number of records, particularly since the 1971 San Fernando earthquake, the database for attenuation studies increased and a number of investigators re-examined their earlier studies, modified their proposed relationships for estimating peak accelerations, and included earthquake magnitude as a parameter. Donovan [(2-23)] compiled a database of more than 500 recorded accelerations from seismic events in the United States, Japan, and elsewhere and later increased it to more than 650 [(2-24)]. The plot of peak ground acceleration versus fault distance for different earthquake magnitudes from his database is shown in Figure 2-9. Even though there is a considerable scatter in the data, the figure indicates that peak acceleration decreases as the distance from the source of energy release increases. Shown in the figure are the least square fit between acceleration and distance and the curves corresponding to mean plus- and mean minus- one and two standard deviations. Also presented in the figure is the envelope curve (dotted) proposed by Cloud and Perez [(2-25)].

Other investigators have also proposed attenuation relationships for peak ground acceleration, which are similar to Figure 2-9. A summary of some of the relationships, compiled by Donovan [(2-23)] and updated by the authors, is shown in Table 2-4. A comparison of various relationships [(2-24)] for an earthquake magnitude of 6.5 with the data from the 1971 San Fernando earthquake is shown in Figure 2-10. This figure is significant because it shows the comparison of various attenuation relationships with data from a single earthquake. While the figure shows the differences in various attenuation relationships, it indicates that they all follow a similar trend.

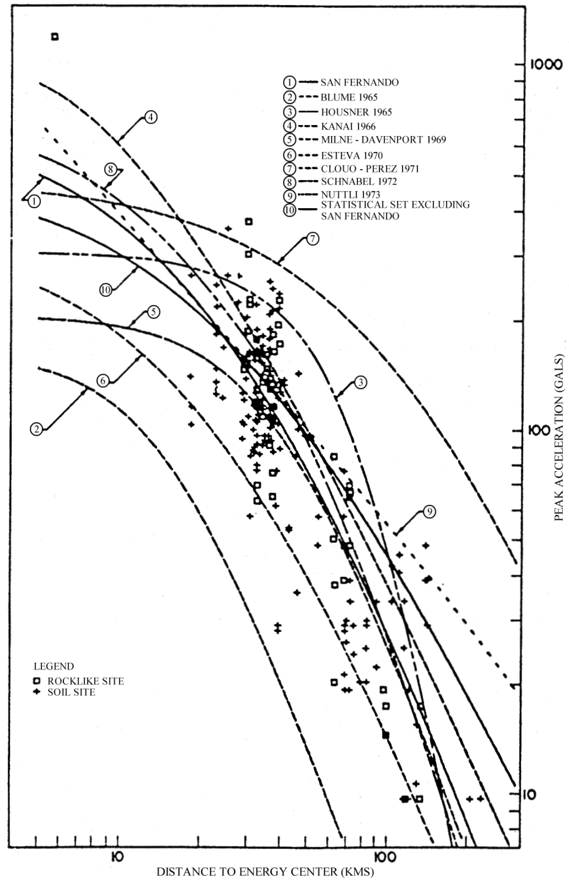

Figure 2-10. Comparison of attenuation relations with data from the San Fernando earthquake of February 9, 1971. [After Donovan (2-24).]

Housner [(2-38)], Donovan [(2-23)], and Seed and Idriss [(2-39)] have reported that at farther distances from the fault or the source of energy release (far-field), earthquake magnitude influences the attenuation, whereas at distances close to the fault (near-field), the attenuation is affected by smaller but not larger earthquake magnitudes. This can be observed from the earthquake data in Figure 2-9.

Table 2-4. Typical Attenuation Relationships

Data Source	Relationship*	Reference
1. San Fernando earthquake February 9, 1971	$\log PGA = 190 / R^{1.83}$	Donovan (2-23)
2. California earthquake	$PGA = y_0 /(1 + (R'/h)^2)$ where $\log y_0 = -(b + 3) + 0.81M - 0.027M^2$ and b is a site factor	Blume (2-26)
3. California and Japanese earthquakes	$PGA = \dfrac{0.0051}{\sqrt{T_G}} 10^{(0.61M - p \log R + 0.167 - 1.83/R)}$ where $P = 1.66 + 3.60/R$ and T_G is the fundamental period of the site	Kanai (2-27)
4. Cloud (1963)	$PGA = 0.0069e^{1.64M} /(1.1e^{1.1M} + R^2)$	Milne and Davenport (2-28)
5. Cloud (1963)	$PGA = 1.254e^{0.8M} /(R + 25)^2$	Esteva (2-29)
6. U.S.C. and G.S.	$\log PGA = (6.5 - 2\log(R'+80)) / 981$	Cloud and Perez (2-25)
7. 303 Instrumental Values	$PGA = 1.325e^{0.67M} /(R + 25)^{1.6}$	Donovan (2-23)
8. Western U.S. records	$PGA = 0.0193e^{0.8M} /(R^2 + 400)$	Donovan (2-23)
9. U.S., Japan	$PGA = 1.35e^{0.58M} /(R + 25)^{1.52}$	Donovan (2-23)
10. Western U.S. records, USSR, and Iran	$\ln PGA = -3.99 + 1.28M - 1.75 \ln[R = 0.147e^{0.732M}]$ - *M* is the surface wave magnitude for *M* greater than or equal to 6, or it is the local magnitude for *M* less than 6.	Campbell (2-30)
11. Western U.S. records and worldwide	$\log PGA = -1.02 + 0.249M - \log \sqrt{R^2 + 7.3^2} - 0.00255\sqrt{R^2 + 7.3^2}$	Joyner and Boore (2-31)
12. Western U.S. records and worldwide	$\log PGA = 0.49 + 0.23(M - 6) - \log \sqrt{R^2 + 8^2} - 0.0027\sqrt{R^2 + 8^2}$	Joyner and Boore (2-32)
13. Western U.S. records	$\ln PGA = \ln \alpha(M) - \beta(M) \ln(R + 20)$ - *M* is the surface wave magnitude for *M* greater than or equal to 6, or it is the local magnitude for smaller *M*. - *R* is the closest distance to source for *M* greater than 6 and hypocentral distance for *M* smaller than 6. - $\alpha(M)$ and $\beta(M)$ are magnitude-dependent coefficients.	Idriss (2-33)
14. Italian records	$\ln PGA = -1.562 + 0.306M - \log \sqrt{R^2 + 5.8^2} + 0.169S$ - *S* is 1.0 for soft sites or 0.0 for rock.	Sabetta and Pugliese (2-34)
15. Western U.S. and worldwide (soil sites)	For *M* less than 6.5, $\ln PGA = -2.611 + 1.1M - 1.75 \ln[R + 0.822e^{0.418M}]$ For *M* greater than or equal to 6.5, $\ln PGA = -2.611 + 1.1M - 1.75 \ln[R + 0.316e^{0.629M}]$	Sadigh et al. (2-35)
16. Western U.S. and worldwide (rock sites)	For *M* less than 6.5, $\ln PGA = -1.406 + 1.1M - 2.05 \ln[R + 1.353e^{0.406M}]$ For *M* greater than or equal to 6.5, $\ln PGA = -1.406 + 1.1M - 2.05 \ln[R + 0.579e^{0.537M}]$	Sadigh et al. (2-35)
17. Worldwide earthquakes	$\ln PGA = -3.512 + 0.904M - 1.328 \ln \sqrt{R^2 + [0.149e^{0.647M}]^2}$ $+ [1.125 - 0.112 \ln R - 0.0957M]F + [0.440 - 0.171 \ln R]S_{sr}$ $+ [0.405 - 0.222 \ln R]S_{hr}$ - $F = 0$ for strike-slip and normal fault earthquakes and 1 for reverse, reverse-oblique, and thrust fault earthquakes. - $S_{sr} = 1$ for soft rock and 0 for hard rock and alluvium - $S_{hr} = 1$ for hard rock and 0 for soft rock and alluvium	Campbell and Bozorgnia (2-36)
18. Western North American earthquakes	$\ln PGA = b + 0.527(M - 6.0) - 0.778 \ln \sqrt{R^2 + (5.570)^2} - 0.371 \ln \dfrac{V_s}{1396}$ - where $b = -0.313$ for strike-slip earthquakes $= -0.117$ for reverse-slip earthquakes $= -0.242$ if mechanism is not specified - V_s is the average shear wave velocity of the soil in (m/sec) over the upper 30 meters - The equation can be used for magnitudes of 5.5 to 7.5 and for distances not greater than 80 km	Boore et al. (2-37)

* Peak ground acceleration *PGA* in *g*, source distance *R* in km, source distance *R'* in miles, local depth *h* in miles, and earthquake magnitude *M*. Refer to the relevant references for exact definitions of source distance and earthquake magnitude.

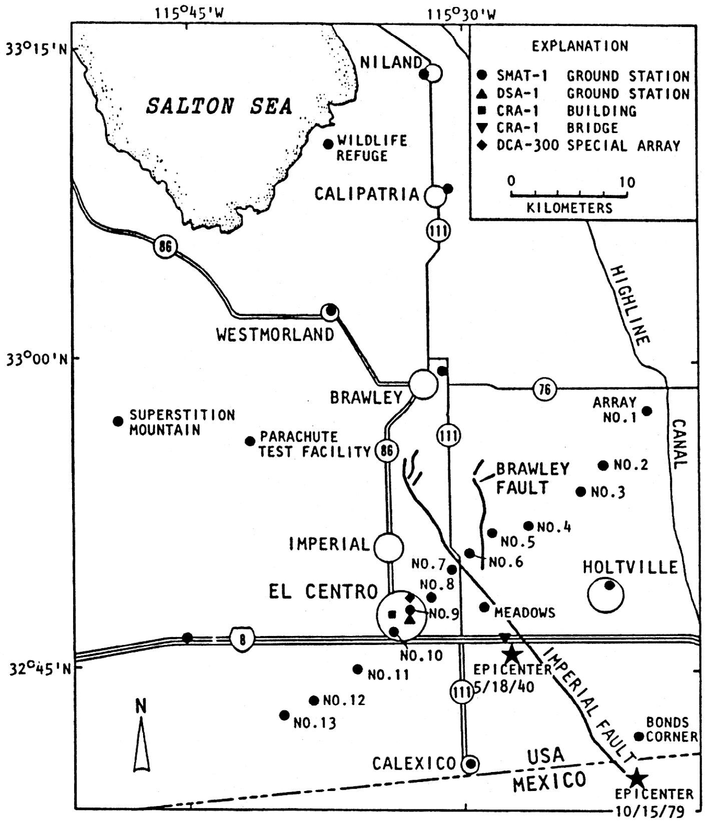

Figure 2-11. Strong motion stations in the Imperial Valley, California. [After Porcella and Matthiesen (2-40); reproduced from (2-39).]

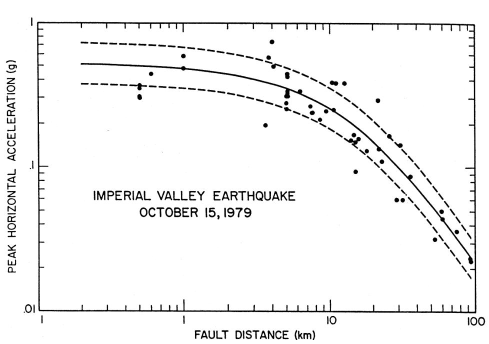

Figure 2-12. Observed and predicted mean horizontal peak accelerations for the Imperial Valley earthquake of October 15, 1979 plotted as a function of distance from the fault. The solid curve represents the median predictions based on the observed values and the dashed curves represent the standard error bounds for the regression. [After Campbell (2-30).]

The majority of attenuation relationships for predicting peak ground motion are presented in terms of earthquake magnitude. Prior to the Imperial Valley earthquake of 1979, the vast majority of available accelerograms were recorded at distances of greater than approximately 10 or 15 km from the source of energy release. An array of accelerometers placed on both sides of the Imperial Fault (2-40) prior to this earthquake (See Figure 2-11) provided excellent acceleration data for small distances from the fault. The attenuation relationship from this array presented by Campbell (2-30) is shown in Figure 2-12. The figure indicates the flat slope of the acceleration attenuation curve for distances close to the source, a phenomenon which is not observed in

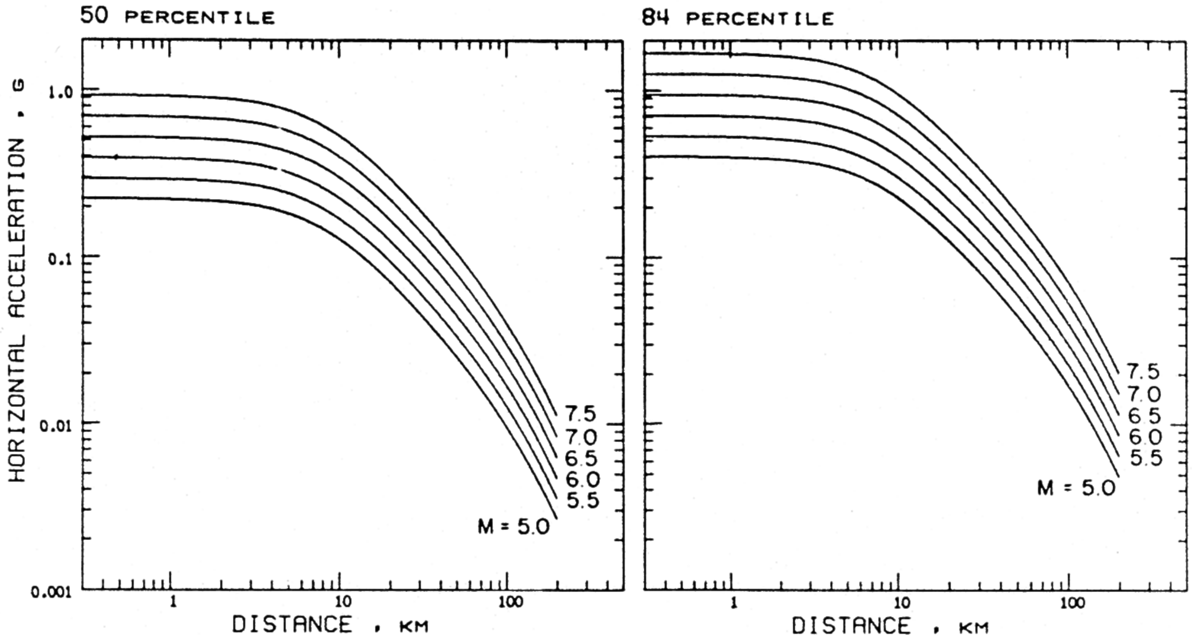

Figure 2-13. Predicted values of peak horizontal acceleration for 50 and 84 percentile as functions of distance and moment magnitude. [After Joyner and Boore (2-31).]

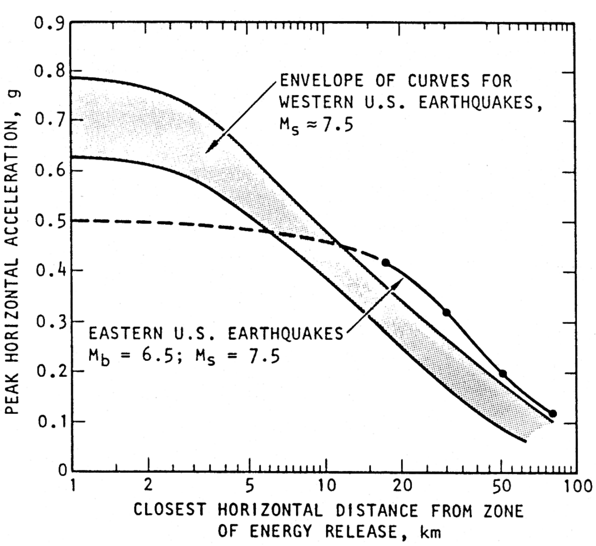

Figure 2-14. Comparison of attenuation curves for the eastern and western U.S. earthquakes. (Reproduced from 2-39.)

the attenuation curves for far-field data. Similar observations can also be made from the attenuation curves (Figure 2-13) proposed by Joyner and Boore [(2-31)]. The majority of attenuation studies and the relationships presented in Table 2-4 are primarily from the data in the western United States. Several seismologists believe that ground acceleration attenuates more slowly in the eastern United States and eastern Canada, i.e. earthquakes in eastern North America are felt at much greater distances from the epicenter than western earthquakes of similar magnitude. A comparison of the attenuation curves for the western and eastern United States earthquakes recommended by Nuttli and Herrmann [(2-41)] is shown in Figure 2-14. Another comparison for eastern North America prepared by Milne and Davenport [(2-28)] is presented in Figure 2-15. Both these figures reflect the slower attenuation of earthquake motions in the eastern United States and eastern Canada. According to Donovan [(2-23)], a similar phenomenon also exists for Japanese earthquakes. Due to the lack of sufficient earthquake data in the eastern United States and Canada, theoretical models which include earthquake source and wave propagation in the surrounding medium are used to study the effect of distance and other parameters on ground motion. The reader is referred to references (2-42 to 2-44) for the detailed procedure.

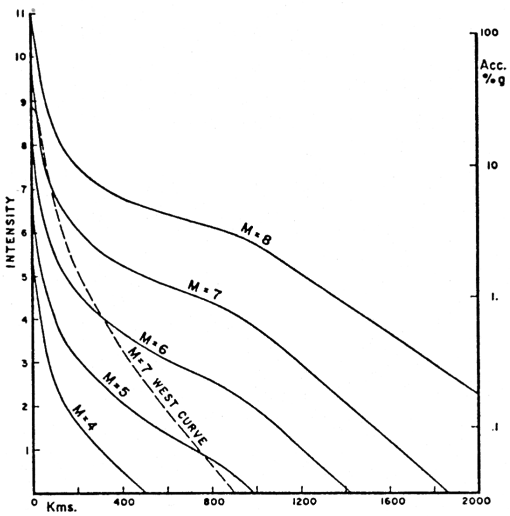

Figure 2-15. Intensity versus distance for eastern and western Canada. [After Milne and Davenport (2-28).]

In addition to source distance and earthquake magnitude, recent attenuation relationships include the effect of source characteristics (fault mechanism) and soil conditions. As an example, Campbell and Bozorgnia (2-36) used 645 accelerograms from 47 worldwide earthquakes of magnitude 4.7 and greater, recorded between 1957 and 1993, to develop attenuation relationship for peak horizontal ground acceleration. The data was limited to distances of 60 km or less to minimize the influence of regional differences in crustal attenuation and to avoid the complex propagation effects at farther distances observed during the 1989 Loma Prieta and other earthquakes. The peak ground acceleration was estimated using a generalized nonlinear regression analysis and given by

$$\begin{aligned}\ln(PGA) &= -3.512 + 0.904 M_W \\ &-1.328 \ln\sqrt{R_s^2 + [0.149\exp(0.647 M_W)]^2} \\ &+[1.125 - 0.112\ln R_s - 0.0957 M_W]F \\ &+[0.440 - 0.171\ln R_s]S_{sr} \\ &+[0.405 - 0.222\ln R_s]S_{hr} + \varepsilon\end{aligned} \tag{2-27}$$

where PGA is the mean of the two horizontal components of peak ground acceleration (g), M_W is the moment magnitude, R_S is the closest distance to the seismogenic rupture[3] on the fault (km), F = 0 for strike-slip and normal fault earthquakes and = 1 for reverse, reverse-oblique, and thrust fault earthquakes, S_{sr} = 1 for soft rock and = 0 for hard rock and alluvium, S_{hr} = 1 for hard rock and = 0 for soft rock and alluvium, and ε is the random error term with a zero mean and a standard deviation equal to $\sigma_{\ln(PGA)}$ which is represented by

$$\sigma_{\ln(PGA)} = \begin{cases} 0.55 & PGA < 0.068 \\ 0.173 - 0.140\ln(PGA) & 0.068 \le PGA \le 0.21 \\ 0.39 & PGA > 0.21 \end{cases} \tag{2-28}$$

with a standard error of estimate 0.021.

More recently, Boore et al. (2-37) used approximately 270 records to estimate the peak ground acceleration in terms of 1) the closest horizontal distance R_{jb} (km) from the recording station to a point on the earth surface that lies directly above the rupture, 2) the moment magnitude M_W, 3) the average shear wave velocity of the soil V_s (m/sec) over the upper 30 meters, and 4) the fault mechanism such that:

$$\begin{aligned}\ln(PGA) &= b + 0.527(M_W - 6.0) \\ &- 0.778\ln\sqrt{R_{jb}^2 + (5.570)^2} - 0.371\ln\frac{V_s}{1396}\end{aligned} \tag{2-29}$$

[3] Seismogenic rupture zone was determined from the location of surface fault rupture, the spatial distribution of aftershocks, earthquake modelling studies, regional crustal velocity profiles, and geodetic and geologic data.

Where b is a parameter that depends on the fault mechanism. They recommended

$$b = \begin{cases} -0.313 & \text{for the strike - slip earthquakes} \\ -0.117 & \text{for the reverse - slip earthquakes} \\ -0.242 & \text{if the fault mechanism is not specified} \end{cases} \quad (2\text{-}30)$$

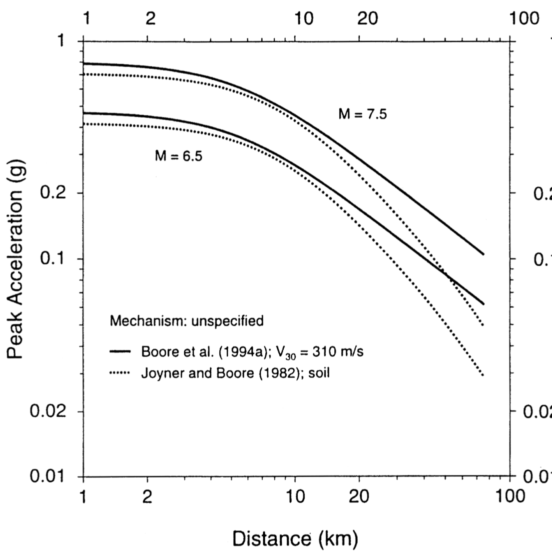

Figure 2-16. Peak ground acceleration versus distance for soil sites for earthquake magnitudes of 6.5 and 7.5. [After Boore et al. (2-37).]

Equation 2-29 is used for earthquake magnitudes of 5.5 to 7.5 and distances less than 80 km. Although Equations 2-27 and 2-29 use different definitions for the source distance, the equations indicate the decaying pattern of the peak ground acceleration with distance. Figure 2-16 shows the variation of the peak ground acceleration with distance computed from Equation 2-29 for earthquakes of magnitude 6.5 and 7.5 with an unspecified fault mechanism and for soils with a shear wave velocity of 310 m/sec. Also shown in the figure is the attenuation relationship proposed by Joyner and Boore [(2-32)] (Equation 12 Table 2-4).

The variation of peak ground velocity with distance from the source of energy release (velocity attenuation) has also been studied by several investigators such as Page et al. [(2-11)], Boore et al. [(2-45, 2-46)], Joyner and Boore [(2-31)], and Seed and Idriss [(2-39)]. Velocity attenuation curves have similar shapes and follow similar trends as the acceleration attenuation. Typical velocity attenuation curves proposed by Joyner and Boore are shown in Figure 2-17. Comparisons between Figures 2-13 and 2-17 indicate that velocity attenuates somewhat faster than acceleration.

The variation of peak ground displacement with fault distance or the distance from the

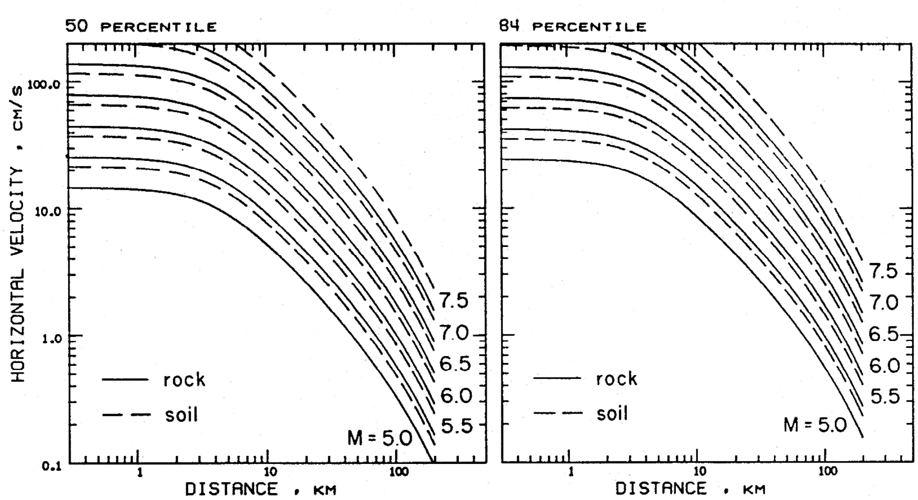

Figure 2-17. Predicted values of peak horizontal velocity for 50 and 84 percentile as functions of distance, moment magnitude, and soil condition. [After Joyner and Boore (2-31).]

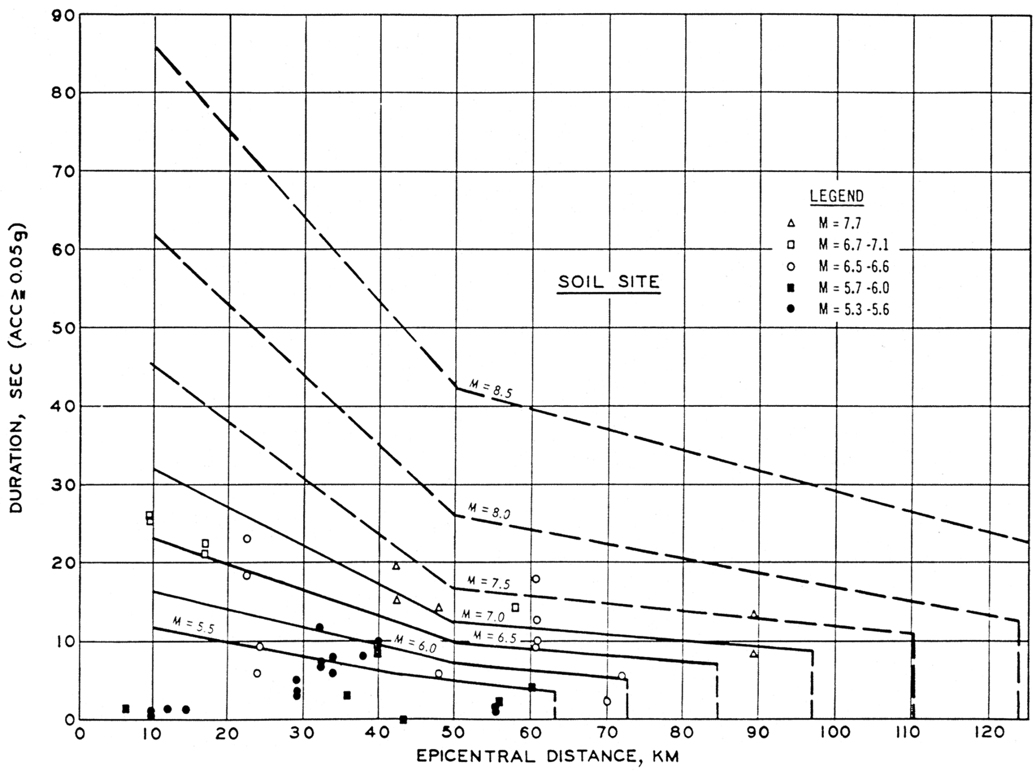

Figure 2-18. Duration versus epicentral distance and magnitude for soil. [After Change and Krinitzsky (2-47).]

source of energy release (displacement attenuation) can also be plotted. Boore et al. [2-45, 2-46] have presented displacement attenuations for different ranges of earthquake magnitude. Only a few studies have addressed displacement attenuations probably because of their limited use and the uncertainties in computing displacements accurately.

Distance also influences the duration of strong motion. Correlations of the duration of strong motion with epicentral distance have been studied by Page et al. [2-11], Trifunac and Brady [2-13], Chang and Krinitzsky [2-47], and others. Page et al., using the bracketed duration, conclude that for a given magnitude, the duration decreases with an increase in distance from the source. Chang and Krinitzsky, also using the bracketed duration, presented the curves shown in Figures 2-18 and 2-19 for estimating durations for soil and rock as a function of distance. These figures show that for a given magnitude, the duration of strong motion in soil is greater (approximately two times) than that in rock.

Using the 90% contribution of the acceleration intensity ($\int a^2\,dt$) as a measure of duration, Trifunac and Brady [2-13] concluded that the average duration in soil is approximately 10-12 sec longer than that in rock. They also observed that the duration increases by approximately 1.0 - 1.5 sec for every 10 km increase in source distance. Although there seems to be a contradiction between their finding and those of Page et al. and Chang-Krinitzsky, the contradiction stems from using two different definitions. The bracketed duration is based on an absolute acceleration level (0.05*g*). At longer epicentral distances, the acceleration peaks are smaller and a shorter duration is to be expected. The acceleration intensity definition of duration is based on the relative measure of the percentile

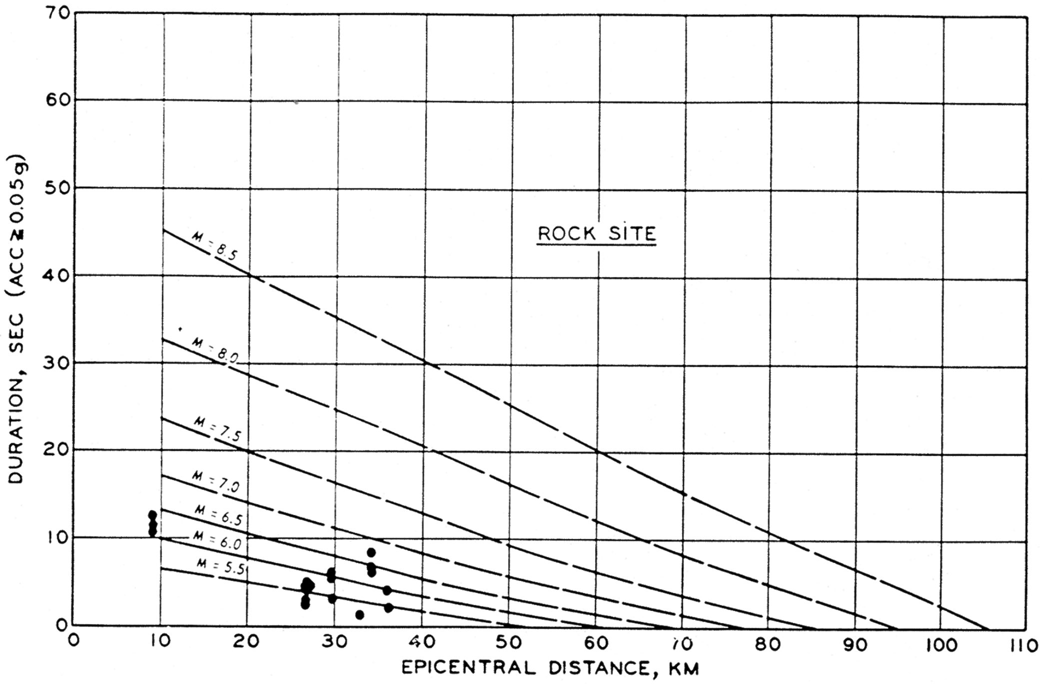

Figure 2-19. Duration versus epicentral distance and magnitude for rock. [After Chang and Krinitzsky (2-47).]

contribution to the acceleration intensity. Conceivably, a more intense shaking within a shorter time may result in a shorter duration than a much less intense shaking over a longer time. According to Housner (2-38), at distances away from the fault, the duration of strong shaking may be longer but the shaking will be less intense than those closer to the fault.

Recently, Novikova and Trifunac (2-48) used the frequency dependent definition of duration developed by Trifunac and Westermo (2-16) to study the effect of several parameters on the duration of strong motion. They employed a regression analysis on a database of 984 horizontal and 486 vertical accelerograms from 106 seismic events. Their study indicated an increase in duration by 2 sec for each 10 km of epicentral distance for low frequencies (near 0.2 Hz). At high frequencies (15 to 20 Hz), the increase in duration drops to 0.5 sec per each 10 km.

Near-Source Effects. Recent studies have indicated that near-source ground motions contain large displacement pulses (ground displacements which are attained rapidly with a sharp peak velocity). These motions are the result of stress waves moving in the same direction as the fault rupture, thereby producing a long-duration pulse. Conse-quently, near source earthquakes can be destructive to structures with long periods. Hall et al. (2-49) have presented data of peak ground accelerations, velocities, and displacements from 30 records obtained within 5 km of the rupture surface. The ground accelerations varied from 0.31*g* to 2.0*g* while the ground velocities ranged from 0.31 to 1.77 m/sec. The peak ground displacements were as large as 2.55 m. Figures 2-20 and 2-21 offer two examples of near-source earthquake ground motions. The first was recorded at the LADWP Rinaldi Receiving Station during the Northridge earthquake of January 17, 1994. The distance from the recording station to the surface projection of the rupture was less than 1.0 km. The figure shows a uni-directional ground

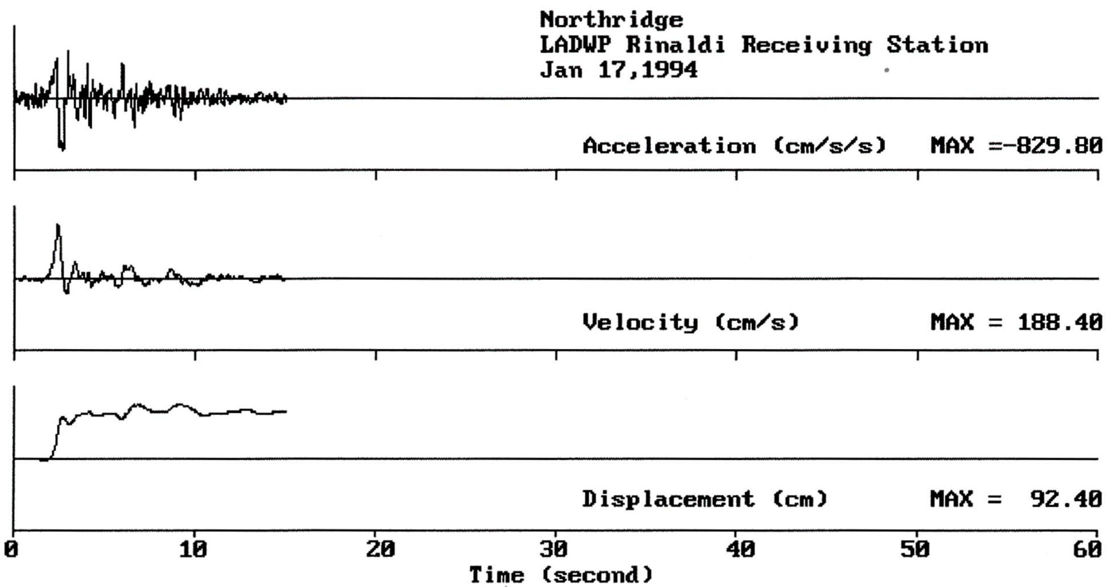

Figure 2-20. Ground acceleration, velocity, and displacement time-histories recorded at the LADWP Rinaldi Receiving Station during the Northridge earthquake of January 17, 1994.

displacement that resembles a smooth step function and a velocity pulse that resembles a finite delta function. The second example, shown in Figure 2-21, was recorded at the SCE Lucerne Valley Station during the Landers earthquake of June 28, 1992. The distance from the recording station to the surface projection of the rupture was approximately 1.8 km. A positive and negative velocity pulse that resembles a single long-period harmonic motion is reflected in the figure. Near-source ground displacements similar to that shown in Figure 2-21 have also been observed with a zero permanent displacement. The two figures clearly show the near-source ground displacements caused by sharp velocity pulses. For further details, the reader is referred to the work of Heaton and Hartzell [(2-50)] and Somerville and Graves [(2-51)].

2.4.2 Site geology

Soil conditions influence ground motion and its attenuation. Several investigators such as Boore et al. [(2-45 and 2-46)] and Seed and Idriss [(2-39)] have presented attenuation curves for soil and rock. According to Boore et al., peak horizontal acceleration is not appreciably affected by soil condition (peak horizontal acceleration is nearly the same for both soil and rock). Seed and Idriss compare acceleration attenuation for rock from earthquakes with magnitudes of approximately 6.6 with acceleration attenuation for alluvium from the 1979 Imperial Valley earthquake (magnitude 6.8). Their comparison shown in Figure 2-22 indicates that at a given distance from the source of energy release, peak accelerations on rock are somewhat greater than those on alluvium. Studies from other earthquakes indicate that this is generally the case for

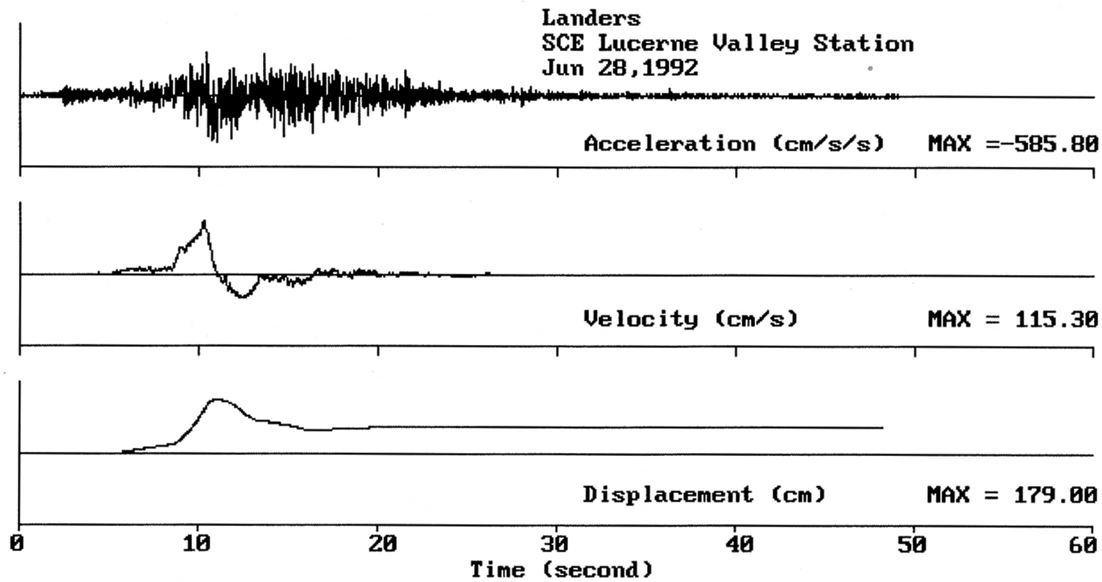

Figure 2-21. Ground acceleration, velocity, and displacement time-histories recorded at the SCE Lucerne Valley Station during the Landers earthquake of June 28, 1992.

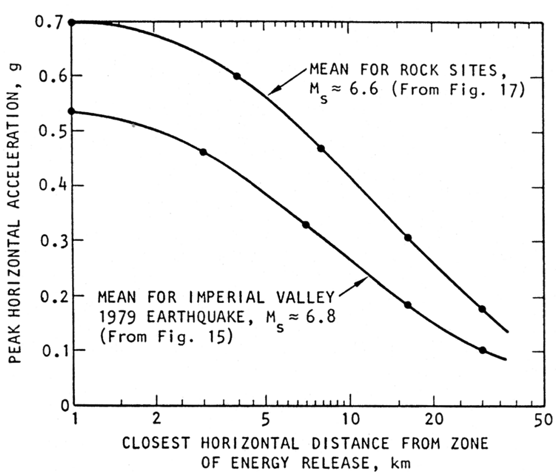

Figure 2-22. Comparison of attenuation curves for rock sites and the Imperial Valley earthquake of 1979. [After Seed and Idriss (2-39).]

acceleration levels greater than approximately 0.1*g*. At levels smaller than this value, accelerations on deep alluvium are slightly greater than those on rock. The effect of soil condition on peak acceleration is illustrated by Seed and Idriss in Figure 2-23. According to this figure, the difference in acceleration on rock and on stiff soil is not that significant. Even though in specific cases, particularly soft soils, soil condition can affect peak accelerations, Seed and Idriss conclude that the influence of soil condition can generally be neglected when using acceleration attenuation curves. In a more recent study, Idriss [(2-52)], using the data from the 1985 Mexico City and the 1989 Loma Prieta earthquakes, modified the curve for soft soil sites as shown in Figure 2-24. In these two earthquakes, soft soils exhibited peak ground accelerations of almost 1.5 to 4 times those of rock for the acceleration range of 0.05*g* to 0.1*g*. For rock accelerations larger than approximately 0.1*g*, the acceleration ratio between soft soils and rock tends to decrease to about 1.0 for rock accelerations of 0.3*g* to 0.4*g*. The figure indicates that large rock accelerations are amplified through soft soils to a lesser degree and may even be slightly de-amplified.

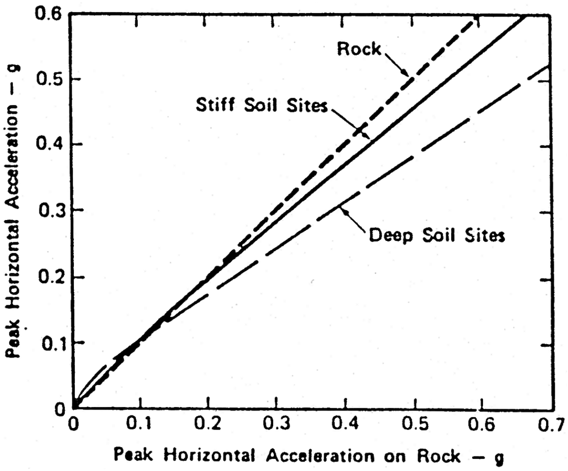

Figure 2-23. Relationship between peak accelerations on rock and soil. [After Seed and Idriss (2-39).]

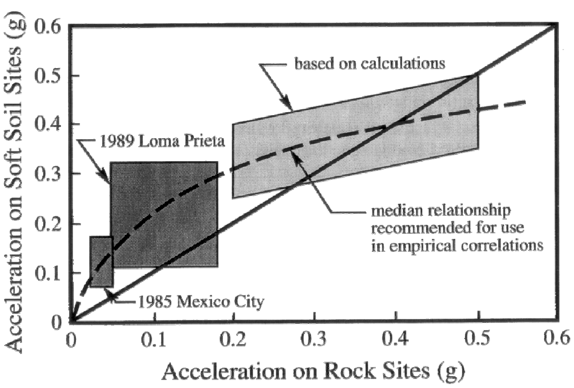

Figure 2-24. Variation of peak accelerations on soft soil compared to rock for the 1985 Mexico City and the 1989 Loma Prieta earthquakes. [After Idriss (2-52).]

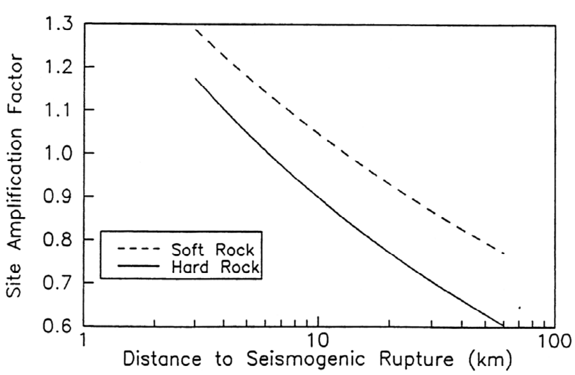

Figure 2-25. Variation of site amplification factors (ratio of peak ground acceleration on rock to that on alluvium) with distance. [After Campbell and Bozorgnia (2-36).]

The effect of site geology on peak ground acceleration can be seen in Equation 2-27 proposed by Campbell and Bozorgnia (2-36). The ratios of peak ground acceleration on soft rock and on hard rock to that on alluvium (defined as site amplification factors) were computed from Equation 2-27 and are shown in Figure 2-25. The figure indicates that rock sites have higher accelerations at shorter distances and lower accelerations at longer distances as compared to alluvium sites, with ground accelerations on soft rock consistently higher than those on hard rock.

Recent studies on the influence of site geology on ground motion use the average shear wave velocity to identify the soil category. Boore et al. (2-37) used the average shear wave velocity for the upper 30 meters of the soil layer to characterize the soil condition in the attenuation relationship in Equation 2-29. The equation indicates that for the same distance, magnitude, and fault mechanism, as the soil becomes stiffer (i.e. a higher shear wave velocity), the peak ground acceleration becomes smaller. The recent UBC code and NEHRP recommended provisions use shear wave velocities to identify the different soil profiles with a shear wave velocity of 1500 m/sec or greater defining hard rock and a shear wave velocity of 180 m/sec or smaller defining soft soil (Section 2.9).

There is a general agreement among various investigators that the soil condition has a pronounced influence on velocities and displacements. According to Boore et al. (2-45 and 2-46), Joyner and Boore (2-31), and Seed and Idriss (2-39); larger peak horizontal velocities are to be expected for soil than rock. A statistical study of earthquake ground motion and response spectra by Mohraz (2-53) indicated that the average velocity to acceleration ratio for records on alluvium is greater than the corresponding ratio for rock.

Using the frequency dependent definition of duration proposed by Trifunac and Westermo (2-16), Novikova and Trifunac (2-48) determined that for the same epicentral distance and earthquake magnitude, the strong motion duration for records on a sedimentary site is longer than that on a rock site by approximately 4 to 6 sec for frequencies of 0.63 Hz and by about 1 sec for frequencies of 2.5 Hz. The records on intermediate sites, furthermore, exhibited a shorter duration than those on sediments. They indicated that for frequencies of 0.63 to 21 Hz, the influence of the soil condition on the duration is noticeable.

2.4.3 Magnitude

Different earthquake magnitudes have been defined, the more common being the Richter magnitude (local magnitude) M_L, the surface wave magnitude M_S, and the moment magnitude M_W (see Chapter 1). As expected, at a given distance from the source of energy release, large earthquake magnitudes result in large peak ground accelerations, velocities, and displacements. Because of the lack of adequate data for earthquake magnitudes greater than 7.5, the influence of the magnitude on peak ground motion and duration is generally determined through extrapolation of data from earthquake magnitudes smaller than 7.5. Attenuation relationships are also presented as a function of magnitude for a given source distance as indicated in Equations 2-27 and 2-29. Both equations show that for a given distance, soil condition, and fault mechanism, the larger the earthquake magnitude, the larger is the peak ground acceleration. Figure 2-16, plotted using Equation 2-29, confirms this observation.

The influence of earthquake magnitude on the duration of strong motion has been studied by several investigators. Housner [2-38 and 2-54] presents values for maximum acceleration and duration of strong phase of shaking in the vicinity of a fault for different earthquake magnitudes (Table 2-5). Donovan [2-23] presents the linear relationship in Figure 2-26 for estimating duration in terms of magnitude. His estimates compare closely with those presented by Housner in Table 2-5. Using the bracketed duration (0.05*g*), Page et al. [2-11] give estimates of duration for various earthquake magnitudes near a fault (Table 2-6). Chang and Krinitzsky [2-47] give approximate upper-bound for duration for soil and rock (Table 2-7). Their values for soil are close to those presented by Page et al., and the ones for rock are consistent with those given by Housner and by Donovan. The study by Novikova and Trifunac [2-48] which uses the frequency dependent definition of duration presents a quadratic expression for the duration in terms of earthquake magnitude. Their study indicates that the duration of strong motion does not depend on the earthquake magnitude at frequencies less than 0.25 Hz. For higher frequencies, the duration increases exponentially with magnitude.

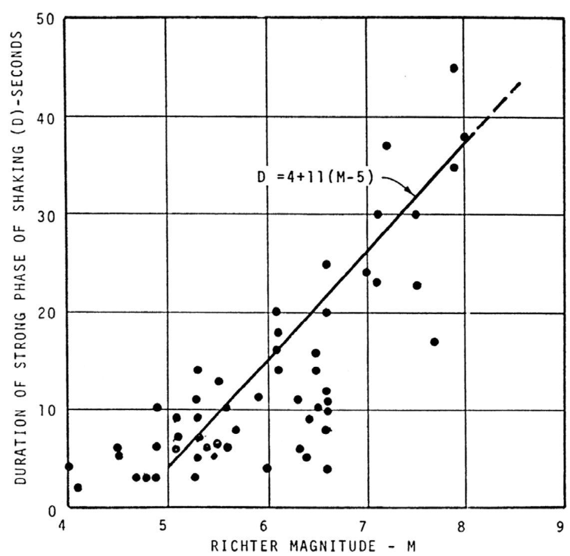

Figure 2-26. Relationship between magnitude and duration of strong phase of shaking. [After Donovan (2-23).]

Table 2-5. Maximum Ground Accelerations and Durations of Strong Phase of Shaking [after Housner (2-54)]

Magnitude	Maximum Acceleration (%g)	Duration (sec)
5.0	9	2
5.5	15	6
6.0	22	12
6.5	29	18
7.0	37	24
7.5	45	30
8.0	50	34
8.5	50	37

Table 2-6. Duration of Strong Motion Near Fault [after Page et al. (2-11)]

Magnitude	Duration (sec)
5.5	10
6.5	17
7.0	25
7.5	40
8.0	60
8.5	90

Table 2-7. Strong Motion Duration for Different Earthquake Magnitudes [after Chang and Krinitzsky (2-47)]

Magnitude	Rock	Soil
5.0	4	8
5.5	6	12
6.0	8	16
6.5	11	23
7.0	16	32
7.5	22	45
8.0	31	62
8.5	43	86

2.4.4 Source characteristics

Factors such as fault mechanism, depth, and repeat time have been suggested by several investigators as being important in determining ground motion amplitudes because of their relation to the stress state at the source or to stress changes associated with the earthquake. Based on the state of stress in the vicinity of the fault, many investigators believe that large ground motions are associated with reverse and thrust faults whereas smaller ground motions are related to normal and strike-slip faults.

The above observations agree with the study by McGarr [2-55, 2-56] who concluded that ground acceleration from reverse faults should be greater than those from normal faults, with strike-slip faults having intermediate accelerations. McGarr also believes that ground motions increase with fault depth. Kanamori and Allen [2-57] presented data showing that higher ground motions are associated with faults with longer repeat times since they experience large average stress drops. Using empirical equations, Campbell [2-58] found that peak ground acceleration and velocity in reverse-slip earthquakes are larger by about 1.4 to 1.6 times than those in strike-slip earthquakes. Joyner and Boore [2-59] believe this ratio should be 1.25.

Recent attenuation relationships include the effects of fault mechanism on ground motion as indicated in Equations 2-27 and 2-29. Equation 2-27 by Campbell and Bozorgnia [2-36] indicates that reverse, reverse-oblique, and thrust fault earthquakes result in larger ground accelerations than strike-slip and normal fault earthquakes. Figure 2-27, computed from Equation 2-27, shows the variation of peak ground acceleration with distance for earthquakes with different magnitudes and fault mechanisms on alluvium. Similar observations can also be made from Equation 2-29 by Boore et al. [2-37] where reverse earthquakes result in higher accelerations than strike-slip earthquakes.

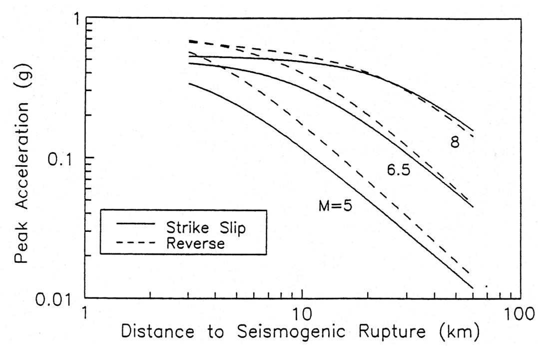

Figure 2-27. Peak ground acceleration versus distance for different magnitudes and fault mechanisms. [After Campbell and Bozorgnia (2-36).]

2.4.5 Directivity

Directivity relates to the azimuthal variation of the angle between the direction of rupture propagation (or radiated seismic energy) and source-to-site vector, and its effect on earthquake ground motion. Large ground accelerations and velocities can be associated with small angles since a significant portion of the seismic energy is channeled in the direction of rupture propagation. Consequently, when a large urban area is located within the small angle, it will experience severe damage.

According to Faccioli [2-60], in the Northridge earthquake of January 17, 1994; the rupture propagated in the direction opposite from downtown Los Angeles and San Fernando Valley, causing moderate damage. In the Hyogoken-Nanbu (Kobe) earthquake of January 17, 1995, the rupture was directed toward the densely populated City of Kobe resulting in significant damage. The stations that lie in the direction of the earthquake rupture propagation will record shorter strong motion durations than those located opposite to the direction of propagation [2-61].

Boatwright and Boore [2-62], believe that directivity can significantly affect strong ground motion by a factor of up to 10 for ground accelerations. Joyner and Boore [2-59] indicate, however, that it is not clear how to incorporate directivity into methods for predicting ground motion in future earthquakes since the angle between the direction of rupture propagation and the source-to-recording-site vector is not known *a priori*. Moreover, for sites close to the source of a large magnitude earthquake, where a reliable estimate of ground motion is important, the angle changes during the rupture propagation. Most ground motion prediction studies do not explicitly include a variable representing directivity.

2.5 EVALUATION OF SEISMIC RISK AT A SITE

Evaluating seismic risk is based on information from three sources: 1) the recorded ground motion, 2) the history of seismic events in the vicinity of the site, and 3) the geological data and fault activities of the region. For most regions of the world this information, particularly from the first source, is limited and may not be sufficient to predict the size and recurrence intervals of future earthquakes. Nevertheless, the earthquake engineering community has relied on this limited information to establish some acceptable levels of risk.

The seismic risk analysis usually begins by developing mathematical models, which are used to estimate the recurrence intervals of future earthquakes with certain magnitude and/or intensity. These models together with the appropriate attenuation relationships are commonly utilized to estimate ground motion parameters such as peak acceleration and velocity corresponding to a specified probability and return period. Among the earthquake recurrence models mostly used in practice is the Gutenberg-Richter relationship [2-63, 2-64] known as the Richter law of magnitude which states that there exists an approximate linear relationship between the logarithm of the average number of annual earthquakes and earthquake magnitude in the form

$$\log N(m) = A - Bm \qquad \text{(2-31)}$$

where $N(m)$ is the average number of earthquakes per annum with a magnitude greater than or equal to m, and A and B are constants determined from a regression analysis of data from the seismological and geological studies of the region over a period of time. The Gutenberg-Richter relationship is highly sensitive to magnitude intervals and the fitting procedure used in the regression analysis [2-65, 2-66, 2-33]. Figure 2-28 shows a typical plot of the Gutenberg-Richter relationship presented by Schwartz and Coppersmith [2-66] for the south-central segment of the San Andreas Fault. The relationship was obtained from historical and instrumental data in the period 1900-1980 for a 40-kilometer wide strip centered on the fault. The box shown in the figure represents recurrence intervals based on geological data for earthquakes of magnitudes 7.5-8.0 [2-67]. It is apparent from the figure that the extrapolated portion of the Gutenberg-Richter equation (dashed line) underestimates the frequency of occurrence of earthquakes with large magnitudes, and therefore, the model requires modification of the B-value in Equation 2-31 for magnitudes greater than approximately 6.0 [2-33].

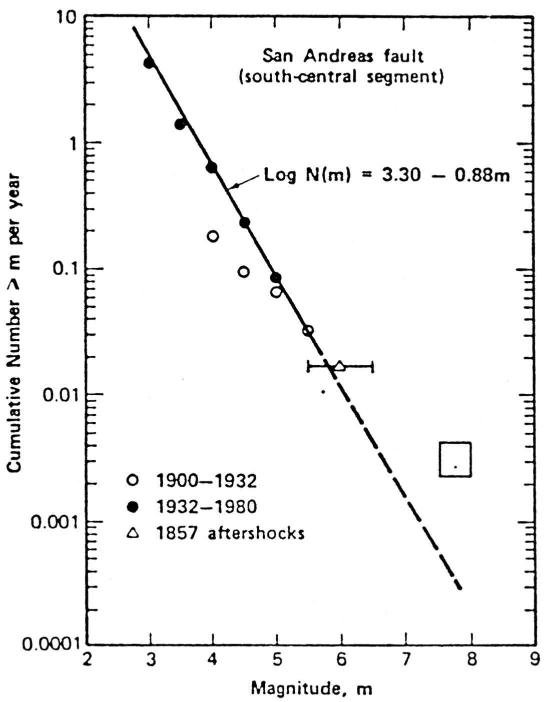

Figure 2-28. Cumulative frequency-magnitude plot. The box in the figure represents range of recurrence based on geological data for earthquake magnitudes of 7.5-8. [After Schwartz and Coppersmith (2-66); reproduced from Idriss (2-33).]

Cornell [(2-68)] introduced a simplified method for evaluating seismic risk. The method incorporates the influence of all potential sources of earthquakes. His procedure as described by Vanmarcke [(2-69)] can be summarized as follows:

1. The potential sources of seismic activity are identified and divided into smaller sub-sources (point sources).
2. The average number of earthquakes per annum $N_i(m)$ of magnitudes greater than or equal to m from the ith sub-source is determined from the Gutenberg-Richter relationship (Equation 2-31) as

$$\log N_i(m) = A_i - B_i m \tag{2-32}$$

where A_i and B_i are known constants for the ith sub-source.

3. Assuming that the design ground motion is specified in terms of the peak ground acceleration a and the epicentral distance from the ith sub-source to the site is R_i, the magnitude $m_{a,i}$ of an earthquake initiated at this sub-source may be estimated from

$$m_{a,\,i} = f(R_i, a) \tag{2-33}$$

where $f(R_i,\ a)$ is a function which can be obtained from the attenuation relationships. Substituting Equation 2-33 into Equation 2-32, one obtains

$$\log N_i(m_{a,i}) = A_i - B_i\left[f(R_i, a)\right] \tag{2-34}$$

Assuming the seismic events are independent (no overlapping), the total number of earthquakes per annum N_a which may result in a peak ground acceleration greater than or equal to a is obtained from the contribution of each sub-source as

$$N_a = \sum_{all} N_i(m_{a,i}) \tag{2-35}$$

4. The mean return period T_a in years is obtained as

$$T_a = \frac{1}{N_a} \tag{2-36}$$

In the above expression, N_a can be also interpreted as the average annual probability λ_a that the peak ground acceleration exceeds a certain acceleration a. In a typical design situation, the engineer is interested in the probability that such a peak exceeds a during the life of structure t_L. This probability can be estimated using the Poisson distribution as

$$P = 1 - e^{-\lambda_a t_L} \tag{2-37}$$

Another distribution based on a Bayesian procedure [2-70] was proposed by Donovan [2-23]. The distribution is more conservative than the Poisson distribution, and therefore more appropriate when additional uncertainties such as those associated with the long return periods of large magnitude earthquakes are encountered. It should be noted that other ground motion parameters in lieu of acceleration such as spectral ordinates may be

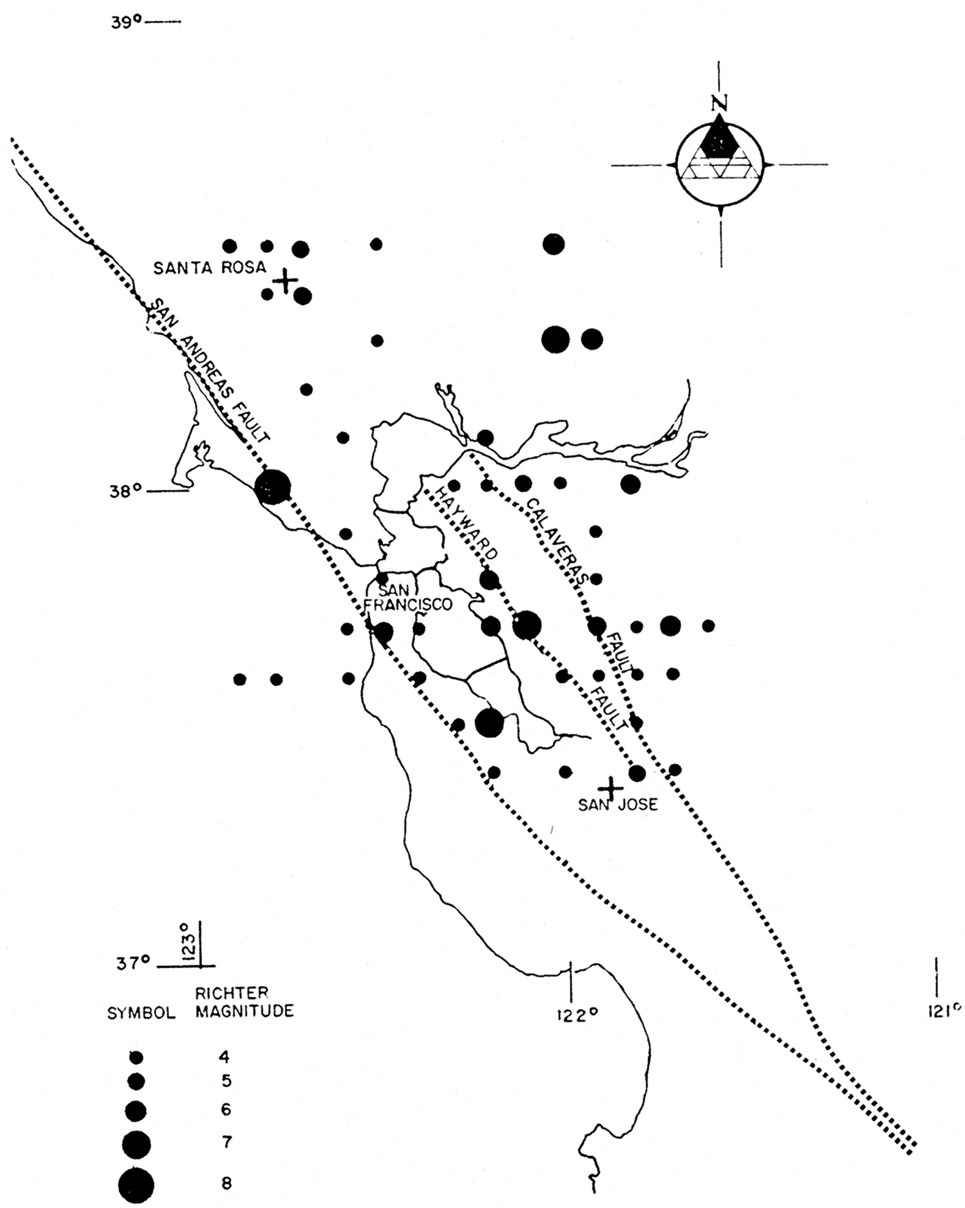

Figure 2-29. Instrumental or estimated epicentral locations within 100 kilometers of San Francisco. [After Donovan (2-23).]

used for evaluating seismic risk. Other procedures for seismic risk analysis based on more sophisticated models have also been proposed (see for example Der Kiureghian and Ang, 2-71).

The evaluation of seismic risk at a site is demonstrated by Donovan [(2-23)] who used as an example the downtown area of San Francisco. The epicentral data and earthquake magnitudes he considered in the evaluation were obtained over a period of 163 years and are depicted in Figure 2-29. The data is associated with three major faults, the San Andreas, Hayward, and Calaveras. Using attenuation relationships for competent soil and rock, Donovan computed the return periods for different peak accelerations (see Table 2-8). He then computed the probability of exceeding various peak ground accelerations during a fifty-year life of the structure which is shown in Figure 2-30. Plots such as those in Figure 2-30 may be used to estimate the peak acceleration for various probabilities. For example, if the structure is to be designed to resist a moderate earthquake with a probability of 0.6 and a severe earthquake with a probability of between 0.1 and 0.2 of occurring at least once during the life of the structure, the peak accelerations using Figure 2-30(b) for rock, are 0.15g and 0.4g, respectively.

Table 2-8. Return Periods for Peak Ground Acceleration in the San Francisco Bay Area [after Donovan (2-23)]

Peak Acceleration	Return Period (years) Soil	Rock
0.05	4	8
0.10	20	30
0.15	50	60
0.20	100	100
0.25	250	200
0.30	450	300
0.40	2000	700

2.5.1 Development of seismic maps

Using the seismic risk principles of Cornell [(2-68)], Algermissen and Perkins [(2-72, 2-73)] developed isoseismal maps for peak ground accelerations and velocities. Figure 2-31 is a map, which shows contours of peak acceleration on rock having a 90% probability of not being exceeded in 50 years. The Applied Technology Council ATC [(2-74)] used this map to develop similar maps for effective peak acceleration (Figure 2-32) and effective peak velocity-related acceleration (Figure 2-33). The effective peak acceleration A_a and the effective peak velocity-related acceleration A_v are defined by the Applied Technology Council [(2-74)] based on a study by McGuire [(2-75)]. They are obtained by dividing the spectral accelerations between periods of 0.1 to 0.5 sec and the spectral

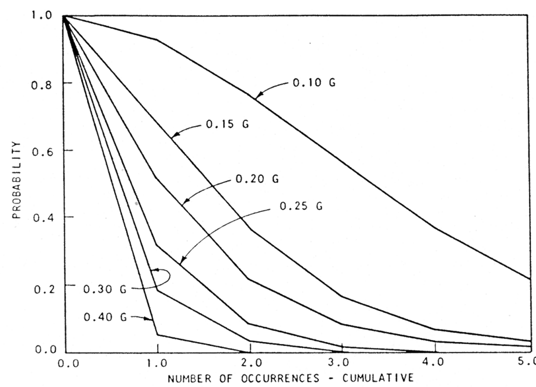

(a) Based on return periods using relationship 9 in Table 2-4

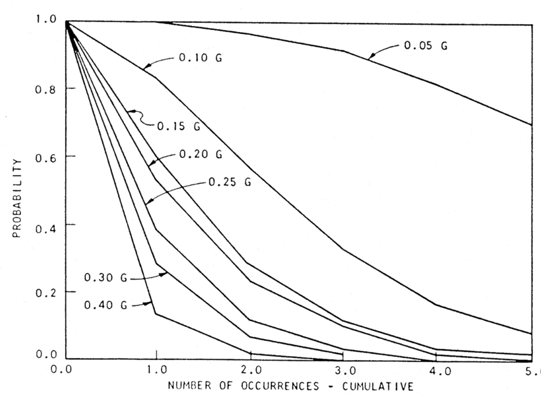

(b) Based on return periods using attenuation equation for rock

Figure 2-30. Estimated probabilities for a fifty year project life. [After Donovan (2-23).]

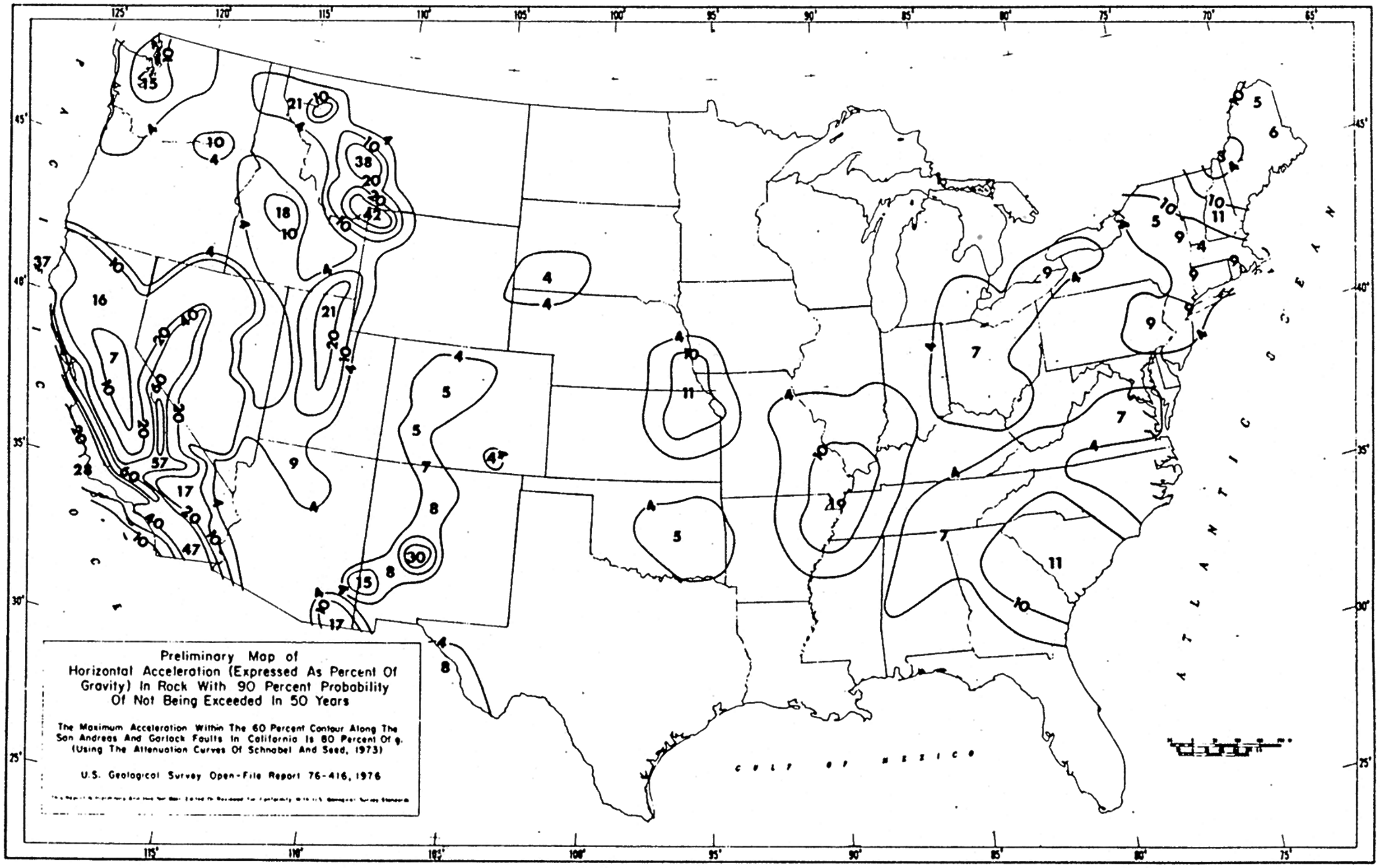

Figure 2-31. Seismic risk map developed by Algermissen and Perkins. (Reproduced from 2-74.)

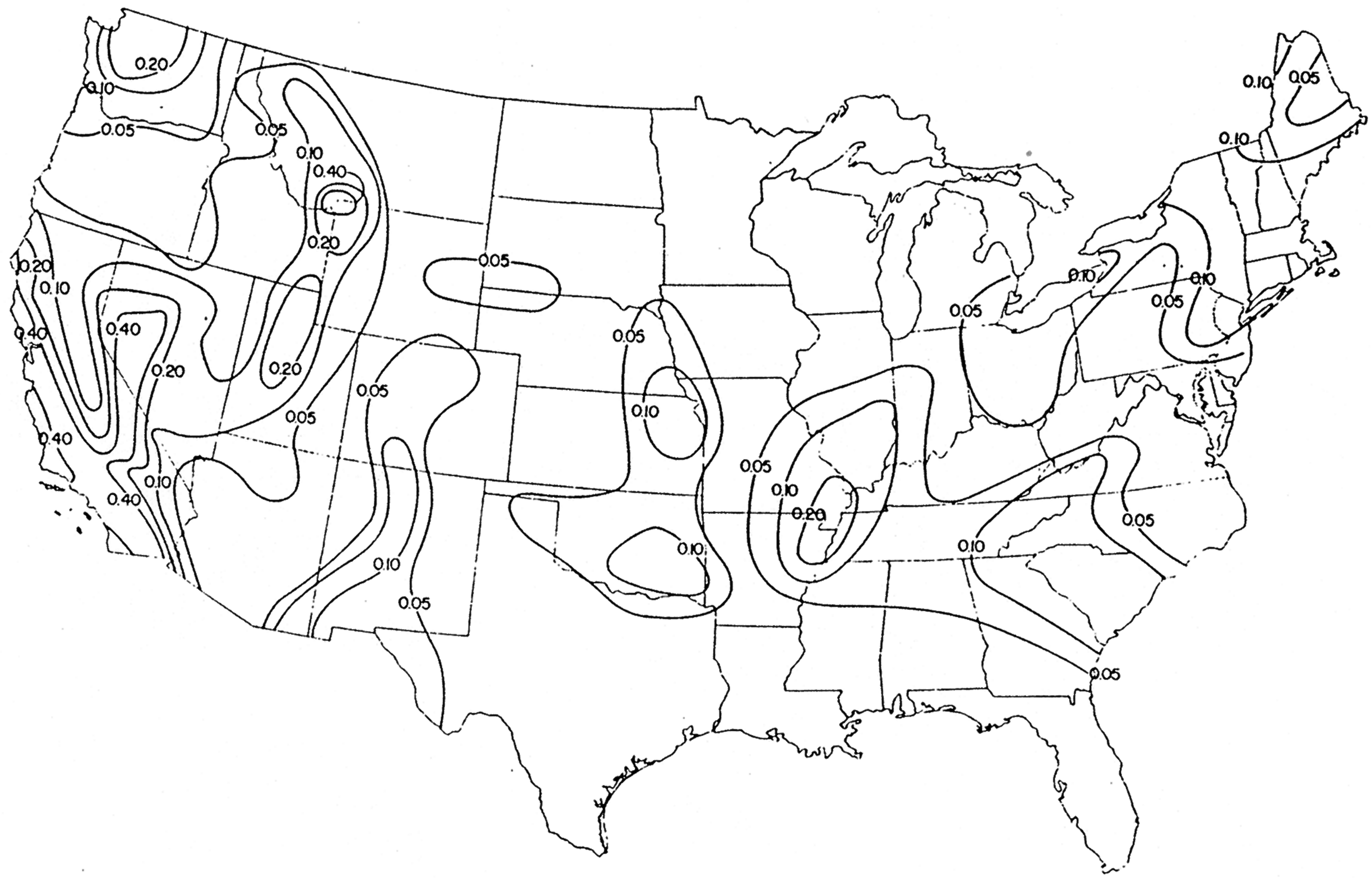

Figure 2-32. Contour map for effective peak acceleration (ATC, 2-74).

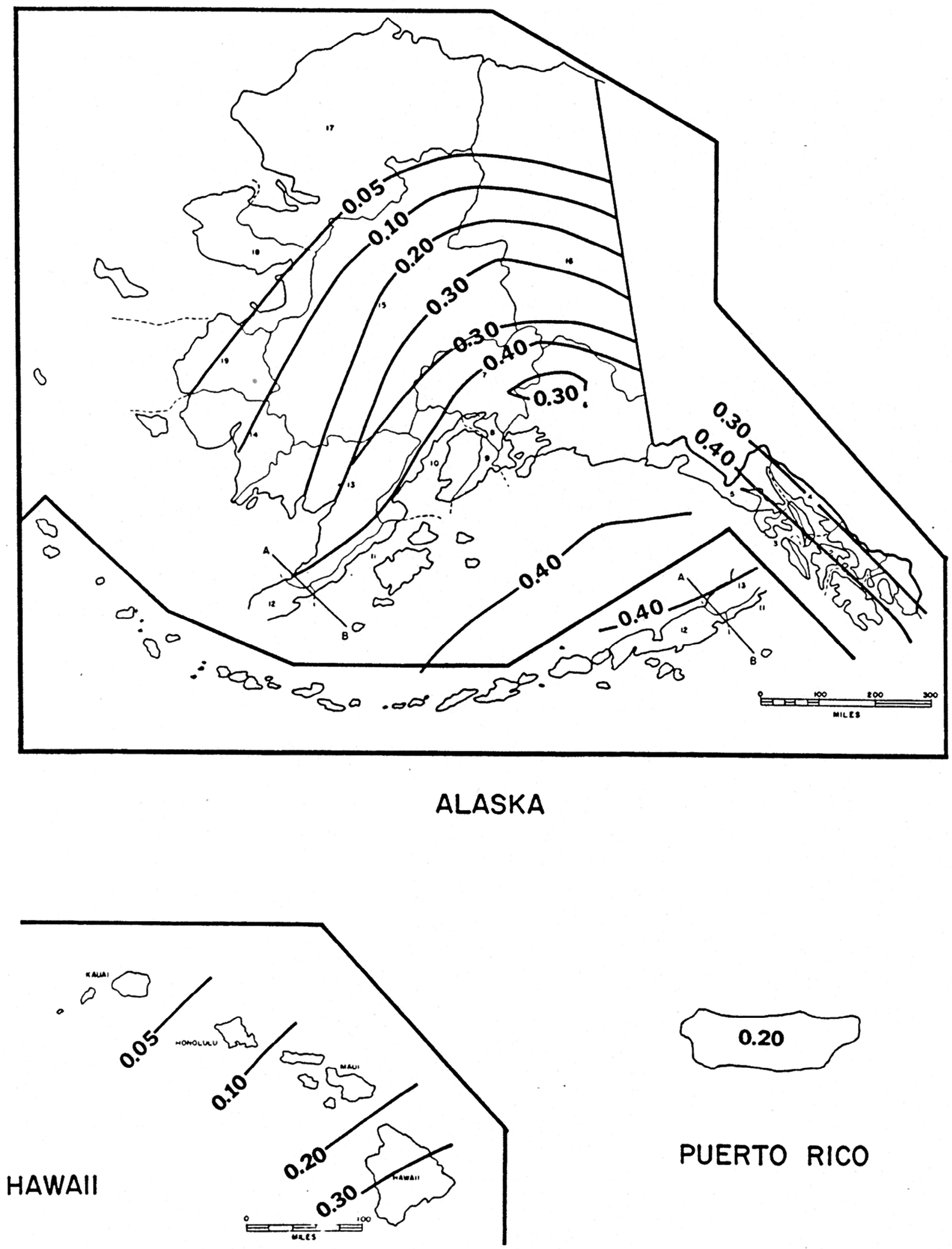

CONTOUR MAP FOR EFFECTIVE PEAK ACCELERATION

Figure 2-32. (continued)

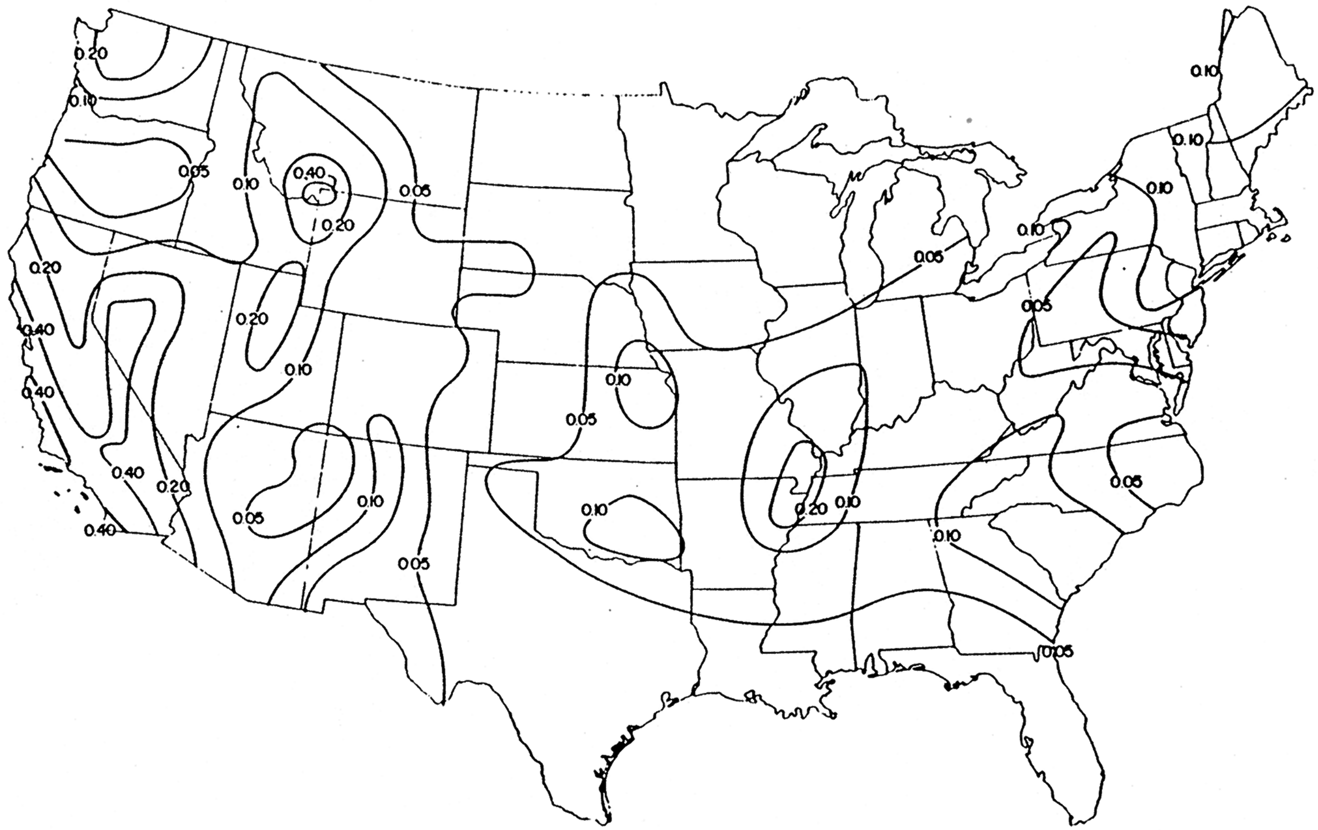

Figure 2-33. Contour map of effective peak velocity-related acceleration (ATC, 2-74).

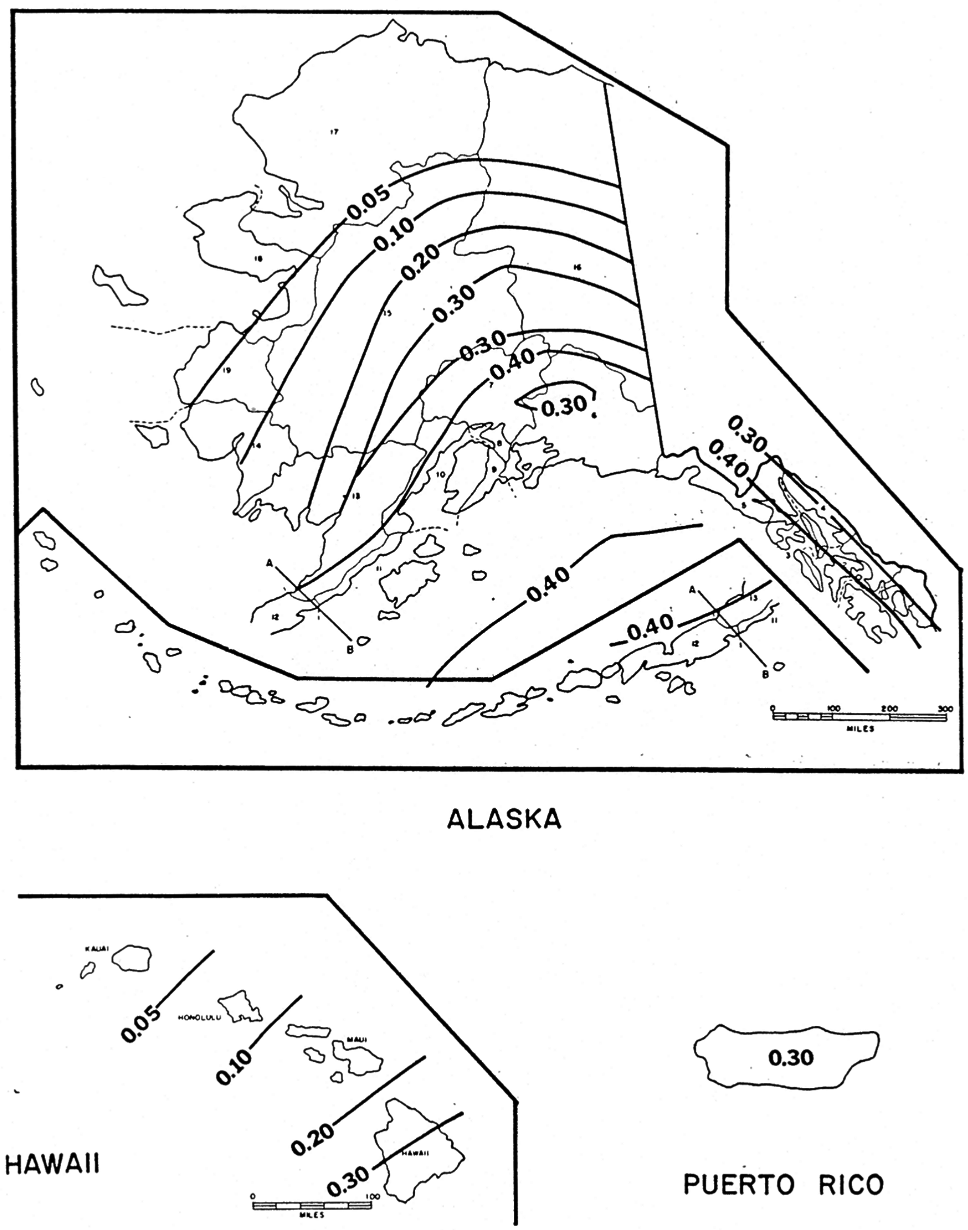

CONTOUR MAP FOR EFFECTIVE PEAK VELOCITY-RELATED ACCELERATION COEFFICIENT

Figure 2-33. (continued)

velocity at a period of approximately 1.0 sec by a constant amplification factor (2.5 for a 5% damped spectrum). It should be noted that the effective peak acceleration will generally be smaller than the peak acceleration while the effective peak velocity-related acceleration is generally greater than the peak velocity [(2-75)].

The A_a and A_v maps developed from the ATC study are in many ways similar to the Algermissen-Perkins map. The most significant difference is in the area of highest seismicity in California. Within such areas, the Algermissen-Perkins map has contours of 0.6*g* whereas the ATC maps have no values greater than 0.4*g*. This discrepancy is due to the difference between peak acceleration and effective peak acceleration and also to the decision by the participants in the ATC study to limit the design value to 0.4*g* based on scientific knowledge and engineering judgment. The ATC maps were also provided with the contour lines shifted to coincide with the county boundaries.

The 1985, 1988, 1991 and 1994 National Earthquake Hazard Reduction Program (NEHRP) Recommended Provisions for Seismic Regulations for New Buildings [(2-76 to 2-79)] include the ATC A_a and A_v maps which correspond to a 10% probability of the ground motion being exceeded in 50 years (a return period of 475 years). The 1991 NEHRP provisions [(2-78)] also introduced preliminary spectral response acceleration maps developed by the United States Geological Survey (USGS) for a 10% probability of being exceeded in 50 years and a 10% probability of being exceeded in 250 years (a return period of 2,375 years). These maps, which include elastic spectral response accelerations corresponding to 0.3 and 1.0 sec periods, were introduced to present new and relevant data for estimating spectral response accelerations and reflect the variability in the attenuation of spectral acceleration and in fault rupture length [(2-78)].

The 1997 NEHRP recommended provisions [(2-80)] provide seismic maps for the spectral response accelerations at the short period range (approximately 0.2 sec) and at a period of 1.0 sec. The maps correspond to the maximum considered earthquake, defined as the maximum level of earthquake ground shaking that is considered reasonable for design of structures. In most regions of the United States, the maximum considered earthquake is defined with a uniform probability of exceeding 2% in 50 years (a return period of approximately 2500 years). It should be noted that the use of the maximum considered earthquake was adopted to provide a uniform protection against collapse at the design ground motion. While the conventional approach in earlier editions of the provisions provided for a uniform probability that the design ground motion will not be exceeded, it did not provide for a uniform probability of failure for structures designed for that ground motion. The design ground motion in the 1997 NEHRP provisions is based on a lower bound estimate of the margin against collapse which was judged, based on experience, to be 1.5. Consequently, the design earthquake ground motion was selected at a ground shaking level that is 1/1.5 or 2/3 of the maximum considered earthquake ground motion given by the maps.

The 1997 NEHRP Guidelines for the Seismic Rehabilitation of Buildings [(2-81)], known as FEMA-273, introduce the concept of performance-based design. For this concept, the rehabilitation objectives are statements of the desired building performance level (collapse prevention, life safety, immediate occupancy, and operational) when the building is subjected to a specified level of ground motion. Therefore, multiple levels of ground shaking need to be defined by the designer. FEMA-273 provides two sets of maps; each set includes the spectral response accelerations at short periods (0.2 sec) and at long periods (1.0 sec). One set corresponds to a 10% probability of exceedance in 50 years, known as Basic Safety Earthquake 1 (BSE-1), and the other set corresponds to a 2% probability of exceedance in 50 years, known as Basic Safety Earthquake 2 (BSE-2), which is similar to the Maximum Considered Earthquake of the 1997 NEHRP provisions [(2-80)]. FEMA-273 also presents a method for adjusting the mapped spectral accelerations for other probabilities of exceedance in 50 years using the spectral accelerations at 2% and 10% probabilities.

The A_a and A_v maps, developed during the ATC study, were also used, after some modifications, in the development of a single seismic map for the 1985, 1988, 1991, 1994, and 1997 editions of the Uniform Building Code [2-82 to 2-86]. The UBC map shows contours for five seismic zones designated as 1, 2A, 2B, 3, and 4. Each seismic zone is assigned a zone factor Z, which is related to the effective peak acceleration. The Z factors for the five zones are 0.075, 0.15, 0.20, 0.30, and 0.40 for zones 1, 2A, 2B, 3, and 4; respectively. The only change in the UBC seismic map occurred in the 1994 edition [2-85] reflecting new knowledge regarding the seismicity of the Pacific Northwest of the United States.

2.6 ESTIMATING GROUND MOTION

In the late sixties and early seventies, the severity of the ground motion was generally specified in terms of peak horizontal ground acceleration. Most attenuation relationships were developed for estimating the expected peak horizontal acceleration at the site. Although structural response and to some extent damage potential to structures can be related to peak ground acceleration, the use of the peak acceleration for design has been questioned by several investigators on the premise that structural response and damage may relate more appropriately to effective peak acceleration A_a and effective peak velocity-related acceleration A_v. Early Studies by Mohraz et al. [2-9], Mohraz [2-53], Newmark and Hall [2-87], and Newmark et al. [2-88] recommended using ground velocity and displacement, in addition to ground acceleration, in defining spectral shapes and ordinates.

Prior to the 1971 San Fernando earthquake where only a limited number of records was available, Newmark and Hall [2-89, 2-90] recommended that a maximum horizontal ground velocity of 48 in/sec and a maximum horizontal ground displacement of 36 in. be used for a unit (1.0g) maximum horizontal acceleration. Newmark also recommended that the maximum vertical ground motion be taken as 2/3 of the corresponding values for the horizontal motion.

With the availability of a large number of recorded earthquake ground motion, particularly during the 1971 San Fernando earthquake, several statistical studies [2-9, 2-91, 2-53] were carried out to determine the average peak ground velocity and displacement for a given acceleration. These studies recommended two ratios: peak velocity to peak acceleration v/a and peak acceleration–displacement product to the square of the peak velocity ad/v^2 be used in estimating ground velocities and displacements. Certain response spectrum characteristics such as the sharpness or flatness of the spectra can be related to the ad/v^2 ratio as discussed later. According to Newmark and Rosenbleuth [2-92], for most earthquakes of practical interest, ad/v^2 ranges from approximately 5 to 15. For harmonic oscillations, ad/v^2 is one and for steady-state square acceleration waves, the ratio is one half.

A statistical study of v/a and ad/v^2 ratios was carried out by Mohraz [2-53] who used a total of 162 components of 54 records from 16 earthquakes. A summary of the v/a and ad/v^2 ratios for records on alluvium, on rock, and on alluvium layers underlain by rock are given in Table 2-9. It is noted that v/a ratios for rock are substantially lower than those for alluvium with the v/a ratios for the two intermediate categories falling between alluvium and rock. Table 2-9 also shows that the v/a ratios for the vertical components are close to those for the horizontal components with the larger of the two peak accelerations. The 50 percentile v/a ratios for the larger of the two peak accelerations from Table 2-9 (24 (in/sec)/g for rock and 48 (in/sec)/g for alluvium) and those given by Seed and Idriss [2-39] (22 (in/sec)/g for rock and 43 (in/sec)/g for alluvium) are in close agreement. The ad/v^2 ratios in Table 2-9

Table 2-9. Summary of Ground Motion Relationships [after Mohraz (2-53)]

Soil Category	Group*	v/a (in/sec)/g	ad/v^2	d/a (in/g)	$a_{vertical}/(a_{horizontal})_L$
	L	24	5.3	8	0.48
Rock	S	27	5.2	10	
	V	28	6.1	12	
<30 ft of alluvium underlain by rock	L	30	4.5	11	0.47
	S	39	4.2	17	
	V	33	6.8	19	
30-200 ft of alluvium underlain by rock	L	30	5.1	12	0.40
	S	36	3.8	13	
	V	30	7.6	18	
	L	48	3.9	23	0.42
Alluvium	S	57	3.5	29	
	V	48	4.6	27	

* L: Horizontal components with the larger of the two peak accelerations
S: Horizontal components with the smaller of the two peak accelerations
V: Vertical components

indicate that, in general, the ratios for alluvium are smaller than those for rock and those for alluvium layers underlain by rock. The d/a ratios are also presented in Table 2-9. The values indicate that for a given acceleration, the displacements for alluvium are 2 to 3 times those for rock. The table also includes the ratio of the vertical acceleration to the larger of the two peak horizontal accelerations where it is apparent that the ratios are generally close to each other indicating that soil condition does not influence the ratios. The ratio of the vertical to horizontal acceleration of 2/3 which Newmark recommended is too conservative, but its use was justified to account for the variations greater than the median and the uncertainties in the ground motion in the vertical direction [(2-91)].

Statistical studies of v/a and ad/v^2 ratios for the Loma Prieta earthquake of October 17, 1989 were carried out by Mohraz and Tiv [(2-93)]. They used approximately the same number of horizontal components of the records on rock and alluvium that Mohraz [(2-53)] used in his earlier study. Their study indicated a mean v/a ratio of 51 and 49 (in/sec)/g and a mean ad/v^2 ratio of 2.8 and 2.6 for rock and alluvium, respectively. The differences in v/a and ad/v^2 ratios from the Loma Prieta and previous earthquakes indicate that each earthquake is different and that site condition, magnitude, epicentral distance, and duration influence the characteristics of the recorded ground motion.

2.7 EARTHQUAKE RESPONSE SPECTRA

Response spectrum is an important tool in the seismic analysis and design of structures and equipment. Unlike the power spectral density which presents information about input energy and frequency content of ground motion, the response spectrum presents the maximum response of a structure to a given earthquake ground motion. The response spectrum introduced by Biot [(2-1, 2-2)] and Housner [(2-3)] describes the maximum response of a damped single-degree-of-freedom (SDOF) oscillator at different frequencies or periods. The detailed procedure for computing and plotting the response spectrum is discussed in Chapter 3 of this handbook and in a number of publications (see for example 2-54, 2-22, 2-94, 2-95). It was customary to plot the response spectrum on a tripartite paper (four-way logarithmic paper) so that at a given frequency

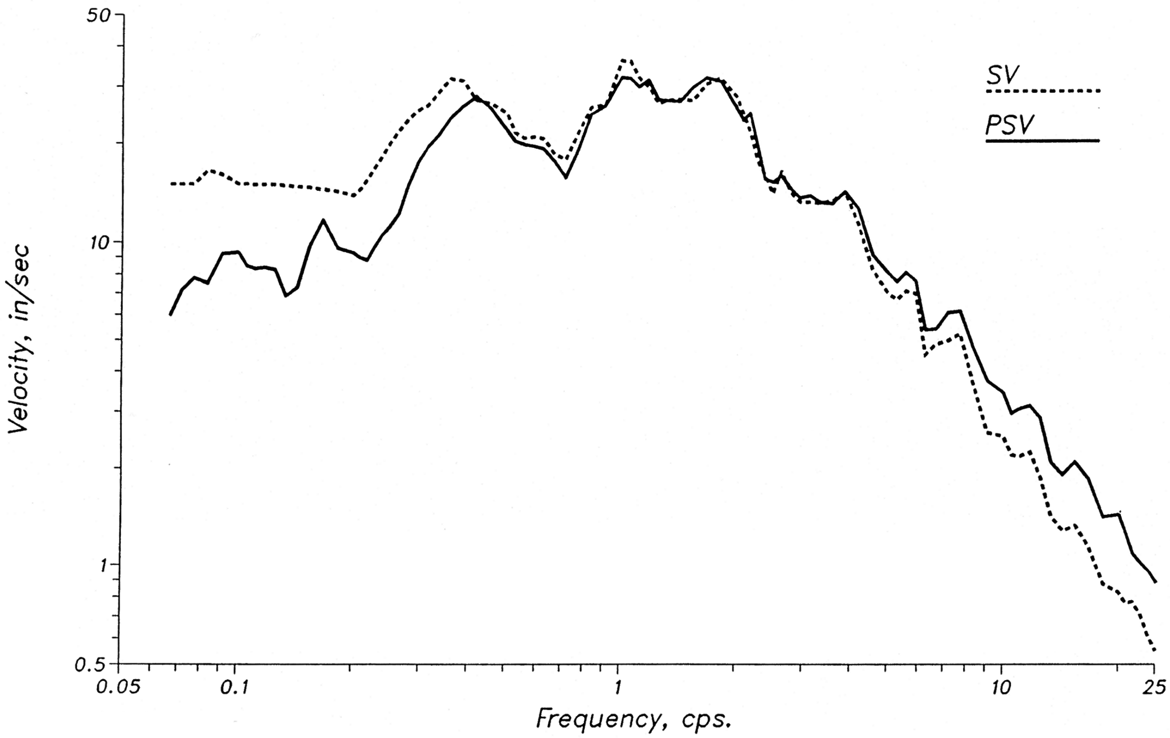

Figure 2-34. Comparison of pseudo-velocity and maximum relative velocity for 5% damping for the S00E component of El Centro, the Imperial Valley earthquake of May 18, 1940.

or period, the maximum relative displacement *SD*, the pseudo-velocity *PSV*, and the pseudo-acceleration *PSA* can all be read from the plot simultaneously. The parameters *PSV* and *PSA* which are expressed in terms of *SD* and the circular natural frequency ω as $PSV = \omega SD$ and $PSA = \omega^2 SD$ have certain characteristics that are of practical interest [(2-87)]. The pseudo-velocity *PSV* is close to the maximum relative velocity *SV* at high frequencies (frequencies greater than 5 Hz), approximately equal for intermediate frequencies (frequencies between 0.5 Hz and 5 Hz) but different for low frequencies (frequencies smaller than 0.5 Hz) as shown in Figure 2-34. In a recent study by Sadek et al. [(2-96)], based on a statistical analysis of 40 damped SDOF structures with period range of 0.1 to 4.0 sec subjected to 72 accelerograms, it was found that the maximum relative velocity *SV* is equal to the pseudo-velocity *PSV* for periods in the neighborhood of 0.5 sec (frequency of 2 Hz). For periods shorter than 0.5 sec, *SV* is smaller than *PSV* while for periods longer than 0.5 sec, *SV* is larger and increases as the period and damping ratio increase. A regression analysis was used to establish the following relationship between the maximum velocity and pseudo-velocity responses:

$$\frac{SV}{PSV} = a_v T^{b_v} \tag{2-38}$$

where $a_v = 1.095 + 0.647\beta - 0.382\beta^2$, $b_v = 0.193 + 0.838\beta - 0.621\beta^2$, T is the natural period, and β is the damping ratio. The relationship between *SV* and *PSV* is presented in Figure 2-35.

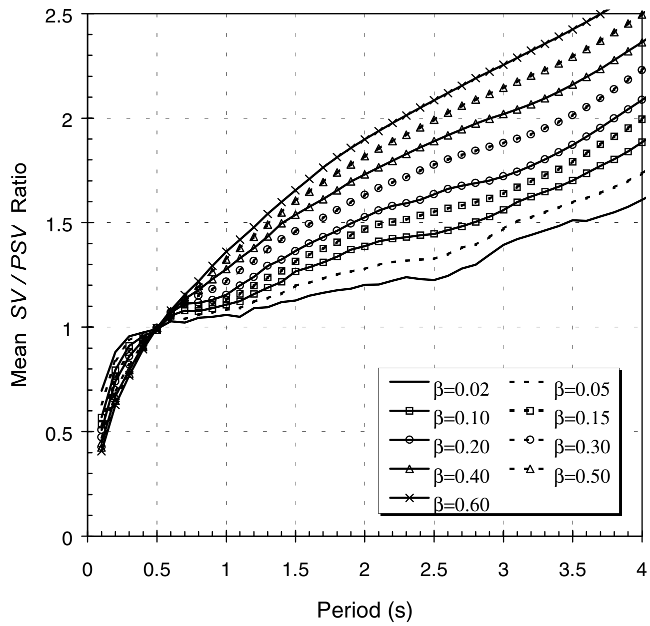

Figure 2-35. Mean ratio of maximum relative velocity to pseudo-velocity for SDOF structures with different damping ratios. [After Sadek et al. (2-96).]

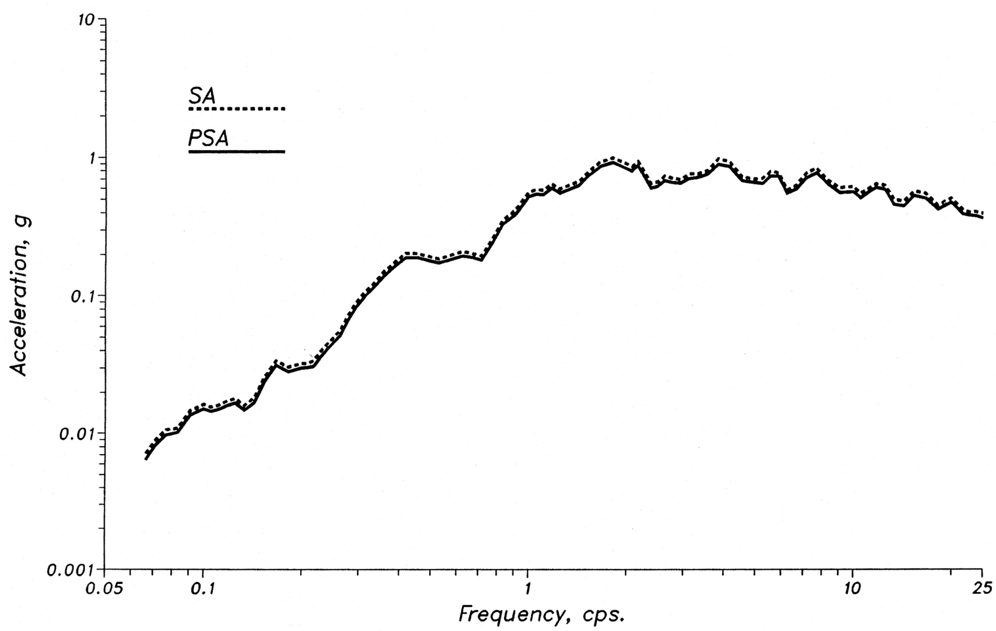

Figure 2-36. Comparison of pseudo-acceleration and maximum absolute acceleration for 5% damping for the S00E component of El Centro, the Imperial Valley earthquake of May 18, 1940.

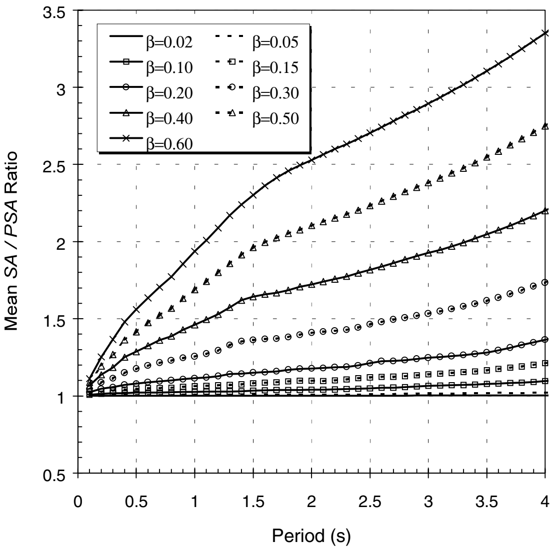

Figure 2-37. Mean ratio of maximum absolute acceleration to pseudo-acceleration for SDOF structures with different damping ratios. [After Sadek et al. (2-96).]

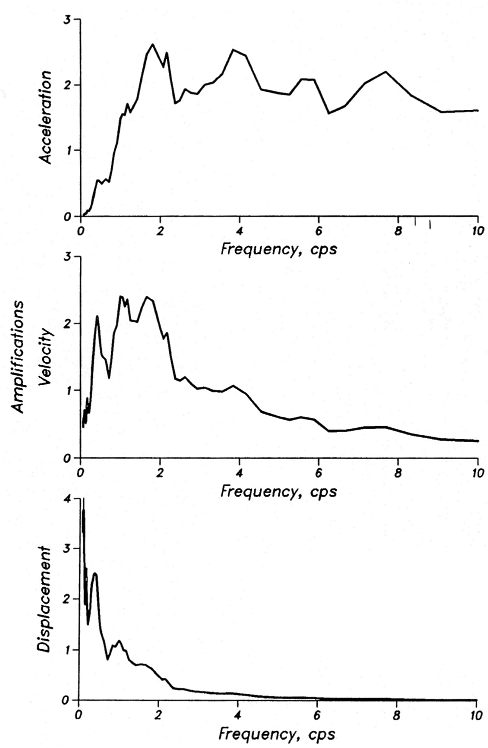

Figure 2-38. Acceleration, velocity, and displacement amplifications plotted as a function of frequency for 5% damping for the S00E component of El Centro, the imperial Valley earthquake of May 18, 1940.

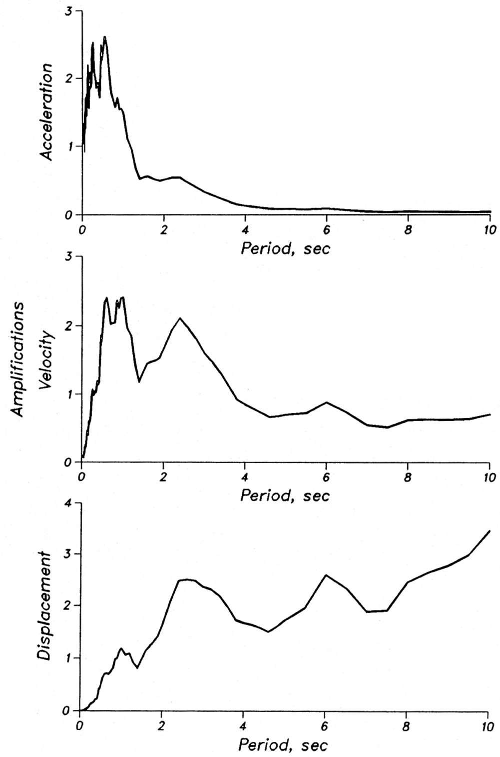

Figure 2-39. Acceleration, velocity, and displacement amplifications plotted as a function of period for 5% damping for the S00E component of El Centro, the Imperial Valley earthquake of May 18, 1940.

For zero damping, the pseudo-acceleration *PSA* is equal to the maximum absolute acceleration *SA*, but for dampings other than zero, the two are slightly different. For the inherent damping levels encountered in most engineering applications, however, the two can be considered approximately equal (see Figure 2-36). When a structure is equipped with supplemental dampers to provide large damping ratios, the difference between *PSA* and *SA* becomes significant, especially for structures with long periods. Using the results of a statistical analysis of 72 earthquake records, Sadek et al. (2-96) described the relationship between *PSA* and *SA* as:

$$\frac{SA}{PSA} = 1 + a_a\, T^{b_a} \tag{2-39}$$

where $a_a = 2.436\beta^{1.895}$ and $b_a = 0.628 + 0.205\beta$. The relationship between *SA* and *PSA* is presented in Figure 2-37.

Arithmetic and semi-logarithmic plots have also been used to represent response spectra. Building codes have presented design spectra in terms of acceleration amplification as a function of period on an arithmetic scale. Typical acceleration, velocity, and displacement amplifications for the S00E component of El Centro, the Imperial Valley earthquake of May 18, 1940 are shown in Figures 2-38 and 2-39 - the former plotted as a function of frequency and the latter as a function of period.

To show how ground motion is amplified in different regions of the spectrum, the peak ground displacement, velocity, and acceleration for the S00E component of El Centro are plotted together on the response spectra, Figure 2-40. Several observations can be made from this figure. At small frequencies or long periods, the maximum relative displacement is large, whereas the pseudo-acceleration is small. At large frequencies or short periods, the relative displacement is extremely small, whereas the pseudo-acceleration is relatively large. At intermediate frequencies or periods, the pseudo-velocity is substantially larger than those at either end of the spectrum. Consequently, three regions are usually identified in a response spectrum: the low frequency or displacement region, the intermediate frequency or velocity region, and the high frequency or acceleration region. In each region, the corresponding ground motion is amplified the most. Figure 2-40 also shows

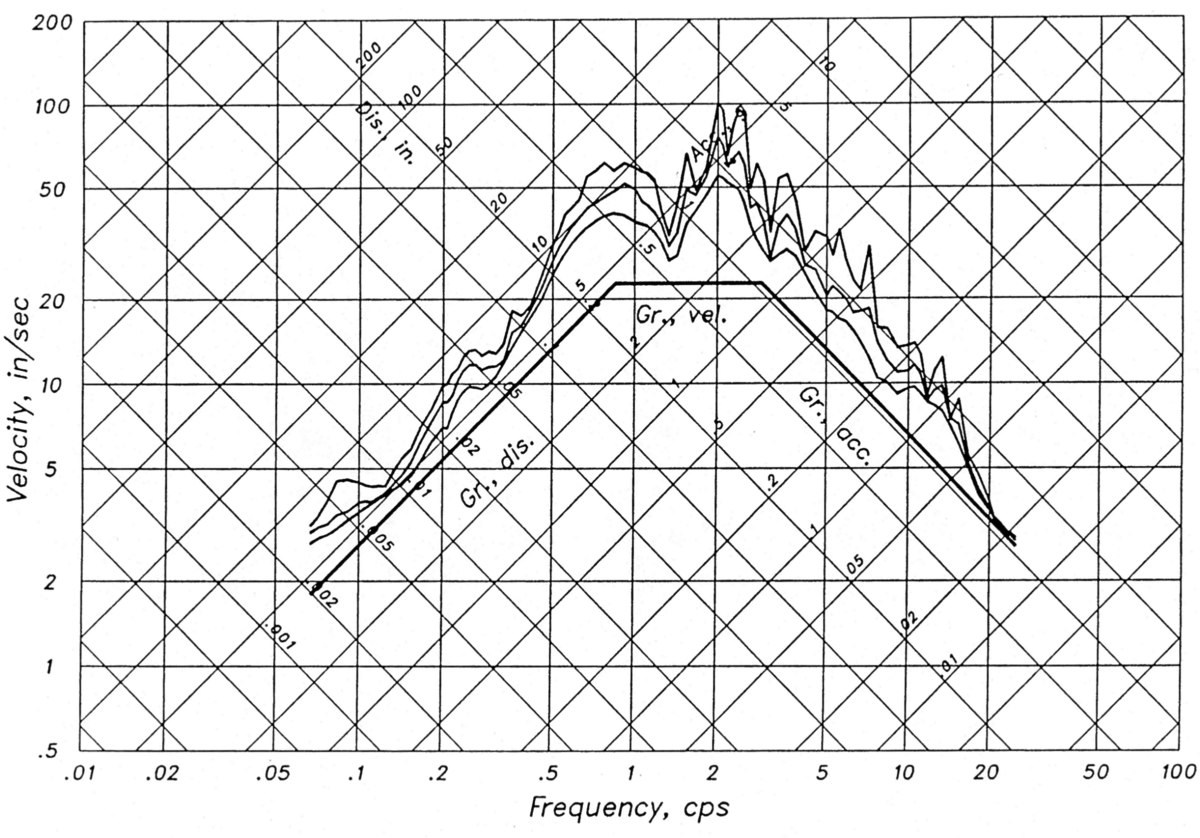

Figure 2-40. Response spectra for 2, 5, and 10% damping for the S00E component of El Centro, the Imperial Valley earthquake of May 18, 1940, together with the peak ground motions.

that at small frequencies (0.05 Hz or less), the spectral displacement approaches the peak ground displacement indicating that for very flexible systems, the maximum displacement is equal to that of the ground. At large frequencies (25-30 Hz), the pseudo-acceleration approaches the peak ground acceleration, indicating that for rigid systems, the absolute acceleration of the mass is the same as the ground. As indicated in Figure 2-40, the response spectra for a given earthquake record is quite irregular and has a number of peaks and valleys. The irregularities are sharp for small damping ratios, and become smoother as damping increases. As discussed previously, the ratio of ad/v^2 influences the shape of the spectrum. A small ad/v^2 ratio results in a pointed or sharp spectrum while a large ad/v^2 ratio results in a flat spectrum in the velocity region. Response spectra may shift toward high or low frequency regions according to the frequency content of the ground motion.

While response spectra for a specified earthquake record may be used to obtain the response of a structure to an earthquake ground motion with similar characteristics, they cannot be used for design because the response of the same structure to another earthquake record will undoubtedly be different. Nevertheless, the recorded ground motion and computed response spectra of past earthquakes exhibit certain similarities. For example, studies have shown that the response spectra from accelerograms recorded on similar soil conditions reflect similarities in shape and amplifications. For this reason, response spectra from records with common characteristics are averaged and then smoothed before they are used in design.

2.8 FACTORS INFLUENCING RESPONSE SPECTRA

Earthquake parameters such as soil condition, epicentral distance, magnitude, duration, and source characteristics influence the shape and amplitudes of response spectra. While the effects of some parameters may be studied independently, the influences of several factors are interrelated and cannot be discussed individually. Some of these influences are discussed below:

2.8.1 Site geology

Prior to the San Fernando earthquake of 1971, accelerograms were limited in number and therefore not sufficient to determine the influence of different parameters on response spectra. Consequently, most design spectra were based on records on alluvium but they did not refer to any specific soil condition. Studies by Hayashi et al. [2-97] and Kuribayashi et al. [2-98] on the effects of soil conditions on Japanese earthquakes had shown that soil conditions significantly affect the spectral shapes. Other studies by Mohraz et al. [2-9] and Hall et al. [2-91] also referred to the influence of soil condition on spectral shapes.

The 1971 San Fernando earthquake provided a large database to study the influence of many earthquake parameters including soil condition on earthquake ground motion and response spectra. In 1976, two independent studies, one by Seed, Ugas, and Lysmer [2-99], and the other by Mohraz [2-53] considered the influence of soil condition on response spectra. The study by Seed et al. used 104 horizontal components of earthquake records from 23 earthquakes. The records were divided into four categories: rock, stiff soils less than about 150 ft deep, deep cohesionless soil with depths greater than 250 ft, and soft to medium clay and sand. The response spectra for 5% damping[4] were normalized to the peak ground acceleration of the records and averaged at various periods. The average and the mean plus one standard deviation (84.1 percentile) spectra for the four categories from their study is presented in Figures 2-41 and 2-42. The ordinates in these plots represent the acceleration amplifications. Also shown in Figure 2-42 is the Nuclear Regulatory Commission (NRC) design spectrum proposed

[4] they limited their study to 5% damping, although the conclusions can easily be extended to other damping coefficients.

by Newmark et al. [2-88, 2-100], see Section 2.9. It is seen that soil condition affects the spectra to a significant degree. The figures show that for periods greater than approximately 0.4 to 0.5 sec, the normalized spectral ordinates (amplifications) for rock are substantially lower than those for soft to medium clay and for deep cohesionless soil. This indicates that using the spectra from the latter two groups may overestimate the design amplifications for rock.

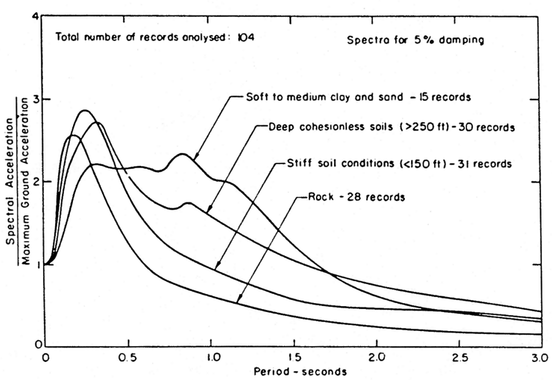

Figure 2-41. Average acceleration spectra for different soil conditions. [After Seed et al. (2-99).]

The study by Mohraz [2-53] considered a total of 162 components of earthquake records divided into four soil categories: alluvium, rock, less than 30 ft of alluvium underlain by rock, and 30 - 200 ft of alluvium underlain by rock. Figure 2-43 presents the average acceleration amplifications (ratio of spectral ordinates to peak ground acceleration) for 2% damping for the horizontal components with the larger of the two peak ground accelerations. Consistent with the study by Seed et al. [2-99], the figure shows that soil condition influences the spectral shapes to a significant degree. The acceleration amplification for alluvium extends over a larger frequency region than the amplifications for the other three soil categories. A comparison of acceleration amplifications for 5% damping from the Seed and Mohraz studies is shown in Figure 2-44. The figure indicates a remarkably close agreement even though the records used in the two studies are somewhat different. Normalized response spectra corresponding to the mean plus one standard deviation (84.1 percentile) for the four soil categories from the Mohraz study are given in Figure 2-45. The plot indicates that for short periods (high frequencies) the spectral ordinates for alluvium are lower than the others, whereas, for intermediate and long periods they are higher.

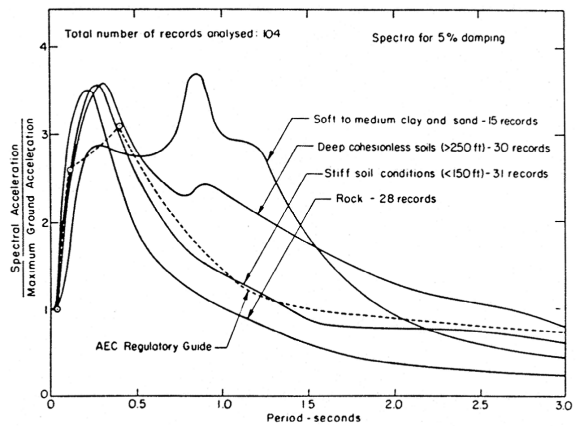

Figure 2-42. Mean plus one standard deviation acceleration spectra for different soil conditions. [After seed et al. (2-99).]

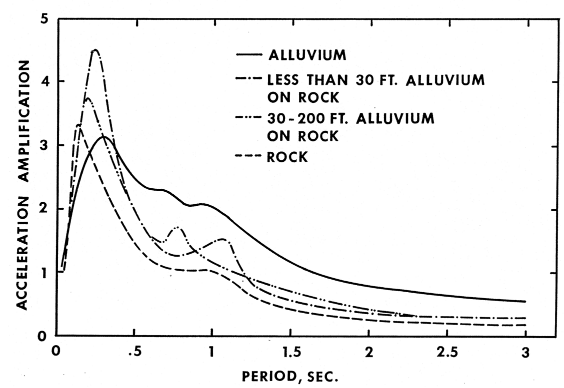

Figure 2-43. Average horizontal acceleration amplifications for 2% damping for different soil categories. [After Mohraz (2-53).]

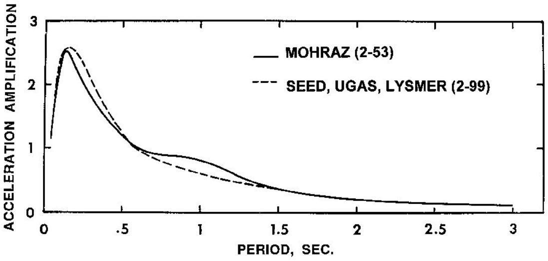

Figure 2-44. Comparison of the average horizontal acceleration amplifications for 5% damping for rock. [After Mohraz (2-53).]

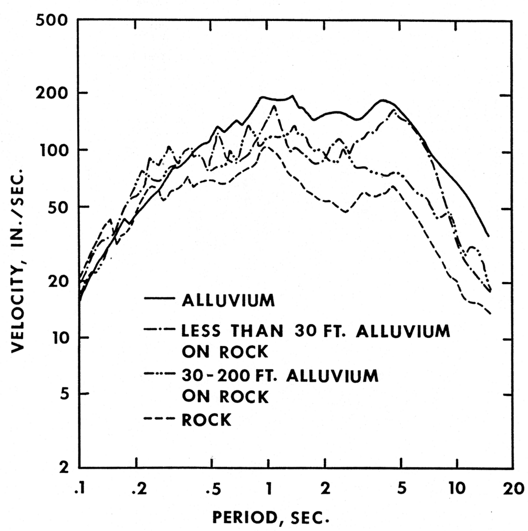

Figure 2-45. Mean plus one standard deviation response spectra for 2% damping for different soil categories, normalized to 1.0*g* horizontal ground acceleration. [After Mohraz (2-53).]

Recent studies indicate that the spectral shape not only depends on the three peak ground motions, but also on other parameters such as earthquake magnitude, source-to-site distance, soil condition, and source characteristics. Similar to ground motion attenuation relationships (Section 2.4), several investigators have used statistical analysis of the spectra at different periods to develop equations for computing the spectral ordinates in terms of those parameters. For example, Crouse and McGuire [(2-101)] used 238 horizontal accelerograms from 16 earthquakes between 1933 and 1992 with surface wave magnitudes greater than 6 to formulate a relationship for pseudo-velocity in terms of various earthquake parameters. The response spectra for 5% damping were computed for four site categories; rock, soft rock or stiff soil, medium stiff soil, and soft soil classified as soil class A through D, respectively. A regression analysis was performed for periods in the range of 0.1 to 4.0 sec. Their proposed equation for the pseudo-velocity (*PSV*) in cm/sec is given as

$$\ln(PSV) = a + bM_s + d\ln[R + c_1 \exp(c_2 M_s)] + eF \tag{2-40}$$

where M_S is the surface wave magnitude, R is the closest distance from the site to the fault rupture in km, and F is the fault type parameter which equals 1 for reverse-slip and 0 for strike-slip earthquakes. The parameters a, b, c_1, c_2, d and e are given in tabular form for different periods and soil categories [(2-101)]. Parameters b, c_1, and c_2 are greater than zero whereas d is less than zero for all periods and different soil conditions. Figure 2-46 presents the spectral shapes for the four soil categories at a distance of 10 km from the source for a strike-slip earthquake of magnitude 7. The figure indicates higher spectral values for softer soils.

A similar study was carried out by Boore et al. [(2-37)] using the average shear wave velocity V_s (m/sec) in the upper 30 m of the surface to classify the soil condition. In their study, the pseudo-acceleration response *PSA* in *g* is given by

$$\ln(PSA) = b_1 + b_2(M_W - 6) + b_3(M_W - 6)^2 + b_5 \ln\sqrt{R_{jb}^2 + h^2} + b_v \ln\frac{V_s}{V_A} \tag{2-41}$$

where M_W and R_{jb} are the moment magnitude and distance (see section 2.4.1), respectively. The parameter b_1 is related to the fault type and is listed for different periods for strike-slip and reverse-slip earthquakes, and the case where the

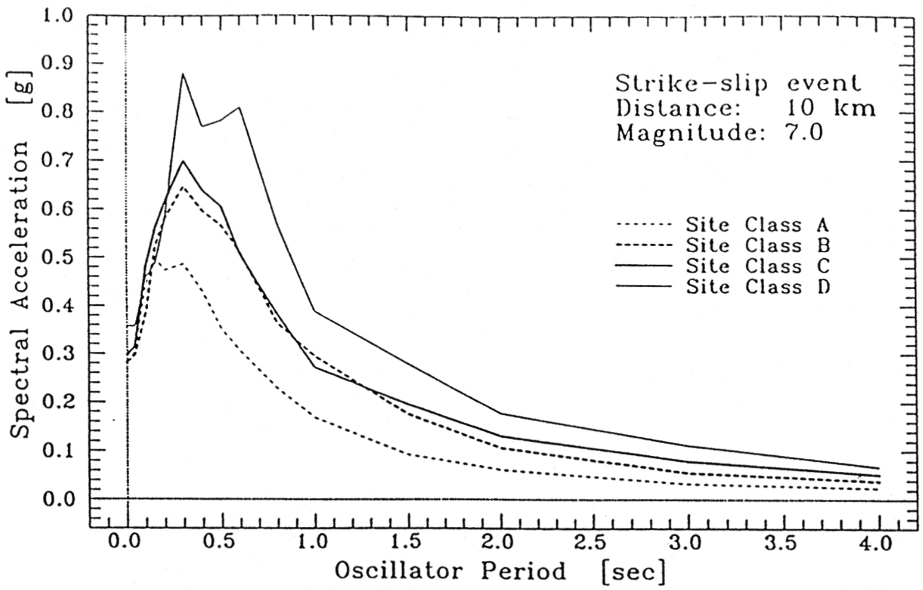

Figure 2- 46. Response spectra for 5% damping for different soil conditions for a magnitude 7 strike-slip earthquake. [After Crouse and McGuire (2-101).]

fault mechanism is not specified. Factors b_2, b_3, b_5, b_v, V_A, and h for different periods are also presented in tabular form [(2-37)]. The parameters b_2, V_A, and h are always positive whereas b_3, b_5, and b_v are always negative. Consistent with the study by Crouse and McGuire [(2-101)], Equation 2-41 indicates that, for the same distance, magnitude, and fault mechanism, as the soil becomes stiffer (a higher shear wave velocity), the pseudo-acceleration becomes smaller since b_v is always negative.

2.8.2 Magnitude

In the past, the influence of earthquake magnitude on response spectra was generally taken into consideration when specifying the peak ground acceleration at a site. Consequently, the spectral shapes and amplifications in Figures 2-41 and 2-42 were obtained independent of earthquake magnitude. Earthquake magnitude does, however, influence spectral amplifications to a certain degree. A study by Mohraz [(2-102)] on the influence of earthquake magnitude on response amplifications for alluvium shows larger acceleration amplifications for records with magnitudes between 6 and 7 than those with magnitudes between 5 and 6 (see Figure 2-47). While the study used a limited number of records and no specific recommendation was made, the figure indicates that earthquake magnitude can influence spectral shapes and may need to be considered when developing design spectra for a specific site.

Equations 2-40 and 2-41 in the previous section include the influence of earthquake magnitude on the pseudo-velocity and pseudo-acceleration, respectively. The equations indicate that spectral ordinates increase with an increase in earthquake magnitude. Figure 2-48 presents the spectral ordinates computed using Equation 2-41 by Boore et al. [(2-37)] for soil with a V_s = 310 m/sec at a zero source distance for earthquakes with magnitudes 6.5 and 7.5 and an unspecified fault mechanism. The figure indicates that the effect of magnitude is more pronounced at longer periods and it also shows a comparison with the spectra computed from an earlier study by Joyner and Boore [(2-32)].

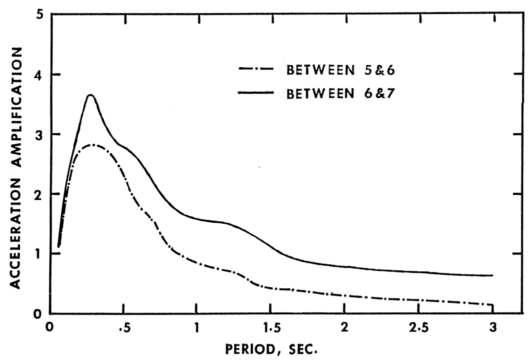

Figure 2-47. Effect of earthquake magnitude on spectral shapes. [After Mohraz (2-102).]

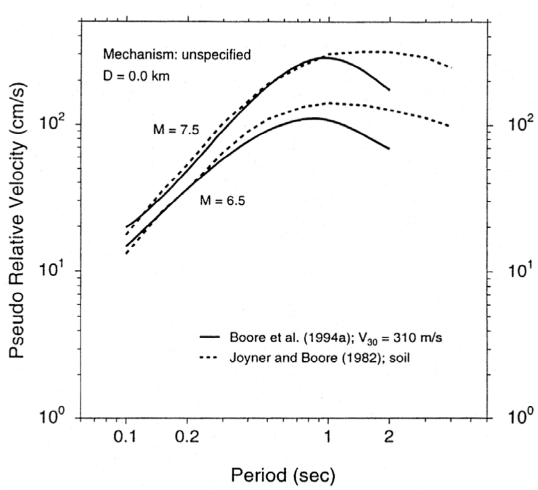

Figure 2-48. Pseudo-velocity spectra for 5% damping on soil and earthquake magnitudes 6.5 and 7.5 at a zero distance. [After Boore et al. (2-37).]

2.8.3 Distance

Recent studies have considered the effect of distance on the shape and amplitudes of the earthquake spectra. Using the data from the Loma Prieta earthquake of October 17, 1989; Mohraz (2-103) divided the records into three groups: near-field (distance less than 20 km), mid-field (distance between 20 to 50 km) and far-field (distance greater than 50 km). The average acceleration amplification (pseudo-acceleration divided by the peak ground acceleration) for the records on rock and on alluvium for the three groups are shown in Figure 2-49. The plots indicate that for sites on rock, the amplifications for the near-field are substantially smaller than those for mid- or far-field for periods longer than 0.5 sec. For shorter periods, however, the amplifications for the near-field are larger. The effect of distance is less pronounced for records on alluvium.

Equation 2-40 proposed by Crouse and McGuire (2-101) shows that the spectral ordinates decay with the logarithm of the distance (parameter *d* in the equation is always negative) for a given soil, earthquake magnitude, and source characteristics. A similar trend is also observed from Equation 2-41 by Boore et al. (2-37). Figure 2-50 shows the pseudo-velocity response computed using Equation 2-41 for sites on soil for a magnitude of 7.5 at various source distances for strike-slip and reverse-slip fault mechanisms. The figure indicates that the spectral ordinates decrease with distance. Since the spectral shapes are nearly parallel to each other for the distance range of 10 to 80 km, it may be concluded that distance does not significantly affect the spectral shape but influences the spectral ordinates through attenuation of ground acceleration.

2.8.4 Source characteristics

Fault mechanism may influence the spectral ordinates. Using Equation 2-40, Crouse and McGuire (2-101), computed the ratios of the spectral ordinates for a reverse-slip fault to ordinates for strike-slip fault for two soil categories: soft rock or stiff soil (site class B) and medium stiff soil (site class C). The ratios, plotted in Figure 2-51, show that the spectral ordinates for reverse-slip faults are greater than the ordinates for strike- slip faults for short periods but not for long periods. Crouse and McGuire concluded, however, that it is difficult to attach any significance on the influence of fault mechanism on the spectral shape. Similar trends and conclusion can also be depicted from

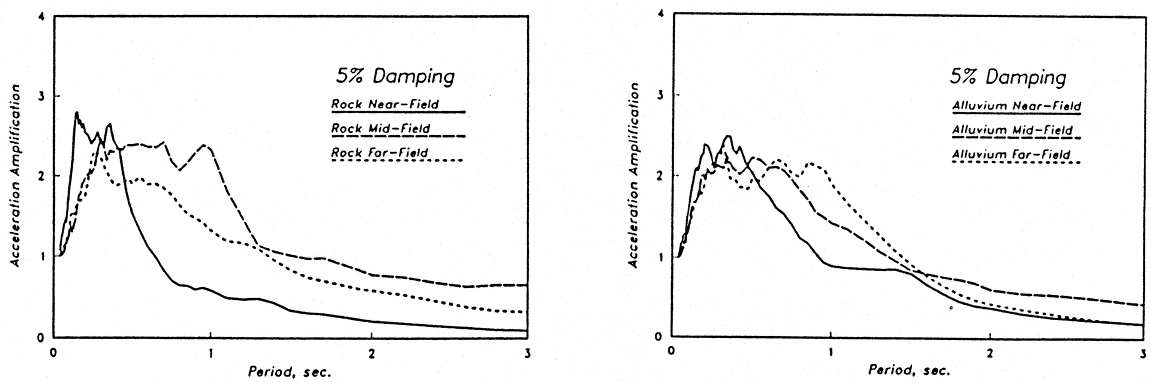

(a) (b)

Figure 2-49. Average acceleration amplification for 5% damping for different distances from the 1989 Loma Prieta earthquake for sites on (a) rock and (b) alluvium. [After Mohraz (2-103).]

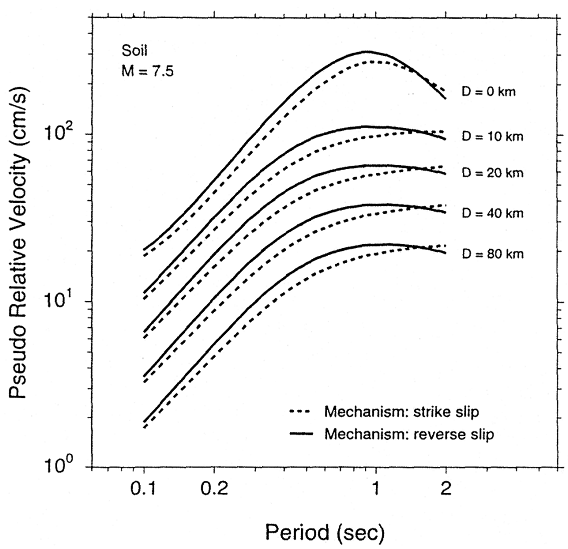

Figure 2-50. Pseudo-velocity spectra for 5% damping on soil and for earthquake magnitude 7.5 at different distances. [After Boore et al. (2-37).]

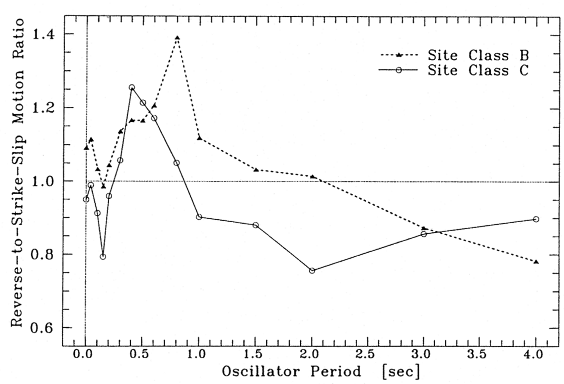

Figure 2-51. Ratio of reverse-slip to strike-slip spectral ordinates for soft rock or stiff soil referenced as site class B and medium stiff soil referenced as site class C. [After Crouse and McGuire (2-101).]

Figure 2-50 by Boore et al. [2-37] where the reverse-slip faults result in a larger response for short periods and the strike-slip faults result in a larger response for long periods. The difference between the response from the two fault mechanisms, however, is not that significant.

2.8.5 Duration

While earthquake response spectra provide the best quantitative description of the intensity and frequency content of ground motion, they do not provide information on the duration of strong shaking -- a parameter that many researchers and practitioners consider to be important in evaluating the damaging effects of an earthquake. The influence of the duration of strong motion on spectral shapes has been studied by Peng et al. [2-104] who used a random vibration approach to estimate site-dependent probabilistic response spectra. Their study shows that long durations of strong motion increase the response in the low and intermediate frequency regions. This is consistent with the fact that accelerograms with long durations have a greater probability of containing long-period wave components which can result in a large response in the long period or low frequency region of the spectrum.

2.9 EARTHQUAKE DESIGN SPECTRA

Because the detailed characteristics of future earthquakes are not known, the majority of earthquake design spectra are obtained by averaging a set of response spectra from records with similar characteristics such as soil condition, epicentral distance, magnitude, source mechanism, etc. For practical applications, design spectra are presented as smooth curves or straight lines. Smoothing is carried out to eliminate the peaks and valleys in the response spectra that are not desirable for design because of the difficulties encountered in determining the exact frequencies and mode shapes of structures during severe earthquakes when the structural behavior is most likely nonlinear. It should be noted that in some cases, determining the shape of the design spectra for a particular site is complicated and caution should be used in arriving at a representative set of records. For example, long period components of strong motion have a pronounced effect on the response of flexible structures. Recent strong motion data indicates that long period components are influenced by factors such as distance, source type, rupture propagation, travel path, and local soil conditions [2-50, 2-105, 2-106]. In addition, the direction and spread of rupture propagation can affect motion in the near-field. For these reasons, the selection of an appropriate set of records in arriving at representative design spectra is important and may require selection of different sets of records for different regions of the spectrum.

The difference between response spectra and design spectra should be kept in mind. A response spectrum is a plot of the maximum response of a damped SDOF oscillator with different frequencies or periods to a specific ground motion, whereas a smooth or a design spectrum is a specification of seismic design force or displacement of a structure having a certain frequency or period of vibration and damping [2-107].

Since the peak ground acceleration, velocity, and displacement for various earthquake records differ, the computed response cannot be averaged on an absolute basis. Various procedures are used to normalize response spectra before averaging is carried out. Among these procedures, two have been most commonly used: 1) normalization according to spectrum intensity [2-108] where the areas under the spectra between two given frequencies or periods are set equal to each other, and 2) normalization to peak ground motion where the spectral ordinates are divided by peak ground acceleration, velocity, or displacement for the corresponding region of the spectrum. Normalization to other parameters such as effective peak acceleration and effective peak velocity-related acceleration has also been suggested and used in development of design spectra for seismic codes.

Table 2-10. Relative Values of Spectrum Amplification Factors (after Newmark and Hall, 2-90)

Percent of Critical Damping	Amplification Factor for		
	Displacement	Velocity	Acceleration
0	2.5	4.0	6.4
0.5	2.2	3.6	5.8
1	2.0	3.2	5.2
2	1.8	2.8	4.3
5	1.4	1.9	2.6
7	1.2	1.5	1.9
10	1.1	1.3	1.5
20	1.0	1.1	1.2

The first earthquake design spectrum was developed by Housner [2-109, 2-110]. His design spectra shown in Figure 2-52 are based on the characteristics of the two horizontal components of four earthquake ground motions recorded at El Centro, California in 1934 and 1940, Olympia, Washington in 1949, and Taft, California in 1952. The plots are normalized to 20% acceleration (0.2g) at zero period (ground acceleration). For any other acceleration, the plots or the information read from them are simply scaled up or down by multiplying them by the ratio of the desired acceleration to 0.2g.

In the late sixties, Newmark and Hall [2-89, 2-90] recommended straight lines be used to represent earthquake design spectra. They suggested that three amplifications (acceleration, velocity, and displacement) which are constant in the high, intermediate, and low frequency regions of the spectrum (Table 2-10) together with peak ground acceleration, velocity, and displacement of 1.0g, 48 in/sec, and 36 in. be used to construct design spectra. Their recommended ground motions and the amplifications were based on

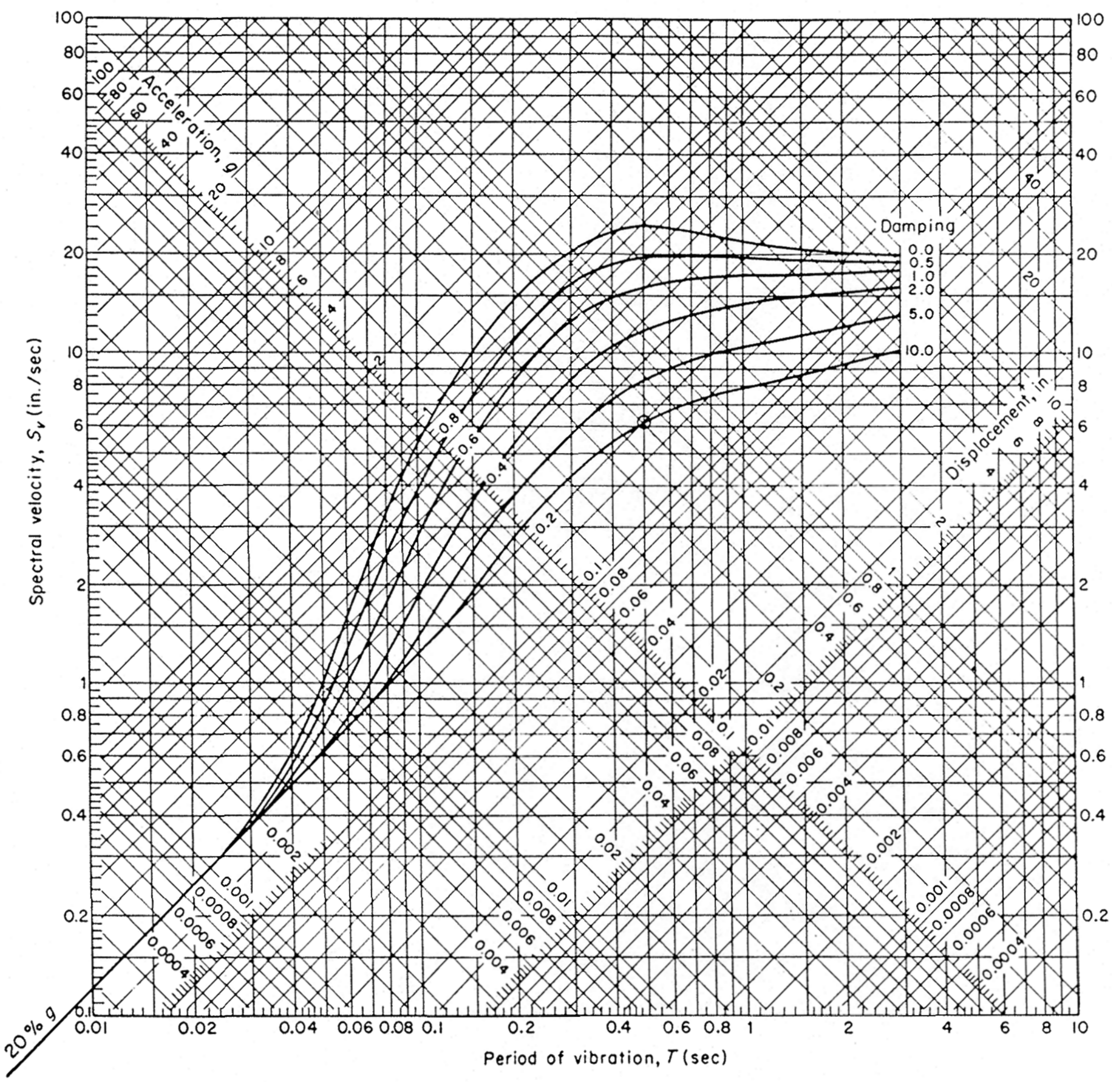

Figure 2-52. Design spectra scaled to 20% ground acceleration. [After Housner (2-110).]

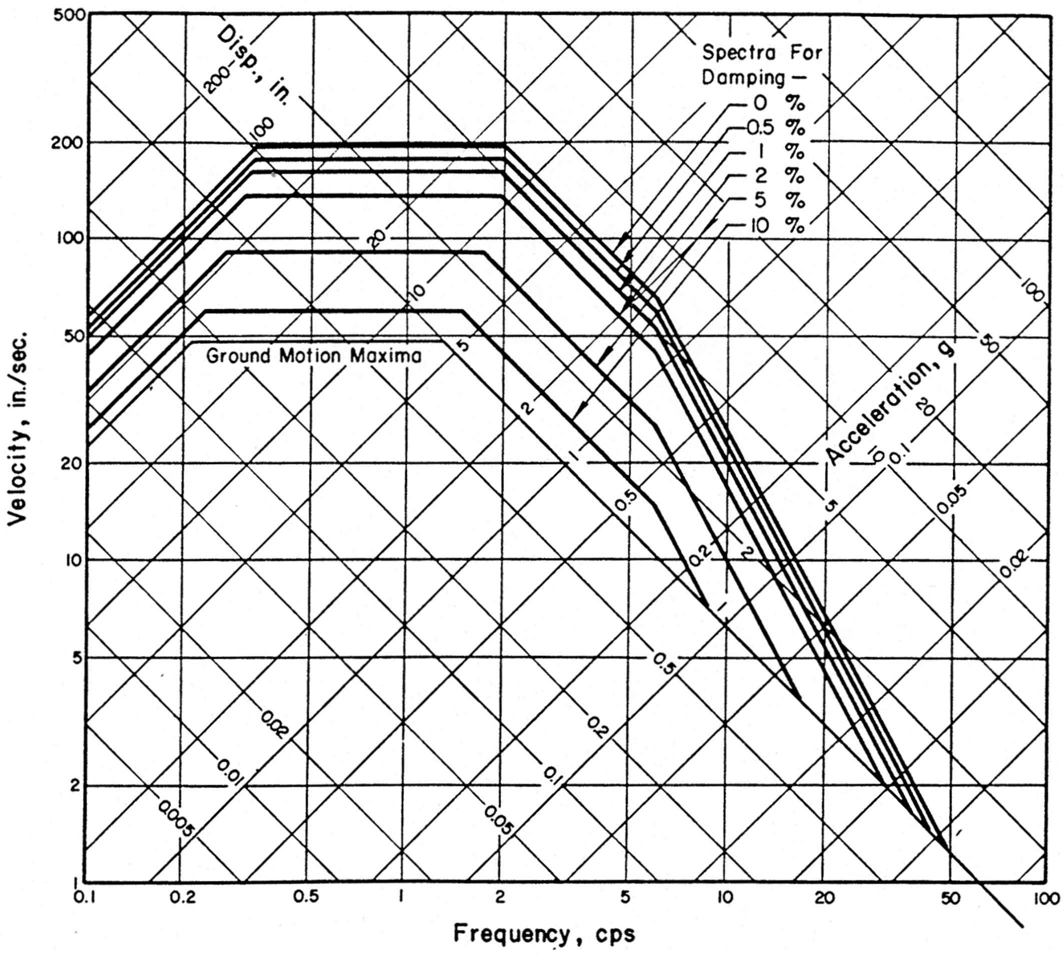

Figure 2-53. Design spectra normalized to 1.0*g*. [After Newmark and Hall (2-90).]

the characteristics of several earthquake records without considering soil condition. The spectral ordinates which are obtained by multiplying the three ground motions by the corresponding amplifications are plotted on a tripartite (four-way logarithmic) paper as shown in Figure 2-53. The spectral displacement, spectral velocity, and spectral acceleration are plotted parallel to maximum ground displacement, ground velocity, and ground acceleration, respectively. The frequencies at the intersections of spectral displacement and velocity, and spectral velocity and acceleration define the three amplified regions of the spectrum. At a frequency of approximately 6 Hz, the spectral acceleration is tapered down to the maximum ground acceleration. It is assumed that the spectral acceleration for 2% damping intersects the maximum ground acceleration at a frequency of 30 Hz. The tapered spectral acceleration lines for other dampings are parallel to the one for 2%. The normalized design spectra in Figure 2-53 can be used for design by scaling the ordinates to the desired acceleration.

In the early seventies with increased activity in the design and construction of nuclear power plants in the United States, the Atomic Energy Commission AEC (later renamed the Nuclear

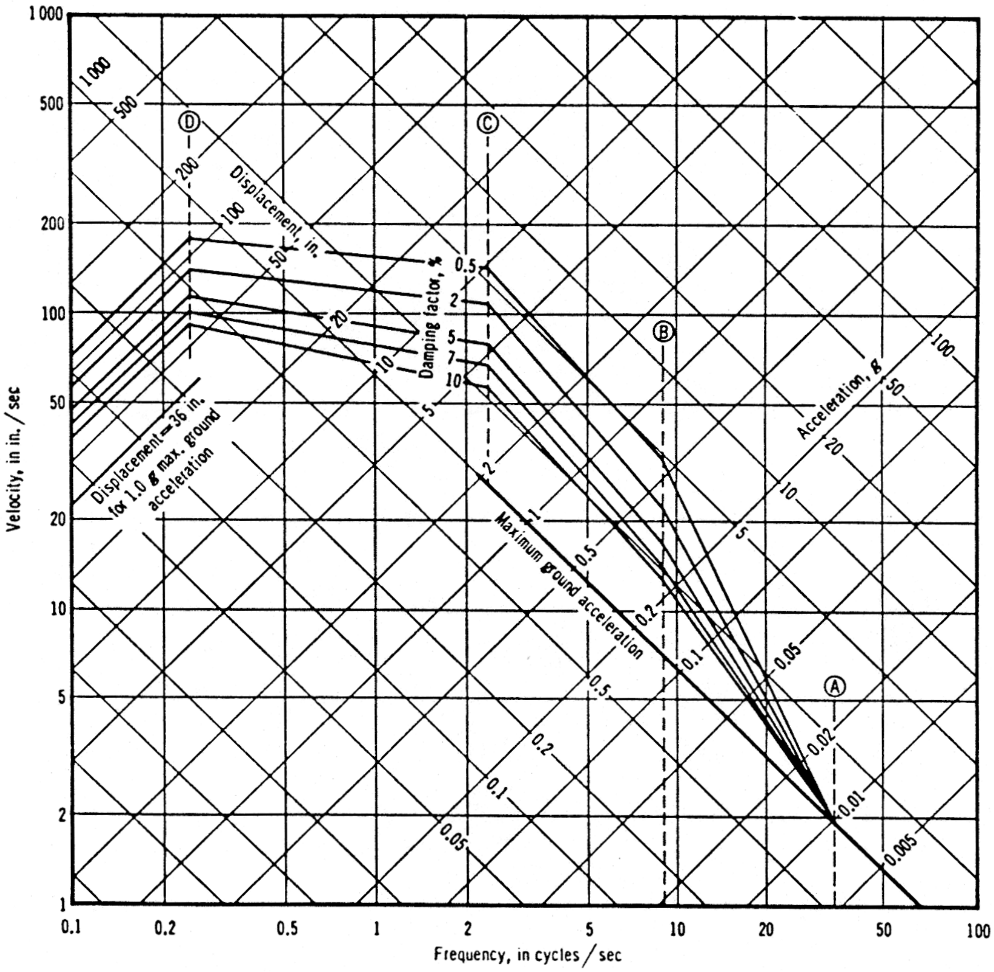

Figure 2-54. NRC horizontal design spectra scaled to 1.0*g* ground acceleration. A, B, C, and D are control frequencies corresponding to 33, 9, 2.5, and 0.25 HZ, respectively.

Regulatory Commission) funded two studies - one by John A. Blume and Associates (2-111) and the other by N. M. Newmark Consulting Engineering Services (2-9) to develop recommendations for horizontal and vertical design spectra for nuclear power plants. These studies which used a statistical analysis of a number of recorded earthquake ground motions and computed response spectra were the basis for the Nuclear Regulatory Commission (NRC) Regulatory Guide 1.60 (2-88, 2-100). The studies recommended that the mean plus one standard deviation (84.1 percentile) response be used for the design of nuclear power plants and equipment. The NRC design spectra are constructed using a set of amplifications corresponding to four control frequencies (Figure 2-54). The spectra are normalized to 1.0*g* horizontal ground acceleration. While the NRC spectra were developed for design of nuclear power plants, they were also used to develop and compare design spectra for other applications.

In 1978, the Applied Technology Council ATC (2-74) recommended a smooth version of the normalized spectral shapes proposed by

Seed et al. [2-99] be used in developing earthquake design spectra for buildings. The spectral shapes in Figures 2-41 and 2-42 were smoothed using four control periods [2-39]. In addition, the four soil categories were reduced to three: rock and stiff soils (soil type 1), deep cohesionless or stiff clay soils (soil type 2), and soft to medium clays and sands (soil type 3). The ATC spectra which was adopted by the Seismology Committee of the Structural Engineers Association of California, SEAOC [2-112] is presented in Figure 2-55. A comparison of the spectral shapes from the study by Mohraz [2-53] and those proposed by ATC is shown in Figure 2-56. The 1985, 1988, 1991, and 1994 editions of the Uniform Building Code [2-82 to 2-85] use the spectral shapes for the three soil conditions recommended by ATC. The design spectra for a given site is computed by multiplying the spectral shapes in Figure 2-55 by the seismic zone factor Z (or the effective peak acceleration) obtained from the seismic maps.

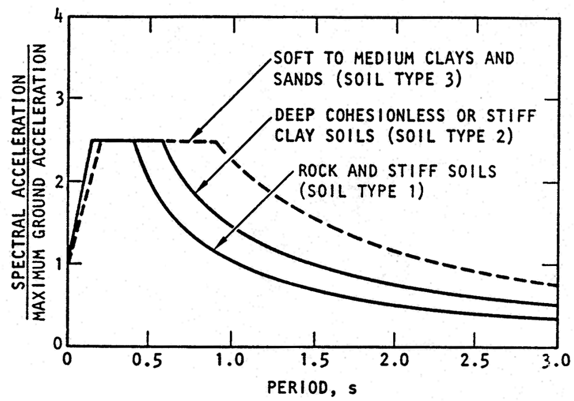

Figure 2-56. Normalized spectral curves recommended for use in building codes. (Reproduced from 2-39).

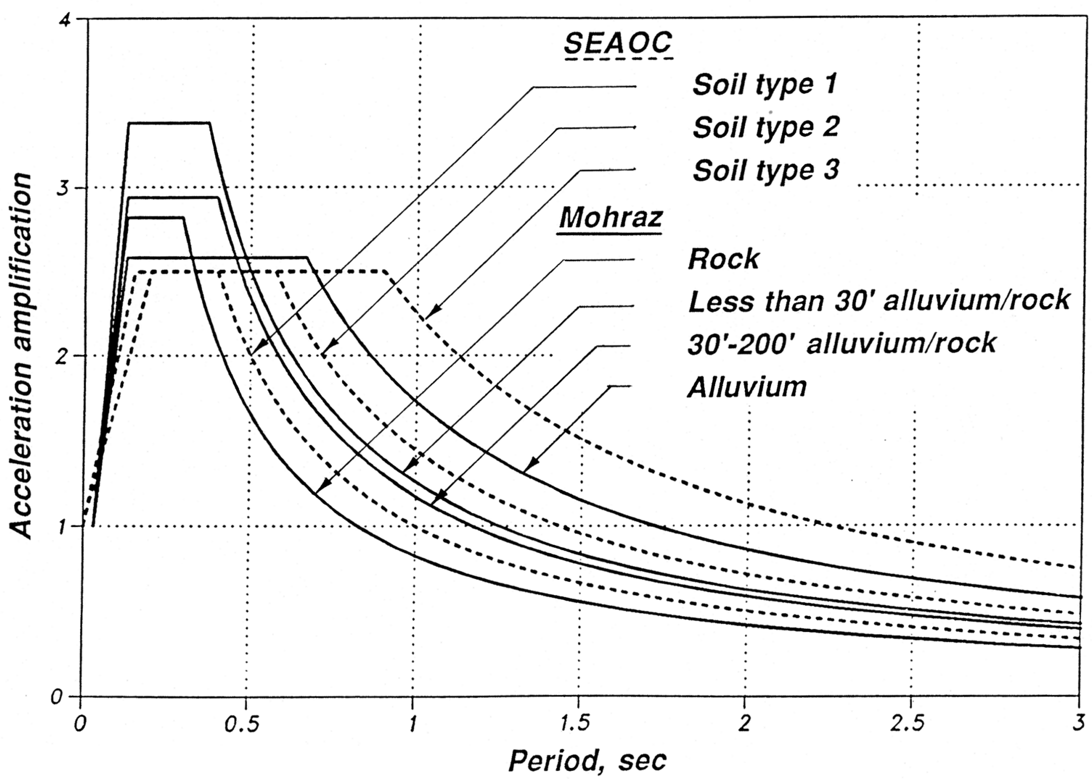

Figure 2-55. Comparison of spectral shapes for 5% damping proposed by Mohraz with those recommended by SEAOC.

The 1985, 1988, and 1991 NEHRP recommended provisions (2-76 to 2-78) present design spectra using the effective peak acceleration A_a and the effective peak velocity-related acceleration A_v. These two factors which are obtained from seismic maps are used to define the constant acceleration and velocity segments of the design spectrum, respectively. Since A_a and A_v for the vast majority of the sites in the United States are the same, the computed spectra are similar to the UBC spectra. While the 1985 NEHRP provisions included the three soil categories defined by ATC (2-74), the 1988 NEHRP provisions (2-77) and the 1988 Uniform Building Code (2-83) included a fourth soil category S_4 based on the experience from the Mexico City earthquake of September 19, 1985 where most of the underlying soil is very soft[5]. Flexible structures (periods in the neighborhood of 2 sec) in that earthquake experienced large acceleration amplifications which resulted in severe and widespread damage. Consequently, it was recommended to compute the spectral shape in the velocity region from that of rock using an amplification of 2.

A new procedure for constructing design spectra and computing the base shears was recommended in the 1991 NEHRP provisions (2-78) by obtaining the spectral acceleration ordinates at periods of 0.3 and 1.0 sec from the spectral maps (see Section 2.5). The ordinate at 0.3 sec is used for the constant acceleration zone whereas the ordinate at 1.0 sec is divided by the period T for the velocity zone. The spectral ordinates from the maps are modified according to the soil category of the site. The maps in the 1991 NEHRP provisions were provided for the soil category S_2 (deep cohesionless or stiff clay soils). The provisions recommended that the spectral ordinates corresponding to the 1.0 sec period be reduced by a factor of 0.8 for soil type S_1 and amplified by factors of 1.3 and 1.7 for soil types S_3 and S_4, respectively.

[5] the shaking was most intense within a region underlain by an ancient dry lake bed composed of soft clay deposits.

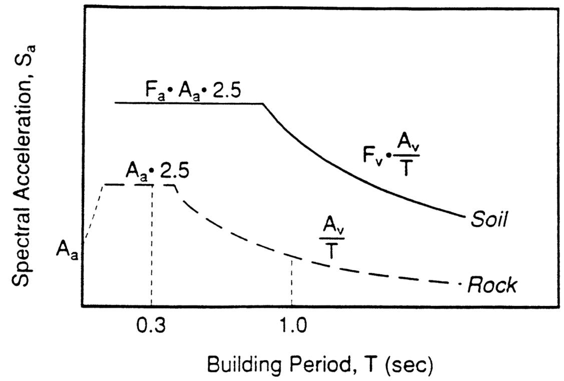

Figure 2-57. Two-factor approach for constructing site-dependent design spectra recommended by the 1994 NEHRP recommended provisions.

In 1992, a workshop on site response during earthquakes was held by the National Center for Earthquake Engineering Research (NCEER), the Structural Engineers Association of California (SEAOC), and the Building Seismic Safety Council (BSSC). The workshop (2-113) recommended that the spectral amplifications at different periods should depend not only on the soil condition but also on the intensity of shaking due to soil nonlinearities. Consequently, a two-factor approach was suggested for constructing the design spectra in order to account for the dependence of the spectral shape on the shaking intensity. The two-factor approach was introduced in the 1994 NEHRP provisions (2-79), see Figure 2-57. The approach uses new seismic coefficients C_a and C_v in terms of the effective peak acceleration A_a and the effective peak velocity-related acceleration A_v such that

$$C_a = A_a F_a \quad \text{and} \quad C_v = A_v F_v \tag{2-42}$$

where F_a and F_v are site amplification coefficients that vary according to soil condition and shaking intensity (seismic zone). The provisions included tables for computing coefficients F_a and F_v as well as C_a and C_v. Six soil categories, designated as A through F, were introduced in the provisions. The first five are based primarily on the average shear wave velocity[6] V_s (m/sec) in the upper 30 meters of the soil profile and the sixth is based on a site specific evaluation. The categories include: (A) hard rock (V_s > 1500), (B) rock (760 < $V_s \leq$ 1500), (C) very dense soil and soft rock (360 < $V_s \leq$ 760), (D) stiff soil profile (180 < $V_s \leq$ 360), (E) soft soil profile ($V_s \leq$ 180), and (F) soils requiring site-specific evaluations such as liquefiable and collapsible soils, sensitive clays, peats and highly organic clays, very high plasticity clays, and very thick soft/medium stiff clays.

The site coefficients F_a and F_v are based primarily on the work of Borcherdt [(2-114)] who used the strong motion data from the Loma Prieta earthquake of October 17, 1989 to compute average amplification factors normalized to firm to hard rock (NEHRP site class B) for short-periods (0.1-0.5 sec), intermediate-periods (0.5-1.5 sec), mid-periods (0.4-2.0 sec), and long-periods (1.5-5.0 sec). Data for ground accelerations of approximately 0.1g were used in an empirical procedure to find amplifications F_a and F_v. Amplification factors for ground accelerations greater than 0.1g (0.2g, 0.3g, and 0.4g) were computed by extrapolation of amplification estimates at 0.1g since few strong motion records were available for ground motions greater than 0.1g for soft soil. The extrapolations were based on results from laboratory experiments and numerical modeling. The amplifications were in good agreement with those computed by Seed et al. [(2-115)] based on a numerical modeling of the data from the Loma Prieta records and those by Dobry et al. [(2-116)] based on a parametric study of several hundred soil profiles.

The amplifications F_a and F_v corresponding to short- and mid- periods with respect to firm to hard rock for different shaking intensities are shown in Figure 2-58. The figure indicates that site amplifications decrease with an increase in shear wave velocity and an increase in ground accelerations. Borcherdt also presented the site amplifications in terms of the average shear wave velocity V_s in the upper 30 meters of the soil profile as:

$$
\begin{aligned}
F_a &= (V_0 / V_s)^{m_a} \\
F_v &= (V_0 / V_s)^{m_v}
\end{aligned}
\tag{2-43}
$$

Where V_O is the average shear wave velocity for a referenced soil profile (V_O = 1050 m/sec for firm to hard rock). Parameters m_a and m_v represent the influence of the ground motion intensity on amplification (see Figure 2-58). Substitution for V_O results in

$$
\begin{aligned}
F_a &= (1050 / V_s)^{m_a} \\
F_v &= (1050 / V_s)^{m_v}
\end{aligned}
\tag{2-44}
$$

The coefficients F_a and F_v recommended by Borcherdt were the basis for those presented in the 1994 NEHRP provisions by computing the coefficients for each site category by substituting the appropriate value for V_s. Borcherdt also provided values for the coefficients F_a and F_v for constructing design spectra in association with the spectral accelerations at periods of 0.3 and 1.0 sec. Since seismic maps for spectral accelerations are for deep cohesionless or stiff clay soils, the coefficients are presented with reference to soft to firm rocks and stiff clays. For this case, Equation 2-43 can be used to compute the coefficients F_a and F_v using a V_0= 450 m/sec.

After the Northridge earthquake of January 17, 1994, Borcherdt [(2-117)] computed coefficients F_a and F_v for accelerograms recorded on different soils in the Los Angeles area. The results indicate that the coefficients are in good agreement with those suggested in his earlier study [(2-114)] and also those included in the 1994 NEHRP provisions [(2-79)] for small shaking intensities. For large intensities, however, the coefficients computed from the Northridge data are greater than those recommended previously.

[6] in addition to the shear wave velocity, other parameters such as average standard penetration, undrained shear strength, and plasticity index are used in the classification.

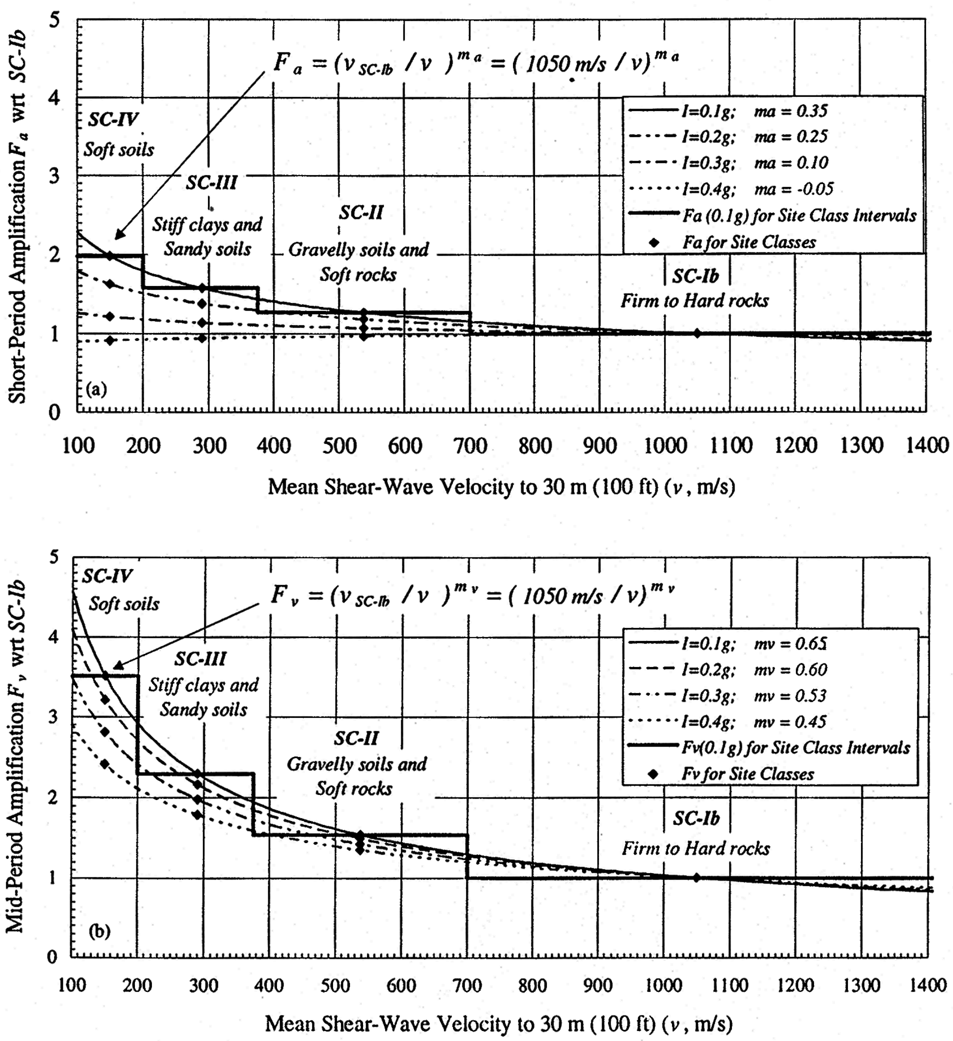

Figure 2-58. Variation of short-period F_a and long-period F_v amplification factors normalized to firm to hard rock with mean shear wave velocity. [After Borcherdt (2-114).]

The 1997 Uniform Building Code [(2-86)] used a method similar to that in the 1994 NEHRP provisions to construct the design spectrum. The design spectrum, Figure 2-59, is defined in terms of the seismic coefficients C_a and C_v. These coefficients are presented for the five UBC seismic zones for different soil categories, which are the same as those used in the 1994 NEHRP provisions. The only difference between the design spectra in the 1997 UBC code and the 1994 NEHRP provisions is that the former includes the near-source factors. These factors were introduced to amplify the spectral ordinates for sites close to a seismic source in the zone with the highest seismicity (zone 4). The near-source factors depend on the distance to the closest active fault and the source type (maximum magnitude, rate of seismic activity, and slip rate).

Design spectra presented in the 1997 NEHRP recommended provisions [(2-80)] can be constructed from the maps of spectral response accelerations at short periods S_S (defined as 0.2 sec) and at 1.0 sec period S_1 corresponding to the maximum considered earthquake (see Section 2.5). Since the maps are provided for rock (site class B), the spectral accelerations for other soil categories are adjusted by multiplying the spectral accelerations for rock by the site coefficients F_a and F_v in the short and the mid to long period ranges, respectively. Similar to the 1994 provisions, F_a and F_v depend on the soil category and the shaking intensity and are given in tabular form based on the study by Borcherdt [2-114]. To construct the spectra for the design earthquake, the adjusted spectral ordinates at the maximum considered earthquake are multiplied by 2/3 (see Section 2.5).

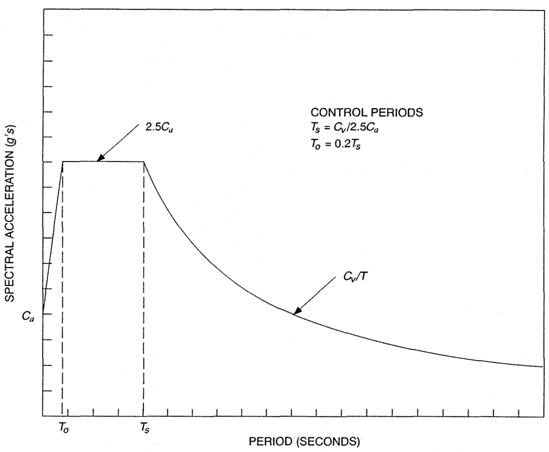

Figure 2-59. Design spectrum recommended by the 1997 Uniform Building Code (2-86).

The 1997 NEHRP Guidelines for the Seismic Rehabilitation of Buildings, FEMA-273 [2-81], uses a procedure similar to that of the 1997 NEHRP Provisions [2-80] to establish the 5% damped design spectra. In addition, FEMA-273 uses damping modification factors in the short- and long-period ranges to reduce the spectral ordinates for damping ratios larger than 5% due to the use of supplemental damping devices in the structure.

2.10 INELASTIC RESPONSE SPECTRA

Structures subjected to severe earthquake ground motion experience deformations beyond the elastic range. To a large extent, the inelastic deformations depend on the intensity of excitation and load-deformation characteristics of the structure and often result in stiffness deterioration. Because of the cyclic characteristics of ground motion, structures experience successive loadings and unloadings and the force-displacement or resistance-deformation relationship follows a sequence of loops known as hysteresis loops. The loops reflect a measure of a structure's capacity to dissipate energy. The shape and orientation of the hysteresis loops depend primarily on the structural stiffness and yield displacement. Factors such as structural material, structural system, and connection configuration influence the hysteretic behavior. Consequently, arriving at an appropriate mathematical model to describe the inelastic behavior of structures during earthquakes is a difficult task.

A simple model which has extensively been used to approximate the inelastic behavior of structural systems and components is the bilinear model shown in Figure 2-60. In this model, unloadings and subsequent loadings are assumed to be parallel to the original loading curve. Strain hardening takes place after yielding initiates. Elastic-plastic (elastoplastic) model is a special case of the bilinear model where the strain hardening slope is equal to zero (α = 0). Other hysteretic models such as stiffness and strength degrading have also been suggested. The elastic-plastic model results in a more conservative response than other models. Because of its simplicity, it was widely used in the development of inelastic response spectra.

Response spectra modified to account for the inelastic behavior, commonly referred to as the inelastic spectra, have been proposed by several investigators. The use of the inelastic spectra in analysis and design, however, has been limited to structures that can be modeled

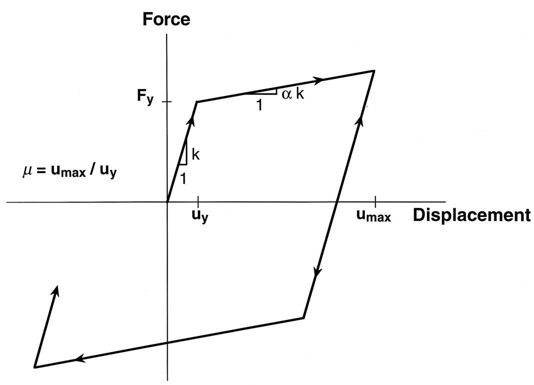

Figure 2-60. Bilinear force-displacement relationship.

as a single-degree-of-freedom. Procedures for utilizing inelastic spectra in the analysis and design of multi-degree-of-freedom systems have not yet been developed to the extent that can be implemented in design. Similar to elastic spectra, inelastic spectra were usually plotted on tripartite paper for a given damping and ductility[7] or yield deformation. When the spectra are plotted for various ductilities, computations are repeated for several yield deformations using an iterative procedure to achieve the target ductility. Depending on the parameter plotted, different names have been used to identify the spectrum (Riddell and

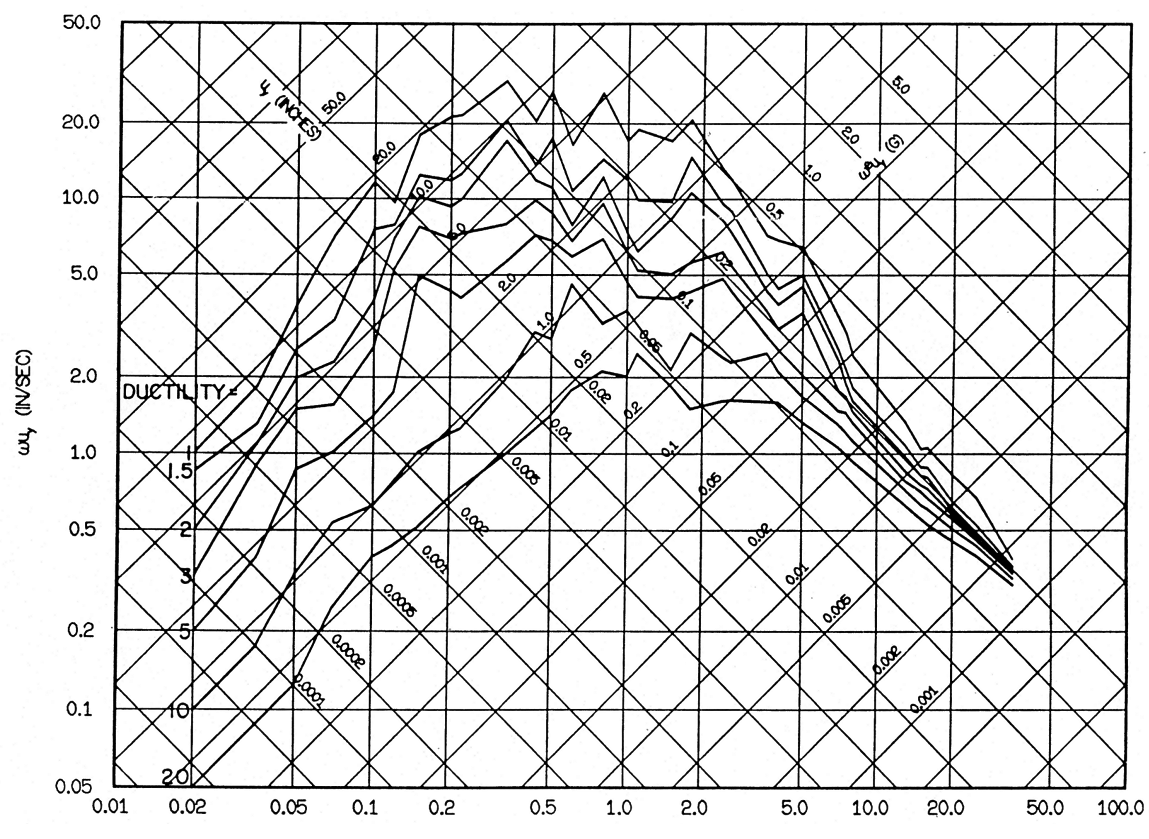

Figure 2-61. Inelastic yield spectra for the S90W component of El Centro, the Imperial Valley earthquake of May 18, 1940. Elastic-plastic systems with 5% damping. [After Riddell and Newmark (2-118).]

[7] ratio of maximum deformation to yield deformation

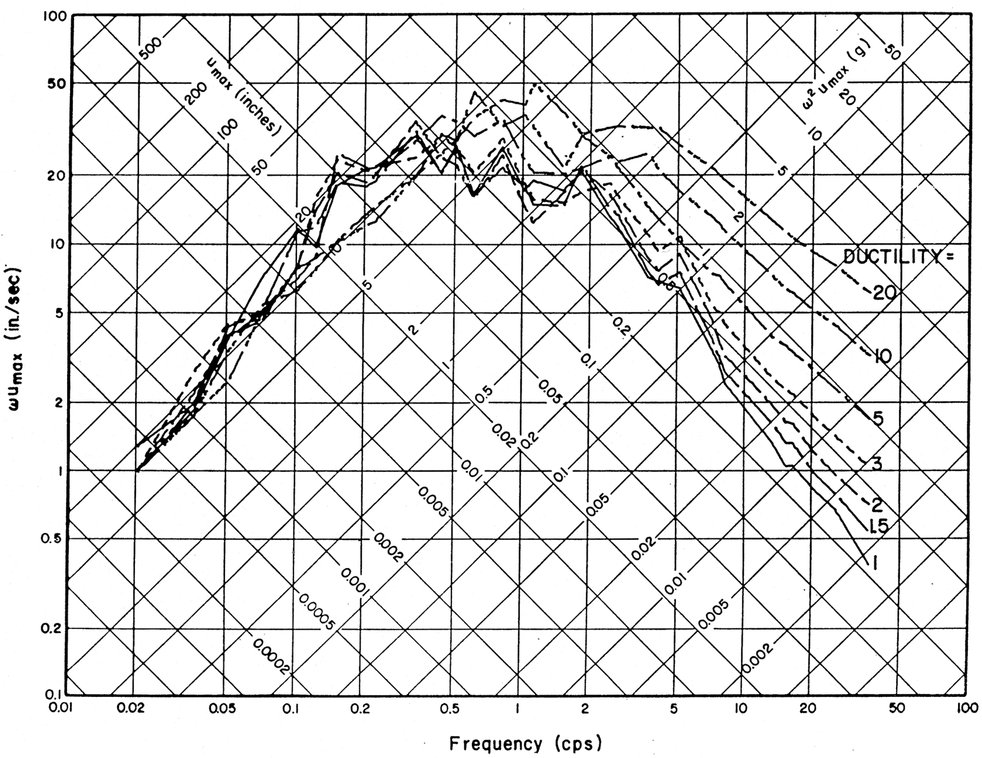

Figure 2-62. Total deformation spectra for the S90W component of El Centro, the Imperial Valley earthquake of May 18, 1940. Elastic-plastic systems with 5% damping. [After Riddell and Newmark (2-118).]

Newmark, 2-118). In the inelastic yield spectrum (IYS), the yield displacement is plotted on the displacement axis; in the inelastic acceleration spectrum (IAS), the maximum force per unit mass is plotted on the acceleration axis; and in the inelastic total displacement spectrum (ITDS), the absolute maximum total displacement is plotted on the displacement axis. For elastic-plastic behavior, the inelastic yield spectrum and the inelastic acceleration spectrum are identical. Examples of inelastic spectra for a 5% damped elastic-plastic system for the S90W component of El Centro, the Imperial Valley earthquake of May 18, 1940 are shown in Figures 2-61 and 2-62. The figures indicate that for inelastic yield and acceleration spectra, the curves for various ductilities fall below the elastic curve (ductility of one), whereas for the inelastic total deformation spectra, they primarily fall above the elastic, particularly in the acceleration region. It should be noted that increasing the ductility ratio smoothes the spectra and minimizes the sharp peaks and valleys that are present in the plots.

A different presentation of inelastic spectra was proposed by Elghadamsi and Mohraz (2-119). The spectrum, referred to as the yield displacement spectrum (YDS), is plotted similar to the inelastic total deformation spectrum except that it is plotted for a given yield displacement instead of a given ductility. The ductility is obtained as the ratio of the maximum displacement to the yield displacement for which the spectrum is plotted. Their procedure offers an efficient computational technique, particularly when statistical studies are used to obtain inelastic design spectra.

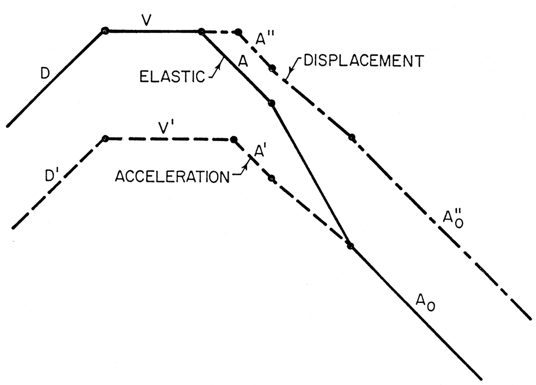

Figure 2-63. Construction of inelastic acceleration and inelastic total displacement spectra from the elastic spectrum. [After Newmark and Hall (2-89).]

Before the Riddell-Newmark study of inelastic response, the most common procedure for estimating inelastic earthquake design spectra was the one proposed by Newmark [(2-120, 2-121)] and Newmark and Hall [(2-89)]. Based on results similar to those in Figures 2-61 and 2-62, and studies by Housner [(2-122)] and Blume [(2-123 to 2-125)], Newmark [(2-121)] observed that: 1) at low frequencies, an elastic and an inelastic system have the same total displacement, 2) at intermediate frequencies, both systems absorb the same total energy, and 3) at high frequencies, they have the same force. These observations resulted in the recommendation by Newmark for constructing inelastic spectra from the elastic by dividing the ordinates of the elastic spectrum by two coefficients in terms of ductility μ. Figure 2-63 shows the construction of the inelastic spectrum from the elastic. The solid lines DVAA$_O$ represent the elastic response spectrum. The solid circles at the intersections of the lines correspond to frequencies which remain constant in obtaining the inelastic spectrum. The lines D'V'A'A$_O$ represent the inelastic acceleration spectrum whereas the lines DVA"A$_O$" show the total displacement spectrum. D' and V' are obtained by dividing D and V by μ. A' is obtained by dividing A by $\sqrt{(2\mu-1)}$ (to insure that the same energy is absorbed by the elastic and the inelastic systems). A" and A$_O$ are obtained by multiplying A' and A$_O$ by μ.

The Riddell-Newmark study [(2-118)] also considered bilinear and stiffness degrading models and concluded that using the elastic-plastic spectrum for inelastic analysis is generally on the conservative side.

2.10.1 De-amplification factors

When inelastic deformations are permitted in design, the elastic forces can be reduced if adequate ductility is provided. Riddell and Newmark [(2-118)] presented a set of coefficients referred to as “de-amplification factors” by which the ordinates of the elastic design spectrum are multiplied to obtain the inelastic yield spectrum. Lai and Biggs [(2-126)], using artificial accelerograms with variable durations of strong motion, presented a set of coefficients referred to as “inelastic acceleration response ratios” by which the ordinates of the elastic spectrum are divided to give the inelastic yield spectrum. Since these two approaches are the inverse of one another, the reciprocal of the Lai-Biggs coefficients represent de-amplification factors. De-amplification factors can also be obtained from the Newmark-Hall [(2-89)] and from the Elghadamsi-Mohraz [(2-119)] procedures for estimating inelastic spectra. Comparisons of the de-amplification factors from the four procedures are shown in Figure 2-64 for a 5% damping ratio and ductilities of 2 and 5. The figure indicates that the Riddell-Newmark de-amplification factors are in general the smallest (largest reduction in the elastic force) compared to the other three. Both Riddell-Newmark and Newmark-Hall de-amplification ratios remain constant over certain frequency segments, whereas those from Lai-Biggs and Elghadamsi-Mohraz follow parallel patterns. While the de-amplification ratios are affected by ductility, they are practically not influenced by damping. Since the elastic spectral ordinates decrease significantly with an increase in damping, the decrease in inelastic spectral ordinates with

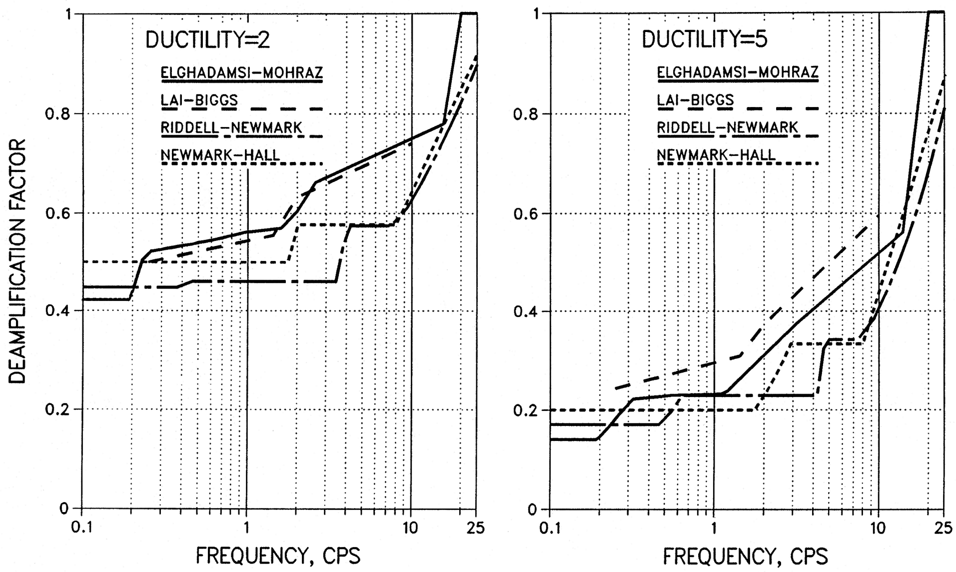

Figure 2-64. Comparison of de-amplification factors for 5% damping. [After Elghadamsi and Mohraz (2-119).]

damping stems primarily from the elastic spectral ordinates.

Elghadamsi and Mohraz (2-119) also presented de-amplification factors for alluvium and rock. Typical de-amplification factors for alluvium and rock for 5% damping is presented in Figure 2-65. According to the figure, de-amplifications are not significantly affected by the soil condition.

The influence of the duration of strong motion on the inelastic behavior of structures has also been studied. In a non-deterministic study of nonlinear structures, Penzien and Liu (2-127) concluded that structures with elastic-plastic and stiffness degrading behavior are more sensitive to the duration of strong motion than elastic structures. Using a random vibration approach and the extreme value theory, Peng et al. (2-128) incorporated the duration of strong motion in estimating the maximum response of structures with elastic-plastic behavior. The effect of duration of strong motion on de-amplification factors from Peng's study is shown in Figure 2-66 which indicates that for a longer duration of strong motion, one should use a larger de-amplification (smaller reduction in elastic force). It should be noted that Lai and Biggs (2-126) conclude that inelastic response spectra are not significantly affected by strong motion duration. They emphasize, however, that this conclusion is valid only when ground motion with varying strong motion durations are compatible with the same prescribed elastic response spectrum.

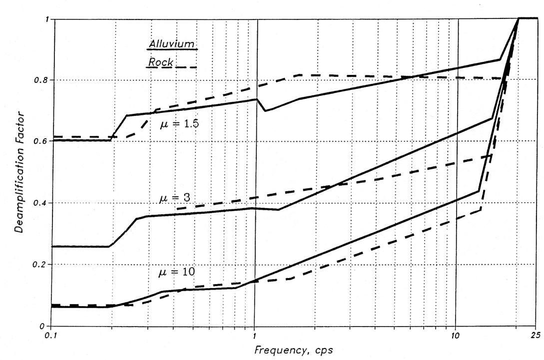

Figure 2-65. De-amplification factors for alluvium and rock for 5% damping. [After Elghadamsi and Mohraz (2-119).]

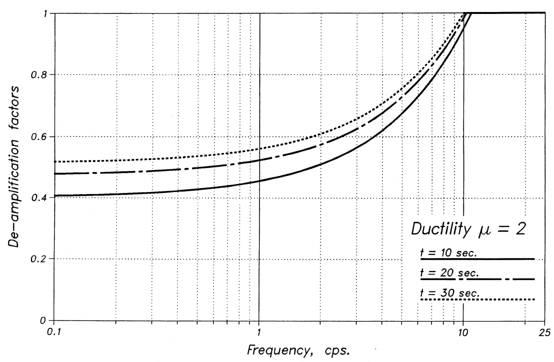

Figure 2-66. Effect of strong motion duration on de-amplification factors for systems with 2% damping. [After page et al. (1-128).]

2.10.2 Response modification factors

Current seismic codes recommend force reduction factors and displacement amplification factors to be used in design to account for the energy absorption capacity of structures through inelastic action. The force reduction factors (referred to as R-factors) are used to reduce the forces computed from the elastic design spectra. A recent study by the Applied Technology Council [2-129] proposes the following expression for computing the R-factors:

$$R = \frac{V_e}{V} = R_s\ R_\mu\ R_R \qquad (2\text{-}45)$$

Where V_e is the base shear computed from the elastic response (elastic design spectrum), and V is the design base shear for the inelastic response. The response modification factor R is the product of the following terms:

1. the period-dependent strength factor R_s which accounts for the reserve strength of the structure in excess of the design strength,
2. the period-dependent ductility factor R_μ which accounts for the ductile capacity of the structure in the inelastic range, and
3. the redundancy factor R_R which accounts for the reliability of seismic framing systems that use multiple lines of framing in each principal direction of the building.

The ductility factor R_μ is defined as the ratio of the elastic to the inelastic displacement for a system with an elastic fundamental period T and specified ductility μ such that

$$R_\mu(T,\mu) = \frac{u_y(T,\mu=1)}{u_y(T,\mu)} \qquad (2\text{-}46)$$

where u_y is the yield displacement. Stated differently, R_μ is the ratio of the maximum inelastic force to the yield force required to limit the maximum inelastic response to a displacement ductility μ, or the inverse of the de-amplification factors presented in Section 2.10.1.

The relationship between displacement ductility and ductility factor has been the subject of several studies in recent years. Earlier studies by Newmark and Hall [2-87, 2-89] provided expressions for estimating the ductility factor R_μ for elastic-plastic systems irrespective of the soil condition. The expressions are

$$R_\mu(T \le 0.03\,\text{sec},\mu) = 1.0$$
$$R_\mu(0.12\,\text{sec} \le T \le 0.5\,\text{sec},\mu) = \sqrt{2\mu - 1} \qquad (2\text{-}47)$$
$$R_\mu(T \ge 1.0\,\text{sec},\mu) = \mu$$

A linear interpolation may be used to estimate R_μ for the intermediate periods. The expressions are plotted in Figure 2-64 for ductility ratios of 2 and 5.

Using a statistical study of 15 ground motion records from earthquakes with magnitudes 5.7 to 7.7, Krawinkler and Nassar [2-130, 2-131] developed relationships for estimating R_μ for rock or stiff soils for 5% damping. Their proposed relationship is

$$R_\mu(T,\mu) = [c(\mu - 1) + 1]^{1/c} \qquad (2\text{-}48)$$

where

$$c = \frac{T^a}{1+T^a} + \frac{b}{T} \tag{2-49}$$

and a and b are parameters that depend on the strain hardening ratio α. They recommend a = 1.00, 1.01, and 0.80 and b = 0.42, 0.37, and 0.29 for strain hardening ratios of 0% (elasto plastic system), 2%, and 10%, respectively.

Miranda and Bertero (2-132) using 124 accelerograms recorded on different soil conditions, developed equations for estimating R_μ for rock, alluvium, and soft soil for 5% damping. Their equation is given by

$$R_\mu(T,\mu) = \frac{\mu - 1}{\Phi} + 1 \tag{2-50}$$

where

$$\Phi(T,\mu) = 1 + \frac{1}{T(10-\mu)} - \frac{1}{2T}\exp[-1.5(\ln T - 0.6)^2]$$

for rock sites

$$\Phi(T,\mu) = 1 + \frac{1}{T(12-\mu)} - \frac{2}{5T}\exp[-2(\ln T - 0.2)^2]$$

for alluvium sites

$$\Phi(T,\mu) = 1 + \frac{T_g}{3T} - \frac{3T_g}{4T}\exp[-3(\ln \frac{T}{T_g} - 0.25)^2]$$

for soft soil sites

(2.51)

and T_g is the predominant period of the ground motion defined as the period at which the relative velocity of a linear system with 5% damping is maximum throughout the entire period range. A comparison of the Nassar-Krawinkler and Miranda-Bertero relationships for rock and alluvium for ductility ratios of 2, 4, and 6 is presented in Figure 2-67. The figure shows that the differences between these relationships are relatively small and may be ignored for engineering purposes.

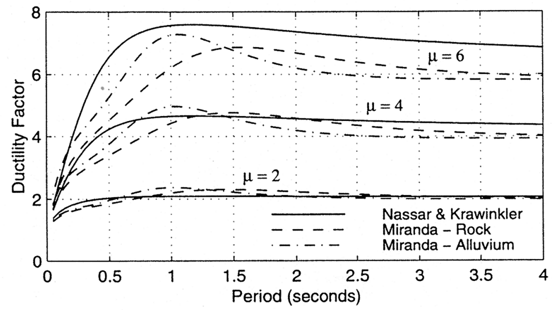

Figure 2-67. Variation of the ductility factor with period for ductility ratios of 2, 4, and 6. [Reproduced from ATC-19 (2-129).]

2.11 ENERGY CONTENT AND SPECTRA

While the linear and nonlinear response spectra, presented in previous sections, have been used for decades to compute design displacements and accelerations as well as base shears, they do not include the influences of strong motion duration, number of response cycles and yield excursions, stiffness and strength degradation, or damage potential to structures. There is a need to re-examine the current analysis and design procedures; especially with the use of innovative protective systems such as seismic isolation and passive energy dissipation devices. In particular, the concept of energy-based design is appealing where the focus is not so much on the lateral resistance of the structure but rather on the need to dissipate and/or reflect seismic energy imparted to the structure. In addition, energy approach is suitable for implementation within the framework of performance-based design since the premise behind the energy concept is that earthquake damage is related to the structure's ability to dissipate energy.

Housner (2-122) was the first to recommend energy approach for earthquake resistant design. He pointed out that ground motion transmits energy into the structure; some of this energy is dissipated through damping and nonlinear behavior and the remainder stored in the structure in the form of kinetic and elastic strain energy. Housner approximated the input energy as one-half of the product of the mass and the square of the pseudo-velocity, $1/2\,m(PSV)^2$. His study provided the impetus for later developments of energy concepts in earthquake engineering.

For a nonlinear SDOF system with pre-yield frequency and damping ratio of ω and β, respectively; subjected to ground acceleration *a(t)* the equation of motion is given by:

$$\ddot{x} + 2\beta\omega\dot{x} + F_S\left[x(t)\right] = -a(t) \qquad (2\text{-}52)$$

where $F_S\left[x(t)\right]$ is the nonlinear restoring force per unit mass. Integrating Equation (2-52) over the entire relative displacement history, results in the following energy balance equation:

$$E_I = E_K + E_D + E_S + E_H \qquad (2\text{-}53)$$

where

$$E_I = \text{Input energy} = \int_0^x a(t)dx = \int_0^t a(t)\dot{x}dt \qquad (2\text{-}54)$$

$$E_K = \text{Kinetic energy} = \int_0^x \ddot{x}dx = \frac{\dot{x}^2}{2} \qquad (2\text{-}55)$$

$$E_D = \text{Dissipative damping energy} = 2\beta\omega\int_0^x \dot{x}dx = 2\beta\omega\int_0^t \dot{x}^2 dt \qquad (2\text{-}56)$$

$$E_S = \text{Recoverable elastic strain energy} = \frac{F_s^2}{2\omega^2} \qquad (2\text{-}57)$$

$$E_H = \text{Dissipative plastic strain energy} = \int_0^x F_s dx - \frac{F_s^2}{2\omega^2} = \int_0^t F_s\dot{x}dt - \frac{F_s^2}{2\omega^2} \qquad (2\text{-}58)$$

The energy terms in the above equations are given in energy per unit mass. Through the remainder of this section, the term "energy" refers to the energy per unit mass.

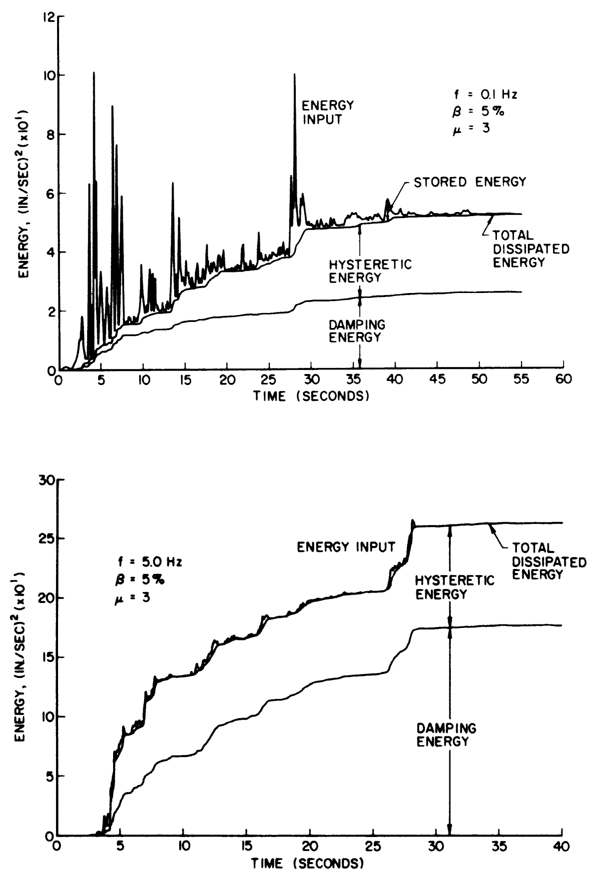

Figure 2-68. Energy time histories for a low and a high frequency, elastic-plastic structure subjected to El Centro ground motion. [After Zahrah and Hall (2-133).]

Figure 2-68 presents the energy response computed by Zahrah and Hall [(2-133)] as a function of time for two elastic-plastic SDOF structures; a low frequency (0.1 Hz) and a high frequency (5 Hz) structure; both with a 5% damping and a ductility of 3.0 subjected to the 1940 El-Centro ground motion. In these plots, the difference between the input energy and the dissipated energy (sum of damping and hysteretic) represents the stored energy (sum of strain and kinetic). The stored energy becomes vanishingly small at the end of motion and the energy dissipated in the structure becomes almost equal to the energy imparted to it. The larger peaks and troughs in the energy response of a low-frequency structure as compared to a high-frequency structure indicate that for low-frequency structures, a larger portion of the energy imparted to the structure is stored in the form of strain and kinetic energies.

Zahrah and Hall [2-133] introduced an energy spectrum as a plot of the numerical value of the input energy E_I at the end of motion as a function of period or frequency for different damping and ductility ratios. Examples of such spectra are shown in Figure 2-69 for linear structures with different damping ratios using the El-Centro record and for nonlinear structures with 2% damping and ductility ratios of 2 and 5 using Taft ground motion. Zahrah and Hall indicated that for linear structures under the same ground motion, input energy spectra are generally similar in shape to response spectra and that the quantity $1/2\, m(PSV)^2$ for an undamped structure is a good estimate of the amount of input energy imparted to the structure. For damped structures, however, this quantity underestimates the input energy. They also indicated that the energy spectral shapes for nonlinear systems are similar to those of linear systems and that the amount of energy input is nearly the same for a linear and a nonlinear structure (with moderate ductility) with the same frequency.

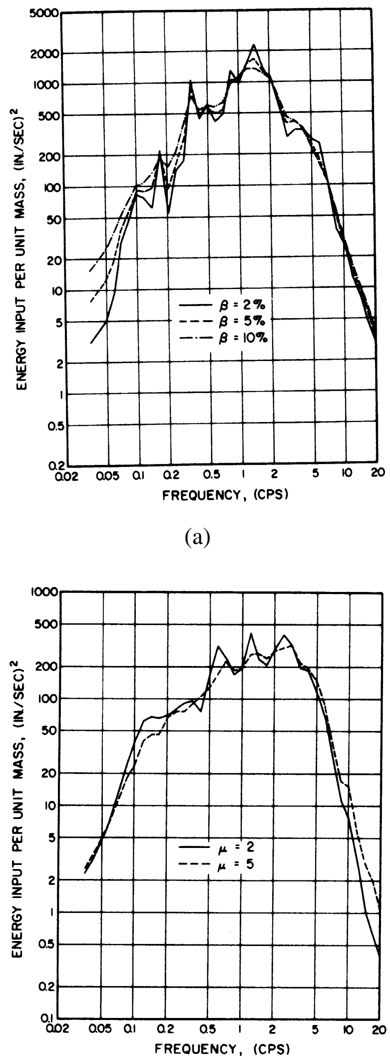

Figure 2-69. Input energy spectra for (a) linear systems with 2, 5, and 10% damping using El Centro ground motion and (b) elstic-plastic systems with 2% damping and ductility ratios of 2 and 5 using Taft ground motion. [After Zahrah and Hall (2-133).]

According to Uang and Bertero [2-134], the energy equations in [2-53] through [2-58] should be considered as "relative energy equations" since the integrations are performed for equations of motion using the relative displacements. For this system of equations, the relative input energy is defined as the work done by the static equivalent lateral force on a fixed-base system. Uang and Bertero introduced the "absolute energy equations" by integrating the equation of motion using the absolute displacements. For

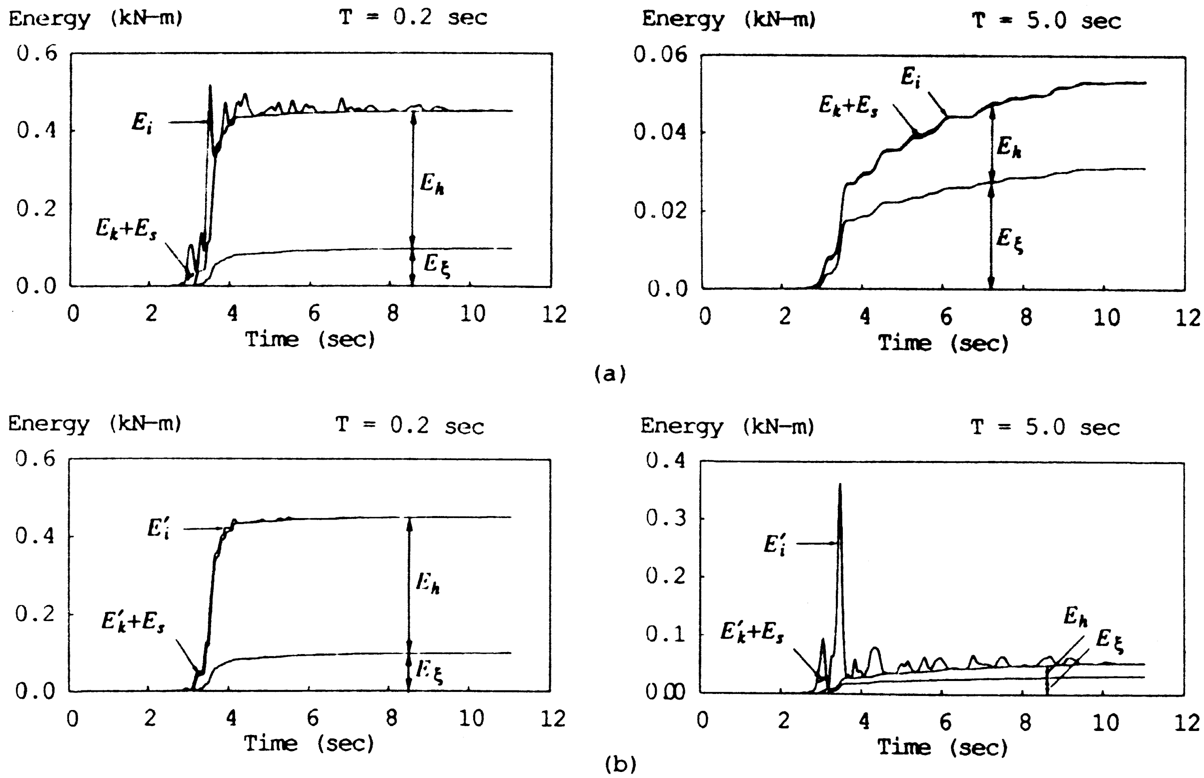

Figure 2-70. (a) Absolute and (b) relative energy time histories for elastic-plastic systems with 5% damping and ductility ratios of 5 subjected to the 1986 San Salvador earthquake. [After Uang and Bertero (2-134).]

the absolute energy terms; E_D, E_S, and E_H are the same as their relative counterparts while the absolute input energy is given as $\int \ddot{x}_t dx_g$ and the absolute kinetic energy is given as $\dot{x}_t^2/2$; where x_t and x_g are the absolute and ground displacement; respectively. The absolute input energy represents the work done by the total base shear on the foundation displacement. The difference between the absolute and relative, input and kinetic energies is given by:

$$E_{I,abs} - E_{I,rel} = E_{K,abs} - E_{K,rel} = \frac{\dot{x}_g^2}{2} + \dot{x}\dot{x}_g \qquad (2\text{-}59)$$

Figure 2-70 shows energy time-histories for a short and a long-period elastic-plastic structure using the relative and absolute energy terms. In addition, Uang and Bertero [(2-134)] converted the input energy to an equivalent velocity such that

$$V_I = \sqrt{2E_I} \qquad (2\text{-}60)$$

where E_I can be the relative or absolute input energy per unit mass. Figure 2-71 presents the relative and absolute input energy equivalent velocity spectra along with the peak ground velocity for three earthquake records. As the plots indicate, the relative and absolute input energies are very close for the mid-range periods (in the vicinity of predominant periods of ground motion). For longer and shorter periods, however, the difference between relative and absolute energies is significant. The figure also shows that the absolute and relative equivalent velocities converge to the

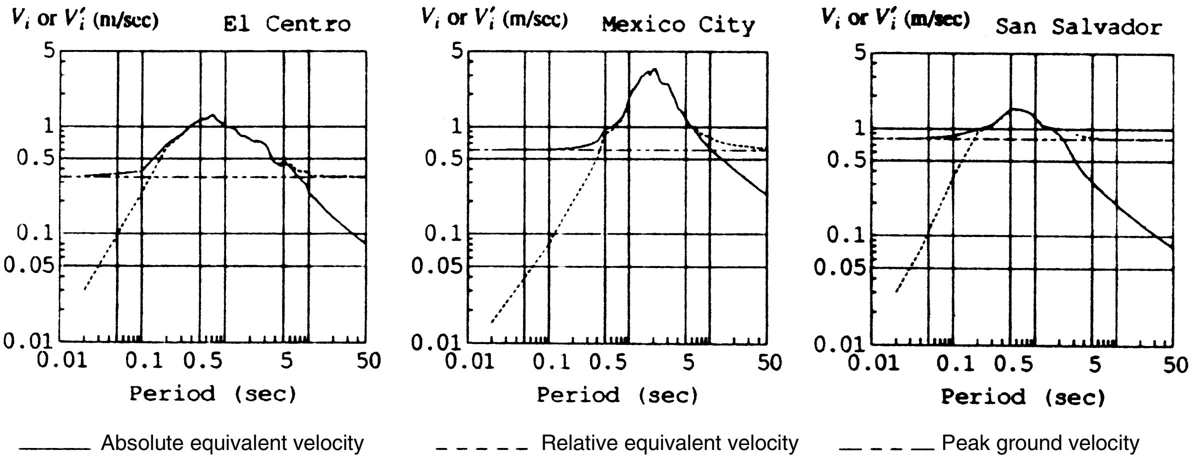

Figure 2-71. Absolute and relative input energy equivalent velocity spectra for elastic-plastic systems with 5% damping and ductility ratio of 5 using three earthquake records. [After Uang and Bertero (2-134).]

peak ground velocity at very short and very long periods, respectively. Subsequently, Uang and Bertero concluded that the absolute input energy can be used as a damage index for short-period structures, while the relative input energy is more suitable for long-period structures. Their study also showed, using energy spectra, that the input energy is insensitive to the ductility ratio. Finally, Uang and Bertero [(2-134)] believed that for linear structures, Housner's use of $1/2\,m(PSV)^2$ to estimate input energy reflects the maximum elastic energy stored in the structure without consideration of damping energy.

It should be noted that at the time of this writing, the energy concept outlined in this section does not provide the basis for seismic design, despite the body of knowledge that has been developed. Further research is required to reliably estimate both the energy demand and energy capacity of structures in order to implement energy approaches in seismic design procedures.

2.12 ARTIFICIALLY GENERATED GROUND MOTION

One major drawback in using the response spectrum method in analysis and design of structures lies in the limitation of the method to provide temporal information on structural response and behavior. Such information is sometimes necessary in arriving at a satisfactory design. For example, the response spectrum procedure can be used to estimate the maximum response in each mode of vibration, and procedures such as square root of the sum of the squares can be used to combine the modal responses. When the natural frequencies are close to each other, however, the square root of the sum of the squares can result in inaccurate estimate of the response. In such cases, the complete quadrature combination[8] CQC, or a time-history analysis may be used. If inelastic deformation is permitted in design, the inelastic spectra and the de-amplification factors presented in the previous sections

[8] An improved procedure for computing modal responses referred to as complete quadrature combination CQC was proposed by Der Kiureghian (see Chapter 3).

cannot be used to compute the response of structures modeled as multi-degree-of-freedom, and one therefore relies on a time-history analysis for computing the inelastic response. In many cases, structures house equipment are sensitive to floor vibrations during an earthquake. It is sometimes necessary to develop floor response spectra from the time-history response of the floor. In addition, when designing critical or major structures such as power plants, dams, and high-rise buildings, the final design is usually based on a complete time-history analysis. The problem which often arises is what representative accelerogram should be used. Artificially generated accelerograms which represent earthquake characteristics such as a given magnitude, epicentral distance, and soil condition of the site have been used for this purpose as well as in research. For example, Penzien and Liu [(2-127)] used artificial accelerograms to investigate the statistical characteristics of inelastic systems and Lai and Biggs [(2-126)] used them to obtain inelastic acceleration and displacement response ratios.

Random models have been used to simulate earthquake ground motion and generate artificial accelerograms. Both stationary and nonstationary random processes have been suggested (see for example 2-135 to 2-138). Other studies have proposed site-dependent power spectral density from recorded ground motion, which can be utilized in generating artificial accelerograms. One of the first attempts in generating artificial accelerograms was by Housner and Jennings [(2-135)] who modeled ground motion as a stationary Gaussian random process with a power spectral density from undamped velocity spectra of recorded accelerograms. They developed a procedure for generating a random function that has the same properties of strong earthquake ground motion and used it to generate eight artificial accelerograms of 30 sec duration which exhibit the same statistical properties of real ground motion.

The detailed description of the procedures for generating artificial accelerograms is beyond the scope of this chapter. It may, however, be useful to briefly mention the basic elements, which are generally needed to generate an artificial accelerogram. In most cases, these elements consist of a power spectral density or a zero-damped response spectrum, a random phase angle generator, and an envelope function. The simulated motion is then obtained as a finite sum of several harmonic excitations. Usually an iterative procedure is needed to check the consistency of the artificial motion by examining its frequency content through its response spectrum or its power spectral density. A typical artificial accelerogram and integrated velocity and displacement generated from the Kanai-Tajimi [(2-19, 2-20)] power spectral density for alluvium using the peak acceleration and the duration of strong motion of the S00E component of El Centro, the Imperial Valley earthquake of May 18, 1940 is shown in Figure 2-72.

2.13 SUMMARY AND CONCLUSION

The state-of-the-art in strong motion seismology and ground motion characterization has advanced significantly in the past three decades. One can now estimate, with reasonable accuracy, the design ground motion and spectral shapes at a given location. Earthquake magnitude, source distance, site geology, fault characteristics, duration of strong motion, etc. influence ground motion and spectral shapes. While building codes and seismic provisions account for some of these influences such as site geology, magnitude, and distance, others such as fault characteristics, travel path, and duration require further studies before they can be implemented.

Response spectrum is used extensively in seismic design of structures. Recent codes recommend acceleration amplifications in terms of seismic coefficients, which account for site geology, shaking intensity, and distance for constructing design spectra and computing the design lateral forces.

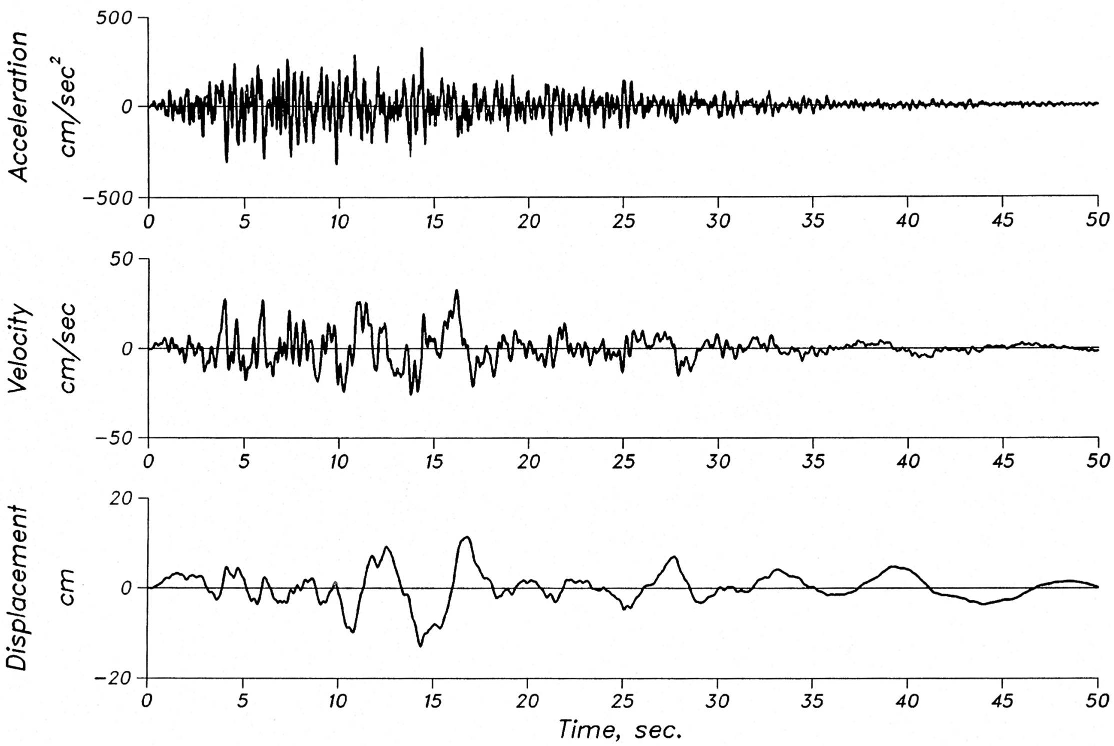

Figure 2-72. Acceleration - time history and integrated velocity and displacement generated from the Kanai-Tajimi power spectral density for alluvium using the peak ground acceleration and the duration of the S00E component of El Centro, the Imperial Valley earthquake of May 18, 1940.

In moderate and strong earthquakes, structures can experience nonlinear behavior and dissipate a portion of the seismic energy through inelastic action. To account for the energy absorption capacity of the structure, seismic codes allow the use of response modification factors, referred to as *R*-factors, to reduce the elastic design forces and amplify the elastic displacements (drifts). Although the application of inelastic spectra is limited to structures which can be modeled as single-degree-of-freedom, inelastic spectra can be used to estimate the ductility demands which are needed to compute response modification or *R*-factors.

In special cases such as design of critical or essential structures, a time-history analysis may be warranted. Determination of a representative set of accelerograms which reflects the earthquake characteristics expected at the site is important. Artificially generated ground motion may be used to determine representative accelerograms.

In most cases, particularly for critical and essential structures, the advice of geologists, seismologists, geotechnical engineers, and structural engineers should be obtained before ground motion and spectral shape estimates are finalized for design.

ACKNOWLEDGMENT

The authors wish to thank Dr. Fawzi E. Elghadamsi who co-authored this chapter in the first edition of the handbook. His contributions, some of which are reflected in this edition, are gratefully acknowledged.

REFERENCES

2-1 Biot, M. A., "A Mechanical Analyzer for Prediction of Earthquake Stresses," *Bull. Seism. Soc. Am*., Vol. 31, 151-171, 1941.

2-2 Biot, M. A., "Analytical and Experimental Methods in Engineering Seismology," *Proc. ASCE* 68, 49-69, 1942.

2-3 Housner, G. W., "An Investigation of the Effects of Earthquakes on Buildings," Ph.D. Thesis, California Institute of Technology, Pasadena, California, 1941.

2-4 Hudson, D. E., "Response Spectrum Techniques in Engineering Seismology," *Proc. 1st World Conf. Earthquake Eng*., 4-1 to 4-12, Berkeley, California, 1956.

2-5 Rojahn, C. and Mork, P., "An Analysis of Strong Motion Data from a Severely Damaged Structure," the Imperial Services Building, El Centro, California, USGS Open File Rep. 81-194, 1981.

2-6 Trifunac, M. D., "Low Frequency Digitization Errors and a New Method for Zero Baseline Correction of Strong-Motion Accelerograms," Earthquake Eng. Research Laboratory, EERL 70-07, California Institute of Technology, Pasadena, California, 1970.

2-7 Hudson, D. E., Brady, A. G., Trifunac, M. D., and Vijayaraghavan, A., "Analysis of Strong-Motion Earthquake Accelerograms-Digitized and Plotted Data, Vol. II, Corrected Accelerograms and Integrated Ground Velocity and Displacement Curves, Parts A through Y," Earthquake Research Laboratory, California Institute of Technology, Pasadena, California, 1971-1975.

2-8 Hudson, D. E., "Reading and Interpreting Strong Motion Accelerograms," Earthquake Eng. Research Institute, Berkeley, California, 1979.

2-9 Mohraz, B., Hall, W. J., and Newmark, N. M., "A Study of Vertical and Horizontal Earthquake Spectra," Nathan M. Newmark Consulting Engineering Services, Urbana, Illinois, AEC Report WASH-1255, 1972.

2-10 Iwan, W. D., Moser, M. A., and Peng, C.-Y., "Some Observations on Strong-Motion Earthquake Measurements Using a Digital Accelerograph," *Bull. Seism. Soc. Am*., Vol. 75, No. 5, 1225-1246, 1985.

2-11 Page, R. A., Boore, D. M., Joyner, W. B., and Caulter, H. W., "Ground Motion Values for Use in the Seismic Design of the Trans-Alaska Pipeline System," USGS Circular 672, 1972.

2-12 Bolt, B. A., "Duration of Strong Motion," *Proc. 4th World Conf. Earthquake Eng*., 1304-1315, Santiago, Chile, 1969.

2-13 Trifunac, M. D. and Brady, A. G., "A Study of the Duration of Strong Earthquake Ground Motion," *Bull. Seism. Soc. Am*., Vol. 65, 581-626, 1975.

2-14 Husid R, Median, H., and Rios, J., "Analysis de Terremotos Norteamericanos y Japonesses," *Rivista del IDIEM*, Vol. 8, No. 1, 1969.

2-15 McCann, W. M. and Shah, H. C., "Determining Strong-Motion Duration of Earthquakes," *Bull. Seism. Soc. Am*., Vol. 69, No. 4, 1253-1265, 1979.

2-16 Trifunac, M. D. and Westermo, B. D., "Duration of Strong Earthquake Shaking," *Int. J. Soil Dynamics and Earthquake Engineering,* Vol. 1, No. 3, 117-121, 1982.

2-17 Moayyad, P. and Mohraz, B., "A Study of Power Spectral Density of Earthquake Accelerograms," NSF Report PFR 8004824, Civil and Mechanical Engineering Dept., Southern Methodist University, Dallas, TX, 1982.

2-18 Elghadamsi, F. E., Mohraz, B., Lee, C. T., and Moayyad, P., "Time-Dependent Power Spectral Density of Earthquake Ground Motion," *Int. J. Soil Dynamics and Earthquake Engineering*, Vol. 7, No. 1, 15-21, 1988.

2-19 Kanai, K., "Semi-Empirical Formula for the Seismic Characteristics of the Ground," Bull. Earthquake Research Institute, Vol. 35, University of Tokyo, Tokyo, Japan, 309-325, 1957.

2-20 Tajimi, H., "A Statistical Method of Determining the Maximum Response of a Building Structure During an Earthquake," *Proc. 2nd World Conf. Earthquake Eng*., Vol. II, 781-797, Tokyo, Japan, 1960.

2-21 Lai, S. P., "Statistical Characterization of Strong Motions Using Power Spectral Density Function," *Bull. Seism. Soc. Am*., Vol. 72, No. 1, 259-274, 1982.

2-22 Clough, R. W. and Penzien, J., *Dynamics of Structures*, McGraw-Hill, New York, 1993.

2-23 Donovan, N. C., "Earthquake Hazards for Buildings," Building Practices for Disaster Mitigation, National Bureau of Standards, U.S. Department of Commerce, Building Research Services 46, 82-111, 1973.

2-24 Donovan, N. C. and Bornstein, A. E., "Uncertainties in Seismic Risk Procedures," *J. Geotechnical Eng. Div*., Vol. 104, No. GT 7, 869-887, 1978.

2-25 Cloud, W. K. and Perez, V., "Unusual Accelerograms Recorded at Lima, Peru," *Bull. Seism. Soc. Am*., Vol. 61, No. 3, 633-640, 1971.

2-26 Blume, J. A., "Earthquake Ground Motion and Engineering Procedures for Important Installations Near Active Faults," *Proc. 3rd World Conf. Earthquake Eng*., Vol. IV, 53-67, New Zealand, 1965.

2-27 Kanai, K., "Improved Empirical Formula for Characteristics of Stray Earthquake Motions," *Proc. Japan Earthquake Symposium*, 1-4, 1966. (In Japanese)

2-28 Milne, W. G. and Davenport, A. G., "Distribution of Earthquake Risk in Canada," *Bull. Seism. Soc. Am.*, Vol. 59, No. 2, 754-779, 1969.

2-29 Esteva, L., "Seismic Risk and Seismic Design Decisions," *Seismic Design for Nuclear Power Plants*, R. J. Hansen, Editor, MIT Press, 1970.

2-30 Campbell, K. W., "Near-Source Attenuation of Peak Horizontal Acceleration," *Bull. Seism. Soc. Am.*, Vol. 71, No. 6, 2039-2070, 1981.

2-31 Joyner, W. B. and Boore, D. M., "Peak Horizontal Acceleration and Velocity from Strong Motion Records Including Records from the 1979 Imperial Valley, California, Earthquake," *Bull. Seism. Soc. Am.*, Vol. 71, No. 6, 2011-2038, 1981.

2-32 Joyner, W. B. and Boore, D. M., "Prediction of Earthquake Response Spectra," *U.S. Geol. Surv. Open File Report 82-977,* 1982.

2-33 Idriss, I. M., "Evaluating Seismic Risk in Engineering Practice," Chapter 6, *Proc. 11th International Conf. Soil Mechanics and Foundation Eng*., 255-320, San Francisco, 1985.

2-34 Sabetta, F. and Pugliese, A., "Attenuation of Peak Horizontal Acceleration and Velocity from Italian Strong-Motion Records," *Bull. Seism. Soc. Am.*, Vol. 77, No. 5, 1491-1513, 1987.

2-35 Sadigh, K., Egan, J., and Youngs, R., "Specification of Ground Motion for Seismic Design of Long Period Structures," *Earthquake Notes*, Vol. 57, 13, 1986.

2-36 Campbell, K. W. and Bozorgnia, Y., "Near-Source Attenuation of Peak Horizontal Acceleration from Worldwide Accelerograms Recorded from 1957 to 1993," *Proc. 5th U.S. National Conf. Earthquake Eng.,* Vol. 3, 283-292, Chicago, Illinois, 1994.

2-37 Boore, D. M., Joyner, W. B., and Fumal, T. E., "Equations for Estimating Horizontal Response Spectra and Peak Acceleration from Western North American Earthquakes: A Summary of Recent Work," *Seismological Research Letters,* Vol. 68, No. 1, 128-153, 1997.

2-38 Housner, G. W., "Intensity of Earthquake Ground Shaking Near the Causative Fault," *Proc. 3rd. World Conf. Earthquake Eng*., Vol. 1, III, 94-115, New Zealand, 1965.

2-39 Seed, H. B. and Idriss, I. M., "Ground Motions and Soil Liquefaction During Earthquakes," Earthquake Engineering Research Institute, Berkeley, California, 1982.

2-40 Porcella, R. L. and Matthiesen, R. B., USGS Open-File Report 79-1654, 1979.

2-41 Nuttli, O. W. and Herrmann, R. B., "Consequences of Earthquakes in Mississippi Valley," ASCE Preprint 81-519, ASCE National Convention, St. Louis, 1981.

2-42 Hanks, T. and McGuire, R., "The Character of High-Frequency Strong Ground Motion," *Bull. Seism. Soc. Am.,* Vol. 71, 2071-2095, 1981.

2-43 Spudich, P. and Ascher, U., "Calculation of Complete Theoretical Seismograms in Vertically Varying Media Using Collocation Methods," *Geophys. J. R. Astron. Soc.,* Vol. 75, 101-124, 1983.

2-44 Atkinson, G. and Boore, D., "Ground Motion Relations for Eastern North America," *Bull. Seism. Soc. Am.,* Vol. 85, No. 1, 17-30, 1995.

2-45 Boore, D. M., Joyner, W. B., Oliver, A. A., and Page, R. A., "Estimation of Ground Motion Parameters," USGS, Circular 795, 1978.

2-46 Boore, D. M., Joyner, W. B., Oliver, A. A., and Page, R. A., "Peak Acceleration, Velocity and Displacement from Strong Motion Records," *Bull. Seism. Soc. Am.*, Vol. 70, No. 1, 305-321, 1980.

2-47 Chang, F. K. and Krinitzsky, E. L., "Duration, Spectral Content, and Predominant Period of Strong Motion Earthquake Records from Western United States," U.S. Army Engineer Waterways Experiment Station, Miscellaneous Paper S-73-1, Vicksburg, Mississippi, 1977.

2-48 Novikova E. I. and Trifunac, M. D., "Duration of Strong Motion in Terms of Earthquake Magnitude, Epicentral Distance, Site Conditions and Site Geometry," *Earthquake Engineering and Structural Dynamics,* Vol. 23, 1023-1043, 1994.

2-49 Hall, J. F., Heaton, T. H., Halling M. W., and Wald, D. J., "Near-Source Ground Motions and its Effects on Flexible Buildings," *Earthquake Spectra,* Vol. 11, No. 4, 569-605, 1995.

2-50 Heaton, T. H. and Hartzell, S. H., "Earthquake Ground Motions," *Annual Reviews of Earth and Planetary Sciences,* Vol. 16, 121-145, 1988.

2-51 Somerville, P. G. and Graves, R. W., "Conditions that Give Rise to Unusually Large Long Period Motions," *Structural design of Tall Buildings,* Vol. 2, 211-232, 1993.

2-52 Idriss, I. M., "Influence of Local Site Conditions on Earthquake Ground Motions," *Proc. 4th U.S. Nat. Conf. Earthquake Engineering,* Vol. 1, 55-57, Palm Springs, California, 1990.

2-53 Mohraz, B., "A Study of Earthquake Response Spectra for Different Geological Conditions," *Bull. Seism. Soc. Am.*, Vol. 66, No. 3, 915-935, 1976.

2-54 Housner, G. W., "Strong Ground Motion," Chapter 4 in *Earthquake Engineering*, R. L. Wiegel, Editor, Prentice-Hall, Englewood Cliffs, N.J., 1970.

2-55 McGarr, A., "Scaling of Ground Motion Parameters, State of Stress, and Focal Depth," *J. Geophys. Res.,* Vol. 89, 6969-6979, 1984.

2-56 McGarr, A., "Some Observations Indicating Complications in the Nature of Earthquake Scaling", *Earthquake Source Mechanics, Maurice*

Ewing Ser. 6, edited by S. Das et al., 217-225, 1986.

2-57 Kanamori, H. and Allen, C. R., "Earthquake Repeat Time and Average Stress Drop," *Earthquake Source Mechanics, Maurice Ewing Ser. 6,* edited by S. Das et al., 227-235, 1986.

2-58 Campbell, K. W., "Predicting strong Ground Motion in Utah," *Evaluation of Regional and Urban Earthquake Hazards and Risks in Utah,* edited by W. W. Hays and P. L. Gori, 1988.

2-59 Joyner, W. B. and Boore, D. M., "Measurement, Characterization, and Prediction of Strong Ground Motion," *Proc. Earthquake engineering and Soil Dynamics II,* GT Div/ASCE, edited by J. L. Von Thun, Park City, Utah, 43-102, 1988.

2-60 Faccioli, E., "Estimating Ground Motions for Risk Assessment," *Proc. of the U.S.-Italian Workshop on Seismic Evaluation and Retrofit,* Edited by D. P. Abrams and G. M. Calvi, Technical Report NCEER-97-0003, National Center for Earthquake Engineering Research, Buffalo, New York, 1-16, 1997.

2-61 Reiter, L., *Earthquake Hazard Analysis: Issues and Insights,* Columbia University Press, New York, 1990.

2-62 Boatwright, J. and Boore, D. M., "Analysis of the Ground Accelerations radiated by the 1980 Livermore Valley Earthquakes for Directivity and Dynamic Source Characteristics," *Bull. Seism. Soc. Am.,* Vol. 72, 1843-1865.

2-63 Gutenberg, B. and Richter, C. F. "Earthquake Magnitude, Intensity, Energy, and Acceleration," *Bull. Seism. Soc. Am*., Vol. 46, No. 2, 143-145, 1956.

2-64 Richter, C. F., *Elementary Seismology*, W. H. Freeman and Co., San Francisco, 1958.

2-65 Bender, B., "Maximum Likelihood Estimation of *b* Values for Magnitude Grouped Data," *Bull. Seism. Soc. Am*., Vol. 73, No. 3, 831-851, 1983.

2-66 Schwartz, D. P. and Coppersmith, K. J., "Fault Behavior and Characteristic Earthquakes: Examples from the Wasatch and San Andreas Fault Zones," *J. Geophs. Res*., Vol. 89, No. B7, 5681-5698, 1984.

2-67 Sieh, K. E., "Prehistoric Large Earthquakes Produced by Slip on the San Andreas Fault at Pallett Creek, California," *J. Geophys. Res*., Vol. 83, No. B8, 3907-3939, 1978.

2-68 Cornell, C. A., "Engineering Seismic Risk Analysis," *Bull. Seism. Soc. Am*., Vol. 58, No. 5, 1583-1606, 1968.

2-69 Vanmarcke, E. H., "Seismic Safety Assessment," *Random Excitation of Structures by Earthquakes and Atmospheric Turbulence*, edited by H. Parkus, International Center for Mechanical Sciences, Course and Lectures No. 225, Springer-Verlag, 1-76, 1977.

2-70 Benjamin, J. R., "Probabilistic Models for Seismic Force Design," *J. Structural Div*., ASCE, Vol. 94, ST5, 1175-1196, 1968.

2-71 Der-Kiureghian, A. and Ang A. H-S., "A Fault-Rupture Model for Seismic Risk Analysis," *Bull. Seism. Soc. Am*., Vol. 67, No. 4, 1173-1194, 1977.

2-72 Algermissen, S. T. and Perkins, D. M., "A Technique for Seismic Risk Zoning, General Considerations and Parameters," *Proc. Microzonation Conf*., 865-877, Seattle, Washington, 1972.

2-73 Algermissen, S. T. and Perkins, D. M., "A Probabilistic Estimate of Maximum Acceleration in Rock in Contiguous United States," USGS Open File Report, 76-416, 1976.

2-74 Applied Technology Council, National Bureau of Standards, and National Science Foundation, "Tentative Provisions for the Development of Seismic Regulations for Buildings," ATC Publication 3-06, NBS Publication 510, NSF Publication 78-8, 1978.

2-75 McGuire, R. K., "Seismic Structural Response Risk Analysis, Incorporating Peak Response Progressions on Earthquake Magnitude and Distance," Report R74-51, Dept. of Civil Engineering, Mass. Inst. of Technology, Cambridge, Mass., 1975.

2-76 NEHRP Recommended Provisions for the Development of Seismic Regulations for New Buildings, 1985 Edition, Building Seismic Safety Council, Washington, D.C., 1985.

2-77 NEHRP Recommended Provisions for the Development of Seismic Regulations for New Buildings, 1988 Edition, Building Seismic Safety Council, Washington, D.C., 1988.

2-78 NEHRP Recommended Provisions for the Development of Seismic Regulations for New Buildings, 1991 Edition, Building Seismic Safety Council, Washington, D.C., 1991.

2-79 NEHRP Recommended Provisions for the Development of Seismic Regulations for New Buildings, 1994 Edition, Building Seismic Safety Council, Washington, D.C., 1994.

2-80 NEHRP Recommended Provisions for the Development of Seismic Regulations for New Buildings, 1997 Edition, Building Seismic Safety Council, Washington, D.C., 1997.

2-81 NEHRP Guidelines for the Seismic Rehabilitation of Buildings, FEMA-273, Building Seismic Safety Council, Washington, D.C., 1997.

2-82 Uniform Building Code, 1985 Edition, International Conference of Building Officials, Whittier, California, 1985.

2-83 Uniform Building Code, 1988 Edition, International Conference of Building Officials, Whittier, California, 1988.

2-84 Uniform Building Code, 1991 Edition, International Conference of Building Officials, Whittier, California, 1991.

2-85 Uniform Building Code, 1994 Edition, International Conference of Building Officials, Whittier, California, 1994.

2-86 Uniform Building Code, 1997 Edition, International Conference of Building Officials, Whittier, California, 1997.

2-87 Newmark, N. M. and Hall, W. J., "Earthquake Spectra and Design," Earthquake Engineering Research Institute, Berkeley, California, 1982.

2-88 Newmark, N. M., Blume, J. A., and Kapur, K. K., "Seismic Design Criteria for Nuclear Power Plants," *J. Power Div*., ASCE, Vol. 99, No. PO2, 287-303, 1973.

2-89 Newmark, N. M. and Hall, W. J., "Seismic Design Criteria for Nuclear Reactor Facilities," *Proc. 4th World Conf. Earthquake Eng*., B-4, 37-50, Santiago, Chile, 1969.

2-90 Newmark, N. M. and Hall, W. J., "Procedures and Criteria for Earthquake Resistant Design," Building Practices for Disaster Mitigation, National Bureau of Standards, U.S. Department of Commerce, Building Research Series 46, 209-236, 1973.

2-91 Hall, W. J., Mohraz B., and Newmark, N. M., "Statistical Studies of Vertical and Horizontal Earthquake Spectra," Nathan M. Newmark Consulting Engineering Services, Urbana, Illinois, 1975.

2-92 Newmark, N. M. and Rosenblueth, E., *Fundamentals of Earthquake Engineering*, Prentice-Hall, Englewood Cliffs, N.J., 1971.

2-93 Mohraz, B. and Tiv, M., "Spectral Shapes and Amplifications for the Loma Prieta Earthquake of October 17, 1989," *Proc. 3rd U.S. Conf. Lifeline Earthquake Eng.,* 562-571, Los Angeles, California, 1991.

2-94 Trifunac, M. D., Brady, A. G., and Hudson, D. E., "Analysis of Strong-Motion Earthquake Accelerograms, Vol. III, Response Spectra, Parts A through Y," Earthquake Eng. Research Laboratory, California Institute of Technology, Pasadena, California, 1972-1975.

2-95 Chopra, A. K., "Dynamics of Structures - A Primer," Earthquake Engineering Research Institute, Berkeley, California, 1981.

2-96 Sadek, F., Mohraz, B., and Riley, M. A., "Linear Procedures for Structures with Velocity-Dependent Dampers," *Journal of Structural Engineering,* ASCE, Vo. 128, No. 8, 887-895, 2000.

2-97 Hayashi, S., Tsuchida, H., and Kurata, E., "Average Response Spectra for Various Subsoil Conditions," *Third Joint Meeting, U.S. - Japan Panel on Wind and Seismic Effects*, UJNR, Tokyo, 1971.

2-98 Kuribayashi, E., Iwasaki, T., Iida, Y., and Tuji, K., "Effects of Seismic and Subsoil Conditions on Earthquake Response Spectra," *Proc. International Conf. Microzonation*, Seattle, Wash., 499-512, 1972.

2-99 Seed, H. B., Ugas, C., and Lysmer, J., "Site-Dependent Spectra for Earthquake-Resistance Design," *Bull. Seism. Soc. Am*., Vol. 66, No. 1, 221-243, 1976.

2-100 Atomic Energy Commission, "Design Response Spectra for Seismic Design of Nuclear Power Plants," Regulatory Guide 1.60, Directorate of Regulatory Standards, Washington, D.C., 1973.

2-101 Crouse, C. B. and McGuire, J. W., "Site Response Studies for Purpose of Revising NEHRP Seismic Provisions," *Earthquake Spectra,* Vol. 12, No. 3, 407-439, 1996.

2-102 Mohraz, B., "Influences of the Magnitude of the Earthquake and the Duration of Strong Motion on Earthquake Response Spectra," *Proc. Central Am. Conf. on Earthquake Eng*., San Salvador, El Salvador, 1978.

2-103 Mohraz, B., "Recent Studies of Earthquake Ground Motion and Amplification," *Proc. 10th World Conf. Earthquake Eng.,* Madrid, Spain, 6695-6704, 1992.

2-104 Peng, M. H., Elghadamsi, F. E., and Mohraz, B., "A Simplified Procedure for Constructing Probabilistic Response Spectra," *Earthquake Spectra*, Vol. 5, No. 2, 393-408, 1989.

2-105 Singh, J. P., "Earthquake Ground Motions: Implications for Designing Structures and Reconciling Structural Damage," *Earthquake Spectra*, Vol. 1, No. 2, 239-270, 1985.

2-106 "Reducing Earthquake Hazards: Lessons Learned from Earthquakes," Earthquake Engineering Research Institute, Publication No. 86-02, Berkeley, California, 1986.

2-107 Housner, G. W. and Jennings, P. C., "Earthquake Design Criteria," Earthquake Engineering Research Institute, Berkeley, California, 1982.

2-108 Housner, G. W., "Spectrum Intensities of Strong-Motion Earthquakes," *Proc. of the Symposium on Earthquakes and Blast Effects on Structures*, Earthquake Engineering Research Institute, 1952.

2-109 Housner, G. W., "Behavior of Structures During Earthquakes," *J. Eng. Mech. Div*., ASCE Vol. 85, No. EM4, 109-129, 1959.

2-110 Housner, G. W., "Design Spectrum," Chapter 5 in Earthquake Engineering, R.L. Wiegel, Editor, Prentice-Hall, Englewood Cliffs, N.J., 1970.

2-111 Blume, J. A., Sharpe, R. L., and Dalal, J. S., "Recommendations for Shape of Earthquake Response Spectra," John A. Blume & Associates, San Francisco, California, AEC Report Wash-1254, 1972.

2-112 Seismology Committee, Structural Engineers Association of California, "Recommended Lateral Force Requirements," 1986.

2-113 Martin, G. M., Editor, *Proceedings of the NCEER/SEAOC/BSSC Workshop on Site Response During Earthquakes and Seismic Code Provisions,* University of Southern California, Los Angeles, 1994.

2-114 Borcherdt, R. D., "Estimates of Site-Dependent Response Spectra for Design (Methodology and Justification)," *Earthquake Spectra,* Vol. 10, No. 4, 617-653, 1994.

2-115 Seed, R. B., Dickenson, S. E., and Mok, C. M., "Recent Lessons Regarding Seismic Response Analyses of Soft and Deep Clay Sites," in *Proc. 4th Japan-U.S. Workshop on Earthquake Resistant Design of Lifeline Facilities and Countermeasures for Soil Liquefaction,* National Center for Earthquake Engineering Research, State University of New York at Buffalo, Vol. I, 131-145, 1992.

2-116 Dobry, R., Martin, G. M., Parra, E., and Bhattacharyya, *Study of Ratios of Response Spectra Soil/Rock and of Site Categories for Seismic Codes,* National Center for Earthquake Engineering Research, State University of New York at Buffalo, 1994.

2-117 Borcherdt, R. D., "Preliminary Amplification Estimates Inferred from Strong-Ground-Motion Recordings of the Northridge Earthquake of January 17, 1994," *Proc. Of the International Workshop on Site Response Subjected to Strong Earthquake Motions,* Japan Port and Harbour Research Institute, Vol. 2, 21-46, Yokosuka, Japan, 1996.

2-118 Riddell, R., and Newmark, N. M., "Statistical Analysis of the Response of Nonlinear Systems Subjected to Earthquakes," Civil Engineering Studies, Structural Research Series 468, Department of Civil Engineering, University of Illinois, Urbana, Illinois, 1979.

2-119 Elghadamsi, F. E and Mohraz, B., "Inelastic Earthquake Spectra," *J. Earthquake Engineering and Structural Dynamics*, Vol. 15, 91-104, 1987.

2-120 Blume, J. A., Newmark, N. M., and Corning, L. H., "Design of Multistory Reinforced Concrete Buildings for Earthquake Motions," Portland Cement Association, 1961.

2-121 Newmark, N. M., "Current Trends in the Seismic Analysis and Design of High-Rise Structures," Chapter 16 in Earthquake Engineering, R.L. Wiegel, Editor, Prentice-Hall, Englewood Cliffs, N.J., 1970.

2-122 Housner, G. W., "Limit Design of Structures to Resist Earthquakes," *Proc. 1st World Conf. Earthquake Engineering*, 5-1 to 5-13, Berkeley, Calif., 1956.

2-123 Blume, J. A., "A Reserve Energy Technique for the Earthquake Design and Rating of Structures in the Inelastic Range," *Proc. 2nd World Conf. Earthquake Engineering*, Vol. II, 1061-1084, Tokyo, Japan 1960.

2-124 Blume, J. A., "Structural Dynamics in Earthquake-Resistant Design," *Transactions*, ASCE, Vol. 125, 1088-1139, 1960.

2-125 Blume, J. A., discussion of "Electrical Analog for Earthquake Yield Spectra," *J. Engineering Mechanics Div*., ASCE, Vol. 86, No. EM3, 177-184, 1960.

2-126 Lai, S. P. and Biggs, J. M., "Inelastic Response Spectra for Aseismic Building Design," *J. Struct. Div*., ASCE, Vol. 106, No. ST6, 1295-1310, 1980.

2-127 Penzien, J. and Liu, S. C., "Nondeterministic Analysis of Nonlinear Structures Subjected to Earthquake Excitations," *Proc. 4th World Conf. Earthquake Engineering*, A-1, 114-129, Santiago, Chile, 1969.

2-128 Peng, M. H., Elghadamsi, F. E., and Mohraz, B., "A Stochastic Procedure for Seismic Analysis of SDOF Structures," Civil and Mechanical Engineering Dept., School of Engineering and Applied Science, Southern Methodist University, Dallas, TX, 1987.

2-129 Applied Technology Council ATC, *Structural Response Modification Factors*, ATC-19 Report, Redwood City, California, 1995.

2-130 Krawinkler, H. and Nassar, A. A., "Seismic Design Based on Ductility and Cumulative Damage Demands and Capacities," *Nonlinear Seismic Analysis and Design of Reinforced Concrete Buildings,* Edited by Fajfar and Krawinkler, Elsevier Applied Science, New York, 1992.

2-131 Nassar, A. A. and Krawinkler, H., *Seismic Demands for SDOF and MDOF Systems,* John A. Blume Earthquake Engineering Center, Report No. 95, Stanford University, Stanford, California, 1991.

2-131 Miranda, E. and Bertero, V. V., "Evaluation of Strength Reduction Factors for Earthquake-Resistant Design," *Earthquake Spectra,* Vol. 10, No. 2, 357-379, 1994.

2-132 Zahrah, T. F. and Hall, W. J., "Earthquake Energy Absorption in SDOF Structures," *Journal of Structural Engineering,* ASCE, Vol. 110, No. 8, 1757-1772, 1984.

2-133 Uang, C. M. and Bertero, V. V., "Evaluation of Seismic Energy Structures," *Earthquake Engineering and Structural Dynamics,* Vol. 19, 77-90, 1990.

2-134 Housner, G. W. and Jennings, P. C., "Generation of Artificial Earthquakes," *J. Engineering Mechanics Div*., ASCE, Vol. 90, 113-150, 1964.

2-135 Shinozuka, M. and Salo, Y., "Simulation of Nonstationary Random Process," *J. Engineering Mechanics Div*., ASCE, Vol. 93, 11-40, 1967.

2-136 Amin, M. and Ang, A. H. - S., "Nonstationary Stochastic Model of Earthquake Ground Motion," *J. Engineering Mechanics Div*., ASCE, Vol. 74, No. EM2, 559-583, 1968.

2-137 Iyengar, R. N. and Iyengar, K. T. S., "A Nonstationary Random Process Model for Earthquake Accelerograms," *Bull. Seism. Soc. Am*., Vol. 59, 1163-1188, 1969.